

1999

A two-component aggregation model

Thomas A. Chisholm Jr

College of William and Mary - Virginia Institute of Marine Science

Follow this and additional works at: <https://scholarworks.wm.edu/etd>



Part of the [Civil Engineering Commons](#), [Environmental Sciences Commons](#), and the [Physical and Environmental Geography Commons](#)

Recommended Citation

Chisholm, Thomas A. Jr, "A two-component aggregation model" (1999). *Dissertations, Theses, and Masters Projects*. William & Mary. Paper 1539616607.

<https://dx.doi.org/doi:10.25773/v5-v9ae-mv55>

This Dissertation is brought to you for free and open access by the Theses, Dissertations, & Master Projects at W&M ScholarWorks. It has been accepted for inclusion in Dissertations, Theses, and Masters Projects by an authorized administrator of W&M ScholarWorks. For more information, please contact scholarworks@wm.edu.

INFORMATION TO USERS

This manuscript has been reproduced from the microfilm master. UMI films the text directly from the original or copy submitted. Thus, some thesis and dissertation copies are in typewriter face, while others may be from any type of computer printer.

The quality of this reproduction is dependent upon the quality of the copy submitted. Broken or indistinct print, colored or poor quality illustrations and photographs, print bleedthrough, substandard margins, and improper alignment can adversely affect reproduction.

In the unlikely event that the author did not send UMI a complete manuscript and there are missing pages, these will be noted. Also, if unauthorized copyright material had to be removed, a note will indicate the deletion.

Oversize materials (e.g., maps, drawings, charts) are reproduced by sectioning the original, beginning at the upper left-hand corner and continuing from left to right in equal sections with small overlaps. Each original is also photographed in one exposure and is included in reduced form at the back of the book.

Photographs included in the original manuscript have been reproduced xerographically in this copy. Higher quality 6" x 9" black and white photographic prints are available for any photographs or illustrations appearing in this copy for an additional charge. Contact UMI directly to order.

UMI[®]

Bell & Howell Information and Learning
300 North Zeeb Road, Ann Arbor, MI 48106-1346 USA
800-521-0600

A TWO-COMPONENT AGGREGATION MODEL

A Dissertation

Presented to

The Faculty of the School of Marine Science

The College of William and Mary in Virginia

In Partial Fulfillment

Of the Requirements for the Degree of

Doctor of Philosophy

by Thomas A. Chisholm, Jr.

1999

UMI Number: 9942547

**Copyright 1999 by
Chisholm, Thomas Alexander, Jr.**

All rights reserved.

**UMI Microform 9942547
Copyright 1999, by UMI Company. All rights reserved.**

**This microform edition is protected against unauthorized
copying under Title 17, United States Code.**

UMI
300 North Zeeb Road
Ann Arbor, MI 48103

APPROVAL SHEET

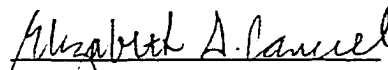
This dissertation is submitted in partial fulfillment of
the requirements of the degree of

Doctor of Philosophy

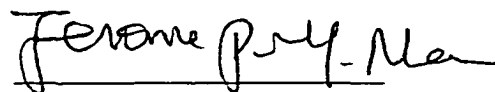

Thomas A. Chisholm, Jr.

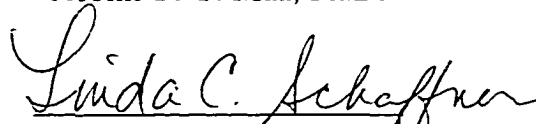
Approved, June 1999


L. Donnelson Wright, Ph.D.
Committee Chairman/ Advisor


Elizabeth A. Canuel, Ph.D.


Albert Y. Kuo, Ph.D.


Jerome P. Y. Maa, Ph.D.


Linda C. Schaffner, Ph.D.

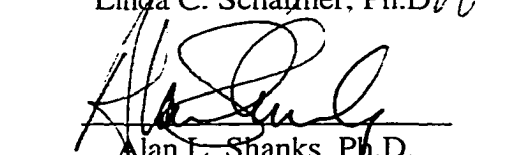

Alan L. Shanks, Ph.D.
University of Oregon, Charleston, OR

TABLE OF CONTENTS

	Page
ACKNOWLEDGMENTS	v
LIST OF TABLES	vi
LIST OF FIGURES	vii
SYMBOLISM	ix
ABSTRACT	xi
INTRODUCTION	2
Particles and Aggregates	2
The Study of Aggregation	8
Sediment Dynamics	8
Objectives	13
LITERATURE REVIEW	15
Aggregation Theory	15
Formation Rates	26
Composition	29
Sizes	30
Fractal Nature of Aggregates	31
Fall Velocity	38
Stickiness	46
Breakup	49
LABORATORY STUDIES	54
Uses of Laboratory Aggregation Devices	54
Device Types	58
Rotating Oscillating Grid Turbulence Aggregation Chamber	59
Analysis of ROGTAC	65
Data Collection	96
Particle Aggregation	98
Proposed Two Component Model Calibration and Verification	100

NUMERICAL MODELING	104
Existing Models	105
Description of Model	109
Discretization Tests	124
Model Testing	129
Effect of Stickiness	137
Variation in Fall Velocity	138
Composition Variation	155
CONCLUSION	171
ROGTAC	171
Aggregation Model	173
APPENDIX	177
LITERATURE CITED	213
VITA	224

ACKNOWLEDGMENTS

The manuscript benefitted from critical review by the dissertation committee members, Elizabeth Canuel, Jerome Maa, Albert Kuo, Linda Schaffner, Alan Shanks, and L. Donnelson Wright. Professor Wright served as committee chairperson.

The Flow Modeling and Control Branch of NASA Langley Research Center generously provided use of their laser Doppler velocimeter. The assistance of William Sellers, Chung-sheng Yao, Jason Lachowicz, and Tim Hepner is appreciated.

Wayne Reisner and Todd Nelson provided support, materials, and tools. Carol Pollard and Ed Kessee provided lab space and advice. Many other donated materials and advice. I am grateful.

Funding was provided by VIMS general funds, the Office of Naval Research, a GSA minigrant, and a VIMS minor research grant.

My wife, Anne, and son, Alex, had more patience with this endeavor than it probably deserved.

LIST OF TABLES

Table	Page
2-1 Fractal Dimension Development	33
2-2 Density - Porosity Relations	37
2-3 Fall Velocity Measurements	44
3-1 Oscillating Grid Turbulence Devices	61
3-2 Viscometers	62
3-3 Rolling Cylinder Devices	62
3-4 Energy Dissipation	95
4-1 Size Re-Center Code	122
4-2 Fractional Composition Re-Center Code	123
4-3 Effect of Stickiness	138
4-4 Fall Velocity Cases	149
4-5 EPA Data	156
4-6 Depth Resolving Model Runs	169
4-7 Depth Resolving Model Output	169
4-8 Concentration Ratios	170

LIST OF FIGURES

Figure	Page
1-1 Particle Sizes	3
1-2 Sediment Dynamics	10
2-1 Differential Settling Aggregation	17
2-2 Shear Aggregation	19
2-3 Syvitski's Fall Velocity Measurements	45
3-1 Oscillating Grid Turbulence Generator	60
3-2 ROGTAC Chamber and Grid	66
3-3 ROGTAC Chamber End View	67
3-4 ROGTAC Support	68
3-5 LDV Velocity Verification	72
3-6 LDV Data Coordinate System	73
3-7 Mean Velocity in XY Plane	77
3-8 Standard Deviation of Velocity in XY Plane	78
3-9 Mean Velocities in XY Plane Across a Grid Cell	79
3-10 Standard Deviation in XY Plane Across a Grid Cell	80
3-11 Measurement Locations	83
3-12 Velocity Measurements in 120 Seconds	84
3-13 Effect of Selecting Evenly Spaced Points	85
3-14 Comparison of Standard Deviation Between Axes	86
3-15 Dissipation for Three Motor Speeds	90
3-16 Dissipation for Motor Speed of 23 Rpm	91
3-17 Dissipation for Motor Speed of 32 Rpm	92
3-18 Dissipation for Motor Speed of 45 Rpm	93
3-19 ROGTAC Aggregation	99
4-1 Differential Settling Kernel	118
4-2 Turbulent Aggregation Kernel	119
4-3 Ratio of Kernels	120
4-4 Cumulative Number of Particles Conserved - Binsize	126
4-5 Number of Particles Per Bin at Steady State - Binsize	127
4-6 Cumulative Number of Particles at Steady State - Binsize	128
4-7 Profile Evolution, One Component	131
4-8 Steady State Convergence Profile, One Component	132
4-9 Steady State Total Number of Particles, One Component	134
4-10 Particle Conservation, Two Components	135
4-11 Steady State, Two Components	136
4-12 Fall Velocity Measurements	140
4-13 Fall Velocity Measurements	141
4-14 Particle Density - Fall Velocity Relationship	143

4-15	Particle Size - Fall Velocity Relationship	144
4-16	Fractal Dimension - Fall Velocity Relationship	145
4-17	Fractal Dimension and Density - Fall Velocity Relationship	146
4-18	Modeled Fall Velocity: Case b1	151
4-19	Modeled Fall Velocity: Case b2	151
4-20	Modeled Fall Velocity: Case b3	152
4-21	Modeled Fall Velocity: Case b4	152
4-22	Modeled Fall Velocity: Case b5	153
4-23	Modeled Fall Velocity: Case b6	153
4-24	Fall Velocity Variation Summary	154
4-25	Module Interaction	158
4-26	Model Convergence with Primary Particle Reference Concentration	164
4-27	Model Convergence with Distributed Reference Concentration	165
4-28	Profile - Distributed Reference Concentrations	166
4-29	Profile - Two Reference Concentrations	167

SYMBOLISM

α	stickiness coefficient	-
β	encounter coefficient	L^3/T
δ	constant	$1/T^2$
ε	turbulent energy dissipation	L^2/T^3
ζ	permeability parameter	-
η_{pl}	Bingham plastic viscosity	M/LT
κ	von Karmen's constant	-
λ	Kolmogorov scale	L
λ_τ	Taylor Microscale	L
μ	molecular viscosity	M/LT
ν	kinematic viscosity	L^2/T
ν_τ	eddy viscosity	L^2/T
ρ	density	M/L^3
ρ_b	bulk density	M/L^3
ρ_c	constituent density	M/L^3
ρ_e	effective density $\rho_b - \rho_f$	M/L^3
ρ_f	fluid density	M/L^3
σ	surface tension	F/L
σ_f	failure stress	F/L^2
τ	stress	F/L^2
τ_y	yield stress	F/L^2
a	radius constant	L
A	constant	-
A_a	area	L^2
B_a	stroke amplitude	L
b	production	L^3/T
B	breakup coefficient	$1/T$
c	collisions	-
C	concentration	L^3
C_D	drag coefficient	-
d	diameter	L
d_o	primary particle diameter	L
D	diffusivity	L^2/T
D_c	constant	-
d_f	fringe spacing	L
e	porosity	-
E	energy	FL
f	fractal dimension	-
F	force	ML/T^2
f_0	Doppler frequency	$1/T$

f_{ip}	permeability fall ratio	-
f_s	stroke frequency	1/T
g	gravitational constant	L/T ²
G	shear	1/T
H	water depth	L
k	permeability	L ²
k_b	Boltzman's constant	ML/Θ
K	breakup size scattering	-
K_c	constant	-
l	length	L
l_a	size a particle	L
l_b	size b particle	L
L	level	-
m	exponent	-
N	number of particles	1/L ³
p	ratio of particle sizes	-
P	pressure	M/LT ²
Q	formation	1/L ³ T
r	radius variable	L
s	stroke length	L
t	time	T
T_c	temperature	Θ
T_p	period	T
U	velocity	L/T
u_s	shear velocity	L/T
V	volume of solids	L ³
V_0	volume primary particle	L ³
W	fall velocity	L/T
W_c	Weber number	-
x	distance	L
y	vertical distance	L
z	distance	L

ABSTRACT

Particle aggregation plays an important role in many fields of study. In addition to marine science, these fields include water and wastewater treatment, process chemical engineering, and atmospheric science. Many investigators have modeled aggregation processes. However, they have assumed that the particles being modeled are all identical. To improve on existing aggregation models, a model which treats two different types of particles was constructed.

The two component model allows specification of primary particle size, density, and fractal dimension for each particle type. Three stickiness values are used, the stickiness of each particle type to itself and the stickiness between particle types. Aggregation mechanisms considered include differential settling and turbulent shear.

The model is used in three forms. In its simplest form, it operates on a closed system with aggregates breaking up when their size approaches the Kolmogorov scale. If the system begins with two types of primary particles, larger aggregates have uniform composition. A second version of the model includes removal of aggregates by settling. In this mode, the stickiness parameters dominate aggregate characteristics. Stickiness between similar particles controls the ratio of the particle type, whereas interparticle stickiness controls the particle removal rate. In the third form, three aggregation models are connected by a Rouse type suspended sediment model. This version models aggregate dynamics in the water column. Comparison of model results with total suspended sediment data and particulate organic carbon data from a site near the Poquoson River suggests that organic and inorganic constituents of suspended sediment do not stick together well.

The dissertation also describes a new type of aggregation device called the rotating oscillating grid turbulent aggregation chamber (ROGTAC). This device combines the advantages of two types of aggregation devices which are commonly used, the oscillating grid device and the rolling cylinder device. Oscillating grid turbulence generators are preferred for creating uniform isotropic turbulence. However, when particles more dense than the fluid are placed in them, the particles settle out. Rotating cylinder devices are effective at keeping particles in suspension. They do this by keeping the fluid in them in solid body rotation, but in this mode the fluid is not experiencing shear. ROGTAC places an oscillating grid in one end of a rotating cylinder. The hydrodynamic characteristics were investigated using laser Doppler velocimetry. Turbulent energy dissipation rates calculated from LDV data agreed well with energy input calculated by applying the quadratic drag law to the grid.

A TWO-COMPONENT AGGREGATION MODEL

INTRODUCTION

In the introduction to a special issue of Deep Sea Research devoted to aggregation, Alldredge and Jackson (1995) state “ The chemical and biological economies of the oceans revolve around particles and their physical and chemical properties. One major process that significantly alters the sizes, characteristics, and abundances of suspended particles is aggregation.” This quotation is based on observations made in oceanic environments by Trent, et al. (1978), Lampitt (1985), and Alldredge and Gotschalk (1990), to name a few. Furthermore, aggregation is important not only to the oceanic environment but also to estuarine, and lacustrine environments as notable papers by Eisma et al. (1980) and Weilenmann et al. (1989) have shown.

Particles and Aggregates

A discussion of aggregated particles begins with a discussion of the particles themselves. Particles are defined operationally. Water is filtered and whatever is large enough to be caught by the filter is considered to be particulate; everything which passes through the filter is considered to be dissolved, even though some of this “dissolved” material is really particles which were too small to be retained by the filter. Particles vary greatly in size. Figure 1-1 shows data on particle size spectra collected by Sheldon et al.

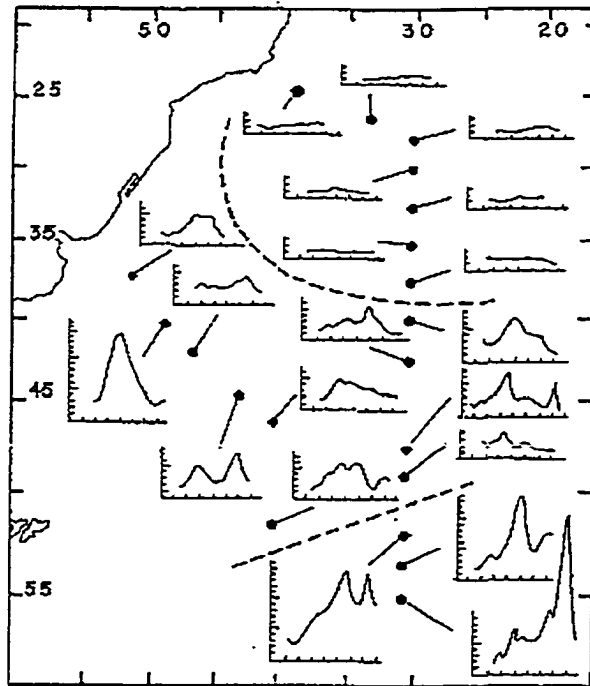


Figure 1-1 Particle Sizes

Distribution of particles in surface waters of the South Atlantic. Dots represent sampling locations and graphs connected to the dots represent particle distributions at the sampling locations. The broken line to the north represents the limit of the subtropical water. The broken line to the south represents the approximate position of the Antarctic Convergence. Particles from 0.63μ to 100μ are plotted. The abscissa are log of volume and the ordinate represents concentration in parts per million. From Sheldon et al. (1972).

(1972) in the South Atlantic. Similar data were collected in the North Atlantic and Pacific Oceans. Krank (1980) describes characteristic shapes of particle spectra. Notable humps in size spectra are normally caused by blooms of particular species of organisms. It should be kept in mind that some studies have used a Coulter Counter to measure particle sizes (e.g., Sheldon et al., 1972). This device breaks up aggregates (Gibbs 1982) so this data represents the particle sizes present, not their aggregated condition.

As already pointed out, particles are defined operationally, by filtering. Filters come in a wide variety of types suitable for various applications. Typical pore sizes are between 0.2 μm and 1 μm , although polycarbonate membrane filters are available with mesh sizes as small as 0.015 μm (Landing et al. 1991). Ultrafiltration, a more specialized technique which pressurizes the fluid, can remove particles as small as 1 nm (Landing et al. 1991). Smaller filter pore sizes result in slower filtering rates. It has been found that a filter with a 0.45 μm pore is a good compromise between filtering rate, cost, and performance and is frequently used.

Most data collected about particles tells us little about their in-situ aggregated condition. Aggregates are generally quite fragile (Aldredge et al. 1990). During sampling by pumps (Gibbs 1981) or bottles (Gibbs and Konwar 1983) aggregates generally are broken apart. It is therefore virtually impossible to determine which of the materials retained by a filter were originally aggregated and which were unaggregated. Furthermore, very small particles which were originally attached to an aggregate may be

stripped from it and not retained on the filter. Sampling aggregates requires specialized techniques. Acuna et al. (1994) developed a device to sample delicate zooplankton which might be useful for studies of aggregates. Trent et al. (1978) collected aggregates while SCUBA diving using small tubes. Sediment traps are particularly effective at capturing aggregates because aggregates comprise much of the settling material (Asper 1987). However, material may be degraded as it sits in a sediment trap (Ducklow et al. 1985).

Research indicates two important functions for aggregates. First, aggregation packages discrete particles into larger aggregates which allow them to settle more rapidly. Second, aggregation provide a mechanism for creating microenvironments.

Larger aggregates make a more significant contribution to the flux of material to the sea bed than do small unaggregated particles because they fall more rapidly through the water column. Almost all the material which reaches the bottom of the deep sea does so in aggregated form (Asper 1987, McCave and Gross 1991). Sedimentation to the deep sea is important for numerous reasons and has received considerable attention. Reasons include: 1) an absence of light precludes photosynthesis so that the energy needed to sustain life must come as materials fall from above; 2) sedimentation and subsequent accumulation forms the geologic record; and 3) the deposition of phytoplankton is the predominant source of most organic matter that ultimately forms petroleum. Creation of petroleum not only creates an important natural resource but also sequesters carbon from the atmosphere over geologic time scales.

Aggregation creates microenvironments because aggregation brings life forms and materials into close proximity. This leads to many interesting ecological effects including the following: First, dissolved oxygen may have difficulty reaching the center of an aggregate. If this causes reducing conditions, nutrients can be mineralized (Shanks and Reeder 1993, Alldredge and Cohen 1987). The mineralized nutrients are vital to organisms, particularly in the generally nutrient poor open ocean. Mineralization is usually fostered by microbial life. Second, several researchers have determined that bacteria residing in aggregates are more productive than free living bacteria (Karner and Herndl 1992, Crump et al. 1998, and Griffith et al. 1994). Third, Shanks and Edmondson (1990) and Bochandsky and Herndl (1992) found higher concentrations of plankton, including larval polychaetes, inside aggregates. Advantages to plankton inside aggregates may include: the aggregate gives the plankton security from predators, the concentration of bacteria provides a food source, and aggregates provide a means of conveyance. Fourth, although aggregates are considered to sink faster than individual particles, Riebesell (1992) found that aggregates can contain pockets of gas which increases their buoyancy. He proposes that the gas is oxygen produced by photosynthesis in phytoplankton. In short, the close proximity of numerous materials and life forms which aggregates provide gives the opportunity for beneficial interactions.

It has been proposed that aggregates are held together by transparent exopolymers (TEP) predominantly composed of mucopolysaccharides (Passow et al. 1994). There is considerable evidence that, at least in oceanic aggregates, TEP is the glue that holds

aggregates together (Alldredge et al. 1993, Decho 1990). The TEP is produced by bacteria and plankton (Biddanda 1985). The importance of TEP in estuaries is less firmly established. Although mucopolysaccharides are present in estuaries, their effect may be diminished by the larger amounts of suspended material to interact with and the relative importance of direct adhesion between clay particles by physicochemical forces.

Particles, both individually and in aggregated form, play important roles in estuarine as well as oceanic environments. However, there are important differences between the two environments. The most obvious difference between the particulate dynamics of oceans and estuaries is that in most estuaries the water is closely coupled with the seabed whereas in oceans most of the water has little contact with the bed. Bottom material in estuaries is frequently resuspended by waves and currents (Dyer 1986). This material has a short distance to settle and can thus be redeposited quickly. In estuaries, aggregates are generally smaller because the higher energy conditions found in estuaries tend to disrupt large aggregates (Eisma 1986). Estuaries are the meeting place between land and sea, and they therefore have not only the wide variety of organic matter found in the ocean but also terrestrial organic matter and large amounts of inorganic clay and silt. Humans who live on the land bordering estuaries cause anthropogenic effects such as pollution. Many pollutants are strongly hydrophobic, meaning they prefer to leave the water and sorb to the particles. Therefore, understanding the fate of the particulates is often the key to understanding the fate of the pollutants (Ongley et al. 1992, Milligan and Loring 1997). Clay is particularly good at sorption because of its very high surface areas

(Grim 1968). However, naturally occurring organic materials may have strong affinities for organic pollutants (Libes 1992). The relative magnitudes of these effects vary.

The Study of Aggregation

Although most of the study of aggregates in marine environments has occurred in the last twenty years, other fields have been studying aggregation processes for much longer. Much of our understanding of the physical process of aggregation dates from Smoluchowski (1917), who created a mathematical model of aggregation early in this century. Smoluchowski was a colloid chemist but many other fields have utilized his work. Water and wastewater branches of civil engineering build structures to facilitate aggregation (Lawler 1986). These structures help make clear, particle free, drinking water. In fact, aggregation processes in fresh water are similar to those in salt water and several studies of aggregation processes have been conducted in lakes (Grossart and Simon 1997). Atmospheric scientists concern themselves with formation of raindrops and aerosols, the tiny particles which are components of air pollution (Pruppacher and Klett 1980). Chemical engineers have addressed numerous processes, including paper making, which rely on particle aggregation. Finally, numerous theoretical researchers, who can be grouped into colloid chemists and hydrodynamicists, have made important contributions to aggregation science. A more in-depth review of this subject is offered in the next chapter.

Sediment Dynamics

Aggregation should be viewed in the context of fluid and sediment dynamics. This section provides a brief overview of sediment dynamics with emphasis on estuaries and the role of aggregation.

The dynamics of sediments in natural bodies of water are governed by the flow of the water, the interaction of the fluid with the sediment, and the interactions between sediment particles (Dyer 1986). The interaction of these mostly nonlinear processes results in an exceedingly complex system. Figure 1-2 is a simplified schematic of this system.

Fluid flow is governed by the equation of motion which is an application of Newton's law of motion to a fluid (Officer 1976). This law states that the acceleration of the fluid is driven by the forces on the fluid. As usually written, the left hand side of this equation describes the acceleration of the fluid and the right hand side describes the forces acting on the fluid. Often, motion caused by variation in the surface elevation of the water, commonly tide, is balanced by the drag force the bottom exerts on the fluid. However, the atmosphere can exert a relatively strong force on the water surface during high winds and in some cases variations in water salinity and temperature create density gradients which also exert a driving force on the fluid.

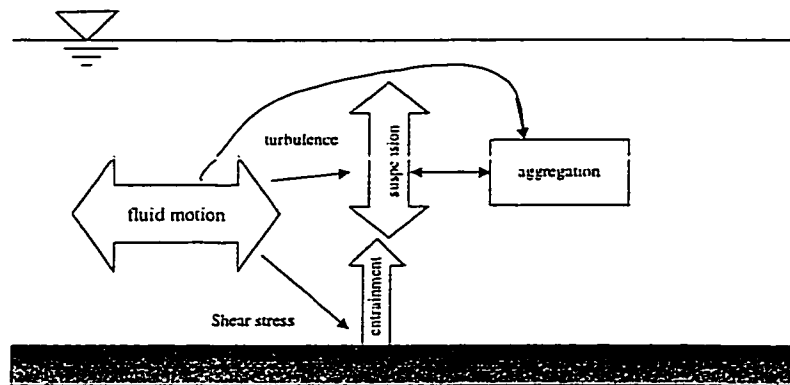


Figure 1-2 Sediment Dynamics

A depiction of the major physical processes controlling sediment dynamics in an estuary.

Because the bottom exerts a force on a moving fluid, the fluid must exert a force on the bottom. This effects sediment dynamics in two ways. The force moves sediment and also creates a turbulent boundary layer. Force is usually converted to the more useful force per unit area, or stress.

If the stress is less than a critical stress, sediment neither moves nor is suspended. The magnitude of the critical stress depends on the bottom type. For relatively coarse bottoms, such as sand, the critical shear stress depends upon the size and weight of individual grains (Buffington 1999). For fine bottoms, such as clay, the critical shear stress depends upon the strength of interparticle forces holding the clay together. Critical shear stresses for fine materials are more difficult to determine and their determination relies more heavily on experimentation (Lee 1995).

Turbulence is created at the boundary layer (Schlichting 1979) and is a function of the shear stress the bottom imposes on the fluid. This shear stress is a function of not only the grain size of the bottom material but also its form, which in turn is caused by the flow (Nielsen 1992). Waves are particularly influential in controlling bottom stresses because they create oscillating flow. Oscillatory flow creates thin boundary layer and relatively high shear stresses (Grant and Madsen 1986). Turbulence fosters mixing of the fluid, and mixing lifts sediment up into the water column. The quantity of suspended sediment is governed by a balance between turbulent mixing lifting the sediment upwards and gravitational settling bringing it back to the bed.

When sediment is suspended the particles bump into each other and stick together. This interaction is caused either by turbulence generated in the turbulent boundary layer or by the particles settling. The number of grains sticking together depends upon not only their stickiness but also how much suspended matter in the water column, which is a function of the turbulence. However, as particles stick together to form larger aggregates their fall velocity increases and effects their suspension dynamics (Eisma et al. 1980). It has been proposed that as aggregates fall into the higher shear region close to the bed they are broken up. These fragments are more easily kept in suspension which contributes to the formation of high concentrations of suspended matter close to the bed (Lick et al. 1992).

To model physical aspects of sediment dynamics in an estuary one must model the coupled processes of fluid flow, fluid-bed interaction, sediment suspension, and interparticle interactions. Even with today's advanced computers, this problem requires simplifications to make it tractable. Most research tackles one relatively small component of the problem. This dissertation will primarily deal with aggregation of particles and investigates the effect of the existence of two distinct types of particles.

Modeling estuarine sediment transport has received attention because of its application to practical problems including contaminant transport and estimating dredging requirements for harbor improvements. A first attempt at modeling estuarine sedimentation includes the familiar Rouse type suspended sediment model (Rouse 1938).

Next attention is paid to fluid flow culminating in a three dimensional numerical model such as the HEM-3D model developed at VIMS (Hamrick 1992). Including aggregation effects is usually a final enhancement of the modeling effort. To date, this has rarely been done even though aggregation can dramatically affect sediment properties (Lick et al. 1992).

Objectives

Most models of sediment dynamics in estuaries assume all the particles are the same. Observation has shown this is not the case (Zabawa 1978, Pierce and Nichols 1986). Fortunately, in estuarine waters the particles neatly break down into the convenient classes of organic particles and inorganic particles. The two types have widely differing densities, are hypothesized to stick together by different mechanisms, and have different affinities for pollutants. It is therefore worthwhile to attempt a modeling effort which investigates differences in behavior of organic and inorganic materials in the water from a particle aggregation standpoint. As part of this dissertation, a model which treats aggregation assuming that two types of particles, with specifiable properties, has been constructed. Because it is computationally much more expensive to run than a one-component model, its primary application will be in the prediction of variation in the behavior of the two components. A two-component model has not previously been written, it is hoped that this effort will represent a contribution to the science of aggregation in its own right and may be used by other fields which use aggregation science.

The primary application for a two-component model is probably in estuaries. The added expense of treating the second component makes it less suited in situations where choice of the two components is not readily apparent. In the open ocean, much of the material is organic and particle densities are less variable. Evidence suggests that ocean aggregates are held together by mucopolysaccharides which are approximately equally effective at binding most types of materials, so it is reasonable to assume there is not one "stickier" particle type. Additionally there have been several efforts at modeling aggregation of oceanic marine snow which have been relatively successful (Hill 1992, Jackson and Lochman 1992). This dissertation seeks to build on that body of work and develop a model more appropriate for use in estuarine environments.

LITERATURE REVIEW

Much effort has been expended studying aggregation and aggregates. This chapter will review previous research and provide a background for modeling and experimental efforts.

Aggregation Theory

Rectilinear Theory

Understanding aggregate properties requires understanding aggregate formation. Virtually all treatments of aggregate formation are built on a model developed by Smoluchowski in 1917. His model recognizes that aggregation is caused by collisions between particles. For the case of two sizes of particles colliding, the number of collisions per unit time equals the concentration of the first size of particle times the concentration of the second size of particle times the volume swept out by the faster particle moving relative to the slower particle. There are several mechanisms which cause variation in particle speed. Models of all aggregation mechanisms include the concentrations of the two size particles, N_i and N_j . The volume swept out per unit time, called the kernel or β , varies among aggregation mechanisms. A final parameter, called the stickiness value or α ,

is the fraction of collisions which result in adhesion. The number of collisions, C_{ij} between aggregates of size i and j which result in adhesion is:

$$c_{ij} = \alpha \beta N_i N_j \quad 2-1$$

It is noted that β can be theoretically derived whereas α is usually empirically derived. Therefore, in practice, α becomes the empirical constant containing not only the likelihood of adhesions after collision but also corrections for the errors in β . In Smoluchowski's simple model, the area swept out is a circle with a diameter equal to the sum of the diameters of the two particles. This area is multiplied by the relative velocities of the two particles. Smoluchowski considered three mechanisms for bringing particles together, differential settling, laminar shear, and Brownian motion.

Differential settling is the easiest to understand. In Figure 2-1, the larger aggregate d_1 settles faster than the smaller aggregate d_2 . The larger particle with diameter d_1 impacts all particles of size d_2 inside diameter d_1+d_2 . The velocity difference between the two particles is calculated by subtracting their Stokes Law (equation 2-2) settling velocities. Stokes Law, which is frequently used in aggregation and particle dynamics studies, is an analytical solution of the balance between buoyancy and drag. Stokes Law gives the fall velocity, W , for a solid impermeable sphere under laminar flow conditions with a kinematic molecular viscosity ν as

$$W = \frac{\left(\frac{\rho_b}{\rho_f} - 1\right)gd^2}{18\nu} \quad 2-2$$

The differential settling kernel, equation 2-4, uses the difference of the Stokes Law settling velocities, equation 2-3, for the two aggregates.

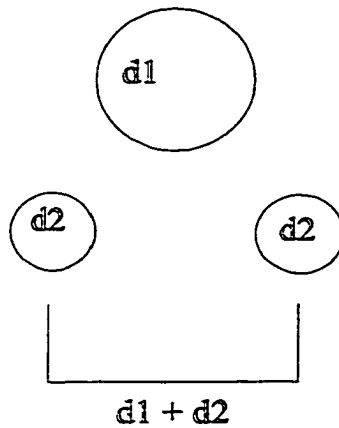


Figure 2 -1 Differential Settling Aggregation

When considering impacts between two aggregates with diameters d_1 and d_2 caused by differential settling, the aggregate with diameter d_1 is assumed to impact all aggregates which lie within the diameter $d_1 + d_2$.

$$\Delta W = \frac{\left(\frac{\rho_b}{\rho_f} - 1\right)g(d_1^2 - d_2^2)}{18\nu} \quad 2-3$$

$$\beta = \frac{\pi}{4}(d_1 + d_2)^2 \Delta W \quad 2-4$$

In equation 1-2, ρ is density with the subscripts b and f denoting the bulk density of the aggregate and the density of the fluid respectively. The d's are the diameters of the two aggregates which are interacting. The gravitational constant and the kinematic viscosity of the fluid are represented by g and ν respectively.

The mechanism of laminar shear is slightly more complicated to describe mathematically than differential settling but identical in principal. Because relative velocity between interacting particles depends on the relative positions of the particles, the area swept out multiplied by the relative velocity must be integrated (equation 2-5). In equation 2-5, G denotes laminar shear.

$$\beta = 4G \int_0^{\frac{d_1 + d_2}{2}} y \sqrt{\frac{(d_1 + d_2)^2}{4} - y^2} dy = \frac{(d_1 + d_2)^3 G}{6} \quad 2-5$$

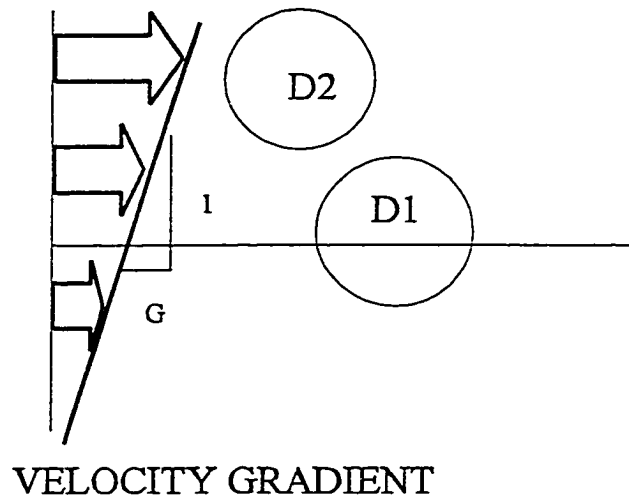


Figure 2-2. Shear Aggregation

In the case of shear flow there is a velocity gradient so the relative velocity between two particles depends upon their relative positions in the direction of the velocity gradient. However, as in the differential settling case, an aggregate with diameter d_1 may impact an aggregate with diameter d_2 within a circle with diameter $d_1 + d_2$.

The Brownian motion kernel considers a sphere around one of the two interacting particles whose diameter is the sum of the diameters of the two particles. The diffusion equation in spherical coordinates, equation 2-6, is solved to determine the likelihood of the second particles entering this sphere around the first particle. A boundary condition of zero particle concentration in the sphere facilitates the solution.

$$\frac{\partial C}{\partial t} = D \frac{1}{r^2} \frac{\partial}{\partial r} \left(r^2 \frac{\partial C}{\partial r} \right) \quad 2-6$$

The diffusion constant is given by the Einstein formula which is satisfactory for order of magnitude estimates (Levich 1962).

$$D = \frac{2k_b T_e}{3\mu\pi(d_1 + d_2)} \quad 2-7$$

In equation 2-7, k_b is the Boltzman constant, T_e is temperature. Brownian motion is only important for particles about 1 μ in diameter and smaller (McCave 1984) and often is not included in aggregation analyses. The models presented later in this dissertation do not include it, but the kernel (McCave 1984) is presented as equation 2-8 for completeness.

$$\beta = \frac{2k_b T_e (d_1 + d_2)^2}{3\mu d_1 d_2} \quad 2-8$$

One consoling aspect of Smoluchowski's formulation is that kernels for separate mechanisms may be added. All mechanisms are presumed to interact linearly, and nonlinear interactions between mechanisms are not considered. For a given size range, one mechanism usually dominates (Han and Lawler 1992).

One mode of aggregation not treated by Smoluchowski is turbulent shear. Camp and Stein (1943) related turbulent and laminar shear by equation 2-9. The turbulent energy dissipation is denoted by ϵ .

$$G = \sqrt{\frac{\epsilon}{\nu}} \quad 2-9$$

This expression can be inserted into Smoluchowski equation for laminar shear. Camp and Stein's relationship was derived from dimensional analysis, but others have used more rigorous methods to determine appropriate constants. Delichatsios and Probstein (1975) proposed two expressions for turbulent shear depending upon whether particles were larger or smaller than the Kolmogorov length scale. For aggregates smaller than the Kolmogorov scale they propose $G=0.26(\epsilon/\nu)^{1/2}$ and for larger $G=1.37(\epsilon d)^{1/3}$. Hill et al. (1992) experimentally explored the regions of applicability of the two equations and concluded that the expression for particles larger than the Kolmogorov scale holds in the region of the Kolmogorov scale. There is some debate about the value of the constant for the smaller than the Kolmogorov scale expression. Saffman and Turner (1956) completed a rigorous analysis and proposed that Camp and Stein's expression be multiplied by 0.1.

Smoluchowski's formulation works remarkably well because its two largest assumptions counteract each other. The kernels give values which are too large because they neglect the effect of large particles pushing small particles out of the way. This effect is sometimes called the "Queen Mary effect", which brings to mind the image of the bow

wake of a large vessel pushing a small buoy out of the way so the two do not hit.

Although when using this image one should remember the Reynolds number of these two situations are vastly different.

Smoluchowski's counteracts the "Queen Mary effect" by assuming that aggregates are nonporous. However, marine aggregates have considerable pore space, and porosity increases with aggregate size (e.g. Logan and Kilps 1995). Porosity is the fraction of the aggregate filled with fluid not particles. The result of Smolukowski not considering porosity is that his approach underestimates aggregate size. However, his assumption of no pore space in the aggregate is valid for coalescence of drops of fluid such as the formation of raindrops in the atmosphere. Despite this, atmospheric scientists have been at the forefront of improving aggregation kernels (Pruppacher and Klett 1980).

Curvilinear Theory

Although inaccurate kernels may be corrected with empirical α 's, the corrections are imperfect because kernel errors are functions of particle size and cannot be corrected with a constant α . The kernels must be improved. The first improvement to the geometrical approach is to include hydrodynamic interaction. This improvement is obtained by multiplying the geometrical kernel by a correction factor which accounts for the fraction of the flow in the geometrical collision area which comes within one small particle diameter's distance of the larger particle. Hill (1992) presented curvilinear

corrections for differential settling and turbulent shear. When $p=d_i/d_j$ and $d_i < d_j$, the differential settling correction is

$$\frac{p^2}{2(1+p)^2} \quad 2-10$$

taken from Pruppacher and Klett (1980) and

$$\frac{(1+p)^5 - (1+5p+5/2p^2)}{(1+p)^5} \quad 2-11$$

for turbulent shear and credited to Landau and Lifshitz (1959).

Further Improvements

Aggregation expressions discussed so far consider only hydrodynamic effects with chemical effects contained in an empirical α . Modeling of particle can be extended beyond hydrodynamic effects to include chemical attractions and repulsions. Calculations of particle motion including both hydrodynamics and chemical interactions are called trajectory analysis. Han and Lawler (1992) review approximately 20 efforts at trajectory analysis which incorporate various assumptions. Han and Lawler (1992) proceeded with their own attempt based on the work of Jeffrey and Onishi (1984). Trajectory analysis is generally too computationally intensive for practical aggregation modeling.

The high porosity of aggregates makes them permeable. This can affect floc behavior in several ways: 1) aggregates filter small particulates out of water flowing through them, 2) permeability reduces aggregate drag coefficients, and 3) permeable aggregates may more easily impact each other because fluid in the space between converging aggregates can leave this space by traveling into the porous aggregate. Porous aggregates are modeled using Brinkman's extension of Darcy's Law (Neale et al. 1973) Assuming the pressure gradient required to produce flow around the aggregate (equation 2-12)

$$\mu \nabla^2 U = \nabla P \quad 2-12$$

and through the aggregates (equation 2-13 which is called Darcy's law)

$$\frac{\mu}{k} U = \nabla P \quad 2-13$$

can be added allows derivation of Brinkman's extension of Darcy's Law.

$$-\frac{\mu}{k} U + \mu \nabla^2 U = \nabla P \quad 2-14$$

In the equations above, μ is molecular viscosity, K is permeability, P is pressure, and U is velocity. It is noted that Brinkman's extension of Darcy's law is an attempt to model flow both around and through an aggregate. Equation 2-13 primarily considers

flow through the aggregate while equation 2-12 pertains to flow around it. Darcy's law is empirical and equation 2-12 is a simplification of the equation of motion. Numerous investigators have considered porous aggregates using Brinkman's extension of Darcy's law. Sutherland and Tan (1970) concluded flow through a floc is unimportant. Neale et al. (1973) extended the work to a swarm of permeable spheres and found permeability is more important in this case. Masliyah et al. (1987) modeled the permeable floc as a solid core with a porous shell. In their experiments they used a hard sphere with threads attached. Veerapaneni and Weisner (1996) considered aggregates with radially varying permeability. They found that for porosities typical of estuarine aggregates the decrease in drag coefficient was less than 10%.

Stolzenbach (1993) considered that a large porous aggregate may act like a filter and remove smaller particles suspended in fluid which flows through the aggregate. If the aggregate is very large and porous and the fluid contains small primary particles this may be significant. However, this derivation has not been experimentally verified and it is uncertain if this effect is larger than uncertainties inherent in the aggregation kernel derivations.

Stolzenbach and Elimelech (1994) investigated a mathematical solution by Wacholder and Sather (1974) of the interaction of 2 solid spheres of varying diameter and density. They observed hollow plastic sphere and solid glass spheres falling in glycerin to verify that small relatively dense particles may be unable to impact large less dense

particles because closed particle paths form near the larger particle preventing particles from impacting the larger particle. Note that this analysis assumes the aggregate to be an impermeable sphere. These two effects considered by Stolzenbach counteract one another which makes it safer to neglect both effects as all applied aggregation models to date have done.

To summarize, calculation of encounter rate coefficients requires balancing the competing objectives of mathematical rigorousness and ease of computation. A good balance between these objectives is the Smoluchowski kernels with the curvilinear improvements (Han and Lawler 1992 Hill 1992).

Formation Rates

Formation times for aggregates in natural settings are not precisely known. Field measured changes in aggregate sizes leave doubt as to whether the changes came from aggregation/ disaggregation or from different size aggregates being advected into the measurement area. However, there is much evidence that aggregation occurs on time scales less than the tidal cycle, probably one to three hours. Wells and Shanks (1987) measured aggregate sizes and abundances in Cape Lookout Bight, N. C. at low, mid, and high tides. Abundances were 395, 291, and 489 per liter while sizes were 8, 71, and 26 μm respectively. These aggregates may not be typical of estuarine aggregates because Cape Lookout Bight is closely connected to the ocean and has little fresh water inflow. Eisma and Li (1993) measured aggregates optically in the Dollard Estuary in Holland.

They took measurements every ½ hour with a camera system at three stations in the estuary. Floc sizes varied noticeably over a tidal cycle. The station closest to the estuary mouth had the largest flocs at both high and low slack water. However, stations further landward in the estuary had larger flocs during ebb tide. Although their paper discusses variations, conclusions are somewhat speculative since each site was occupied on individual days and for only 13 hours.

Laboratory experiments show that aggregation usually occurs on time scales of a few minutes to an hour. The most extensive set of experiments are presented in Lick and Lick (1988). These experiments were done in a viscometer, an aggregation device composed of two concentric cylinders which shears the fluid between the cylinders when one of them moves. They allowed aggregates to form at various shear rates then changed the shear rates and allowed aggregates to reform. There appeared to be characteristic aggregate sizes for each shear rate and particle concentration. Steady state occurred in 30 to 60 minutes. They proposed formulae for time to steady state as $T_s = 12.2 (CG)^{-0.36}$ and $T_s = 4.95 (CG)^{-0.44}$ for freshwater and seawater, respectively. These dimensional equations require T_s , time, in minutes and CG , concentration and shear, in $g (s \text{ cm}^3)^{-1}$. These results were obtained for concentrations between 50 and 800 mg l^{-1} and shears between 100 and 400 sec^{-1} . Note that for the scaling relationships $\epsilon = u_*^3 / z$ and $G = (\epsilon / \nu)^{1/2}$ to give a shear of 100 sec^{-1} one meter above the bottom, they require a u_* shear velocity, of 21.5 cm sec^{-1} . This is unrealistically large for most estuarine situations; 2 cm sec^{-1} is a more realistic value. However, a concentration of 1 gm l^{-1} and shear of 10 sec^{-1}

gives a time to equilibrium of 38 minutes which appears reasonable. However, Lick et al. (1993) performed further experiments with a differential settling device and found that at concentrations of 50 mg l^{-1} , steady state is not achieved for 30 hours. Lower concentrations and less energetic environments form larger aggregates but take much longer to form them. Al Ani et al. (1991) reported that it takes about 30 minutes for aggregates to form in a cruciform vane type aggregation chamber using mud from the Tamer Estuary. For their concentrations between 0.1 and 1 g l^{-1} and shear values of 40 sec^{-1} , Lick's formula gives formation times between 20 and 56 minutes. Casson and Lawler (1990) reported that aggregation takes about 30 minutes to approach steady state in an oscillating grid aggregation chamber with neutrally buoyant particles. However, the particle spectrum continued to evolve for about 180 minutes. Hanson and Cleasby's (1990) performed experiments using 25 mg l^{-1} of kaolin particles and a stator and rotor mixing device, which generated 22 sec^{-1} shear, to find that the number and size of aggregates approached steady state in 30 minutes. However, Lick's formula for these conditions for saltwater predicts 156 minutes.

Shanks and Edmondson (1989) reported that aggregates formed in about 3.5 hours in their rolling cylinder tanks. Water for these experiments was collected from Cape Lookout Bight, N. C. From the variety of data available on formation rates, it is concluded that aggregation usually occurs on a time scale less than a tidal cycle, about 6 hours.

Composition

Aggregates can have diverse compositions. More effort has been expended toward examining marine snow than other types of aggregates. Alldredge and Silver (1988), in a review paper, group marine snow found on the California coast into four types: 1) phytoplankton 2) appendicularium (zooplankton) houses 3) miscellaneous debris, and 4) fecal pellets. This grouping is based on their observations and those of Trent et al. (1978) who reported observing diatoms, dinoflagellates, bacteria, crustacean nauplii, detritus, fecal pellets, copepod exoskeletons, and some unidentifiable objects in marine snow. Riebesell (1991) found aggregates occurring in the North Sea to be composed mostly of diatoms and detritus. His paper includes dramatic SEM pictures. Without discussing the many observations of oceanic marine snow it can be concluded that marine snow's composition is virtually all organic material.

There has been less study of aggregates formed in estuaries and close to shore than in the ocean. Shanks and Edmondson (1989) determined the composition of aggregates in Cape Lookout Bight, N. C. This area is partially separated from the ocean but has free water exchange with the Atlantic Ocean, so its aggregates are oceanic despite its location in what appears to be an estuary. Shanks and Edmondson (1990) examine concentrations of larvae on marine snow. They found large percentages of competent polychaete and nematode larvae but small percentages of noncompetent larvae and holoplankton attached to marine snow. Kiorboe et al. (1994) studied aggregates in the Isefjord estuary in Denmark. They centered their study on phytoplankton dynamics and gave cursory

treatment to detritus in aggregates. They identified phytoplankton by species and found *Skeletonema costatum* to be most abundant.

Two studies of aggregate composition using scanning electron microscopes have been conducted in Chesapeake Bay. Zabawa (1978) collected aggregates near Tolchester Beach and found them to contain mostly fecal pellets and mineral grains. Pierce and Nichols (1986) observed aggregates from the Rappahannock River and found some mineral grains to be clean while others were other coated. Aggregates contained feces, organic material, and fly ash.

Sizes

The first measurements one naturally considers when beginning to study aggregates are counting them and measuring their size. The most straightforward approach to size measurement is to photograph aggregates and analyze the images. Data on aggregate size is best presented as plots of mass or volume versus particle size.

Syvitski et al. (1995) photographed aggregates in Halifax inlet and found 500 μm aggregates most common but some as large as 2mm. Their system could resolve particles as small as 50 microns. Lick et al. (1993) investigated equilibrium aggregate diameters and found power law relations between aggregate diameter and particle concentration multiplied by shear. Their relations are $d=1.05 \times 10^{-3} (\text{CG})^{-0.4}$ for salt water and $d=9 \times 10^{-4} (\text{CG})^{-0.56}$ for fresh water. Note that these relations are dimensional and require d in cm

and CG in $g/(s\text{ cm}^3)$. More shear and higher particle concentrations cause a smaller equilibrium aggregate size to form more rapidly.

Fractal Nature of Aggregates

Most recent discussions of aggregate structure and properties use fractal geometry to describe aggregates. Fractals, as will be discussed in more depth in this section, relate aggregate size to porosity.

Density Size Relationship

It is well known from both visual observation and densities calculated from fall velocity measurements that aggregates have high porosities (Tambo and Watanabe 1979). Porosity increases with size in approximately a powerlaw relationship. The concept of fractals gives a physical explanation of why the power law relationship between aggregate size and porosity holds. Figure 2-3 and the equations that follow it demonstrates this. The use of fractals aids in understanding, but for most applications empirical power law relationships contains the same information. One could argue that introducing fractal terminology only serves to add unnecessary complexity to the discussion.

There are two ways in which aggregates might grow. First, primary particles could stick to the outside of the growing aggregate one at a time. In this case, the porosity of the aggregate would stay the same as it grew. Alternatively, in what is called the fractal view of aggregation, a few primary particles could stick together to form a

cluster. Clusters would stick together, then clusters of clusters would stick together. The clusters would have void space since primary particles do not fit together perfectly. The clusters of clusters would have the void space in the clusters plus the additional void space occurring because the clusters do not fit together perfectly, so porosity would increase as size increased. Table 2-3 presents a model of this phenomena. Note that the p used below equals $e/(1-e)$ where e is the porosity.

The conceptual model of aggregation presented in Table 2-1 will now be related to fractal dimension. Constants at level L are the number of primary particles per cluster and the packing factor of the primary particles. These should relate to the fractal dimension. Fractal dimension is defined by equation 2-15 (Lin et al. 1989). In this equation the exponent f is fractal dimension; V_0 and d_0 are the volume and diameter of primary particles; V is the volume of solids in the aggregate; and d is its diameter.

$$\left(\frac{V}{V_0}\right) = \left(\frac{d}{d_0}\right)^f \quad 2-15$$

The equation for the volume of solids in Table 2-1 can be substituted into the numerator of the left side of equation 2-15. If clusters have their size and volume related by $V=Ad^3$, we can convert the expression for volume of the aggregate in Table 2-1 into an expression for aggregate diameter and substitute it into the right side numerator of equation 2-15. Assuming clusters and primary particles are the same shape allows use of

Table 2-1 Fractal Dimension Development

clusters of primary particles	n V_0 nV_0 pnV_0 $nV_0 + pnV_0$ $(1+p)nV_0$	spheres per cluster volume per sphere solid volume per cluster pore space per cluster total volume per cluster
level 2 (clusters of clusters)	nnV_0 $n((1+p)nV_0)+pn((1+p)nV_0)$ $n(1+p)nV_0(1+p)$ $n^2(1+p)^2V_0$	volume of solids total volume
level 3	n^3V_0 $n[n^2(1+p)^2V_0] + pn[n^2(1+p)^2V_0]$ $n^3(1+p)^3V_0$	volume solids total volume
level L	$n^L V_0$ $n^L(1+p)^L V_0$	volume solids total volume

the $V=Ad^3$ to obtain a final substitution into the denominator of equation 2-15 to obtain equation 2-16.

$$\left(\frac{n^L V_0}{V_0}\right) = \frac{\left(\frac{n^L(1+p)^L V_0}{A}\right)^{f/3}}{\left(\frac{V_0}{A}\right)^{f/3}} \quad 2-16$$

Equation 2-16 simplifies to

$$n^L = (n^L(1+p)^L)^{f/3} \quad 2-17$$

then taking the logarithms and rearranging gives

$$f = \frac{3\ln(n)}{\ln(n(1+p))} \quad 2-18$$

Because this derivation does not give fractal dimension as a function of L, aggregates which grow in the manner described in Table 2-1 can be described by fractal dimensions. In other words, the fractal dimension describes the change in porosity of an aggregate with size if the aggregate grows as described in Table 2-1.

It is useful to relate fall velocity to fractal dimension. With a few assumptions this is easily done. Recasting the fractal equation, equation 2-15, assuming spherical aggregates and considering the definition of V ,

$$V = \frac{\pi}{6}(1 - e)d^3 \quad 2-19$$

one obtains

$$1 - e = \left(\frac{d}{d_0}\right)^{f-3} \quad 2-20$$

Substituting

$$\rho_b = \rho_c(1 - e) + \rho_f e \quad 2-21$$

into Stokes Law, equation 2-2, gives

$$W = \frac{\left(\frac{\rho_c}{\rho_f} - 1\right)(1 - e)gd^2}{18\nu} \quad 2-22$$

Combining equations 2-20 and 2-22 gives

$$W = \frac{\left(\frac{\rho_c}{\rho_f} - 1\right)gd^{f-1}}{18\nu d_0^{f-3}} \quad 2-23$$

If a power law such as $W=Ad^m$ is fit to fall velocity values it is apparent that $m=f-1$ and

$$A = \frac{\left(\frac{\rho_c}{\rho_f} - 1\right)g}{18\nu d_0^{f-3}} \quad 2-24$$

A is thus a function of the density of the solids in an aggregate and the size of the primary particles.

Density Relations

Table 2-2 shows relationships between fall velocity, W , excess density, ρ_c , porosity, e , and fractal dimension, f . Porosity determination requires knowledge of the density of the constituent particles of a floc. Fractal dimension expressions include primary particle diameter. However, if fall velocity is determined as a power law, fractal dimension can be determined by equating exponents of aggregate diameter. Using relationships, one is able to solve for particle size. These equations assume aggregates and primary particles are spheres and that Stokes Law, which assumes impermeable spheres with Reynolds numbers less than 1, holds.

-

Table 2-2 Density - Porosity Relations

W_f	ρ_c	e	f
	$W_f = \frac{\rho_c g d^2}{\rho_f 18 \nu}$	$W_f = \frac{(1-e)(\rho_c - \rho_f) g d^2}{\rho_f 18 \nu}$	$W_f = (\frac{\rho_c}{\rho_f} - 1) \frac{g d_0^{3-f} d^{f-1}}{18 \nu}$
$\rho_c = \frac{W_f \rho_f 18 \nu}{g d^2}$		$\rho_c = (\rho_c - \rho_f)(1-e)$	$\rho_c = (\rho_c - \rho_f) d_0^{3-f} d^{f-3}$
$e = \frac{-W_f \rho_f 18 \nu}{g d^2 (\rho_c - \rho_f)} + 1$	$e = 1 - \frac{\rho_c}{\rho_c - \rho_f}$		$e = 1 - d_0^{3-f} d^{f-3}$
$f = \frac{\ln[\frac{d W_f \rho_f 18 \nu}{g d_0^3 (\rho_c - \rho_f)}]}{\ln[\frac{d}{d_0}]}$	$f = \frac{\ln[\frac{d^3 \rho_c}{d_0^3 (\rho_c - \rho_f)}]}{\ln[\frac{d}{d_0}]}$	$f = \frac{\ln[\frac{d^3 (1-e)}{d_0^3}]}{\ln[\frac{d}{d_0}]}$	

Fall Velocity

Aggregates in most cases leave the water column by settling. How fast they settle, their fall velocity, is therefore very important in determining their fate. It also governs the magnitude of the differential settling kernel.

Theory

A discussion of fall velocity begins with Stoke's Law, equation 2-2. Stoke's Law is derived by equating the buoyant force of the particle to the drag force the surrounding fluid exerts on the falling particle. Drag force is calculated by an analytic solution of flow around a hard impermeable object with the Reynolds number less than one.

For higher Reynolds numbers, empirical results are used. One for sand is presented by Wright (1995) and credited to Gibbs et al. (1971). The constants are based on cgs units.

$$W = \frac{-3v + [9v^2 + d^2(\frac{\rho_b}{\rho_f} - 1)(0.003869 + 0.02480d)]^{\frac{1}{2}}}{0.011607 + 0.07440d} \quad 2-25$$

Two factors which can affect fall velocity but are usually not considered by models include aggregate shape and permeability. Most of our knowledge of these effects comes from studies in fields other than marine science.

Matsumoto and Saganuma (1977) experimentally investigated the permeability and fall velocities of balls of steel wool. They compared their experimental results with analytical results in the literature, notably Neale et al. (1973). They give the analytical solution for the ratio of the fall velocities of permeable to impermeable objects, f_{ip} , as

$$f_{ip} = \frac{\zeta}{\zeta \tanh \zeta} + \frac{3}{2\zeta^2} \quad 2-26$$

The nondimensional ζ is the aggregate radius, r , divided by the square root of the permeability, k . The challenge now is to determine a permeability. Matsumoto and Saganuma (1977) presented an equation relating porosity, e , of a ball of steel wool to its permeability, k in the form,

$$k = 1.42 \times 10^7 (1 - e)^{-1.575} \quad 2-27$$

Fennessy et al. (1994) use field data collected in the Tamar Estuary to estimate that a 100 micron aggregate has a porosity of 0.97. This results in an f_{ip} value of 7.5. In other words, porosity may rapidly increase fall velocity. Gmachowski (1996) related permeability to fractal dimension. Using our fractal dimension of 1.8 gives a permeability of $4.8 \times 10^{-6} \text{ cm}^2$ and thus an f value of 2. Stolzenbach (1993) used a permeability equation originally attributed to Davies (1952) which is more widely used in the marine aggregate literature

$$k = \frac{d_0}{[16(1-e)^{1.5}(1+56(1-e)^3)]} \quad 2-28$$

In this equation, d_0 is the primary particle size. If the primary particle size is 5 micron for our 100 micron aggregate and $p=0.97$, f_p equals 1.25. If this last, most widely used, formulation is correct, the effect of permeability on aggregate fall velocity may be safely ignored.

Swamee and Ojha (1991) processed data from Schulz et al. (1954) on the effect of nonspherical shape on particle fall velocities. They use equation 2-23 to relate drag coefficient to fall velocity.

$$W = \sqrt{\frac{4(\rho_e / \rho_f)gd}{3C_D}} \quad 2-29$$

For a Reynolds number of one, the drag coefficient varies from 25 to 34 for various shapes tested. The fall velocity resulting from the lower drag coefficient is 1.14 times faster than that from the higher drag coefficient. This indicates that the effects of aggregate shape on fall velocity can be safely ignored.

Allredge and Gotschalk (1988) photographed, measured the fall velocities of, then collected oceanic aggregates off the southern California coast. Upon returning to the

lab with these samples, they dried and weighted them. Using this data, including measurements of the shape of the aggregates obtained from the photographs, they determined that shape made essentially no effect on aggregate fall velocity.

Measurements

Because aggregates are delicate, numerous investigators have tried to measure fall velocity without transporting particles to the lab. Either bulk fall velocity (i.e., the total concentration of material with a given fall velocity) or fall velocities of individual particles are measured. The classic bulk fall velocity measurement device is the Owen tube (Burt 1984). The Owen tube operates by capturing a tube of water at depth then bringing it on board a research vessel in the horizontal position. On board it is rotated to the vertical position. Water samples are removed from the tube at specified elevations and times. Sediment concentration in these samples is determined and concentration as a function of fall velocity is easily calculated.

If the fall velocity and size of individual flocs is required, the individual aggregates must be observed. They must be isolated from ambient turbulence in a stilling tube. Any camera system equipped with a stilling tube which can take pictures separated by known small time intervals is capable of collecting data for determining fall velocity.

Photographic fall velocity data which will be discussed in this section have been obtained by Syvitski et al. (1995) and ten Brinke (1994). Syvitski's camera, described in Heffler et al. (1991), is an Olympus OM2 controlled by Tattletale controllers. Three cameras

provided a redundant stereo view of a 17 x 26 x 3 cm volume so particle positions can be determined in three dimensional space. They claimed accuracies of $\pm 20\mu\text{m}$ in size and $\pm 2\text{ m}/24\text{ hours}$ in fall velocity. Ten Brinke (1994) used a video camera directed at a stilling well as described by van Leussen and Cornelisse (1993). The camera had a 25 mm lens with a 15 mm extension tube so that each of the 288 x 604 pixels had dimensions of 10 x 15 μm .

Virtually all investigators agree that there is a power law relationship between fall velocity and aggregate diameter (Syvitski et al. 1995). However, power law relationships are dimensional and many units have been used. Results presented herein have been converted so fall velocity is given in cm sec^{-1} and aggregate diameter is given in cm. Fall velocity relates to other aggregate properties which may be of interest. Some investigators report their fall velocity measurements as excess densities, ρ_e . These values readily convert to fall velocity by assuming Stokes Law is valid.

Syvitski et al. (1995) measured fall velocities in situ in the Bedford Estuary in Canada for several successive days, which are plotted in Figure 2-3. Their results showed considerable day to day variation in floc fall velocity, although they did not present data on environmental conditions or floc composition with which to explain the variation. Ten Brinke (1994) made measurements in the Oosterschelde Estuary in situ in November and September. He states "The density of the aggregates in September was higher at high water slack (HWS), $W=5.59d^{0.84}$, than at low water slack $W=16.2d^{1.29}$." Aggregate

density at HWS in September was higher than that at flood and HWS in November, $W=0.683d^{0.48}$, especially for large aggregates."

Other investigators have made laboratory measurements of fall velocities and sizes of aggregates formed in the field. Gibbs (1985) collected aggregates from the water column in Chesapeake Bay and obtained $W=0.222d^{0.777}$. Kawana and Tanimoto (1984) collected aggregates from near the bottom of Osaka Bay on three different days. Their collection methods may have disturbed the sample but the present fall velocities of $W=10.63d^{1.2}$, $W=14.17d^{1.24}$, and $W=8.66d^{1.17}$. Note that values for marine snow are not directly comparable to relationships developed using clay aggregates because of density differences. Shear intensities and detailed information on aggregate composition are not available from the above sources.

Other investigators have measured fall velocities of aggregates created in the laboratory. Burban et al.(1990) presented results obtained using 6 micron clay collected from Lake Erie which was aggregated in a viscometer. Their results are summarized in Table 2-2. They fit fall velocity data to a power law, $W=Ad^m$. Although the concentrations they used are realistic, the shears are quite high as discussed earlier in this chapter. Higher shears and concentrations give faster settling velocities for a given aggregate size. Lick et al.(1993) performed tests in a differential settling aggregation chamber and obtained results much different than those obtained in the viscometer device. In these tests, $W=46.6d^{1.5}$ in freshwater, and $W=30d^{1.58}$ in salt water.

Table 2-3 Fall Velocity Measurements Burban et al. (1990)

conc.	shear	fresh	fresh	salt	salt
mg l ⁻¹	l sec ⁻¹	a cm sec ⁻¹	m	a cm sec ⁻¹	m
10	100	32.7	2.1	0.095	0.7
	200	7.79	1.6	0.039	0.37
	400	0.275	0.79	0.127	0.54
100	100	0.251	0.85	0.513	0.87
	200	0.24	0.7	0.511	0.74
	400	0.22	0.59	0.12	0.5
400	100	0.305	0.69	0.074	0.47
	200	0.779	0.85	0.238	0.55
	400	0.045	0.26	0.091	0.29

Constants for power law fits to the fall velocity data collected by Lick et al. (1993). The constant is a and m is the exponent. Fresh and salt denote the salinity of the water.

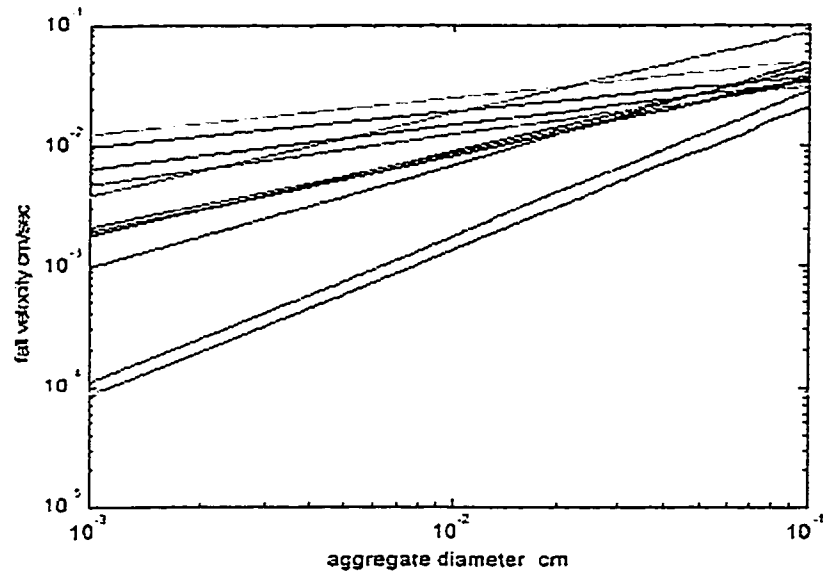


Figure 2-3 Syvitski's Fall Velocity Measurements
Power law curves fitted to fall velocity data collected by Syvitski et al. in the Bedford Estuary on 11 days in May of 1991. Note the large scatter in measurements.

Considering that it is advantageous to minimize handling of aggregates, the in-situ measurements can be considered more representative of aggregates created in estuaries. These fall velocity measurements were converted to fractal dimensions. Average fractal dimensions are 1.67 for Syvitski's data and 1.87 for ten Brinke's data. It is thus likely typical fractal dimensions for estuarine aggregates are slightly less than 2, possibly 1.8.

Stickiness

Theory

Aggregation models usually break the adhesion process into 2 steps, encounter and sticking. This neatly divides the problem between the fields of fluid mechanics and chemistry. Unfortunately, close examination shows that the division is not so neat. The "chemical processes" exert forces on particles that influence the likelihood that they will encounter one another. Before using the typical description of the problem with aggregation described by the ubiquitous α and β , it is worth discussing what is known about the mechanics of adhesion processes.

The classical description of adhesion is presented by DLVO theory, named after Derjaguin and Landau of Russia and Verwey and Overbeek of the Netherlands who independently developed the theory in the 1940's. Descriptions of DLVO theory are commonly available in the literature, e.g. Levich (1962). DLVO theory describes adhesion as a linear superposition of attraction due to van der Waals forces and repulsion due to

the electrical double layers. Particles are negatively charged and surrounded by positively charged ions. These positive ions repel neighboring particles which are also surrounded by positive ions. As the ionic content of the water increases, more positive ions are available and they pack more densely around the particles causing the electrical double layers to become thinner. Eventually the layer becomes thin enough that neighboring flocs can come close enough, about 1 nm, that the short range van der Waals forces dominate and the particles adhere. This mechanism explains the enhanced aggregation that occurs when fresh water enters an estuary and starts to become saline. In this case the suspended material carried by a river aggregates when the river water mixes with the estuarine water and become slightly, a few parts per thousand, saline.

In a review paper, Isrealachivili and McGuiggan (1988) described four forces between surfaces in liquids. The two DLVO forces assume the fluid is a continuum. When two surfaces are close together, less than ten water molecule diameters or 2.5 nm, the fluid can no longer be considered a continuum. Solvation forces become important. Water molecules are squeezed out of the gap between the surfaces one at a time. This results in a repulsion force which builds until a water molecule is ejected. The two surfaces are then drawn together to fill the gap caused by the departing water molecule. As surfaces are brought these solvation forces oscillate as each water molecule is ejected.

Additionally, surfaces that are hydrophilic experience a monotonic repulsion force since the water is more difficult to remove from the gap between surfaces. In the case of

hydrophobic surfaces an adhesive force results. This force has a range similar to or slightly longer than the DLVO forces. Flexible surfaces such as organic coatings can move as affected by the solvation forces. This affects the magnitude of the interparticle forces. However, much of the phenomena remains to be explained.

Alpha Values

Numerous investigators have experimentally considered adhesion coefficients. Alldredge and McGillivray (1991) used the direct approach and observed interparticle collisions. One advantage of this method is that it does not rely on an aggregation model to calculate α . They found an average α value of 0.77 but it varied with the type of aggregate. Diatom flocs were the stickiest with α of 0.88 while amorphous aggregates had a value of 0.6. This seems reasonable since it is generally assumed that more refractory material is less sticky (Alldredge and McGillivray 1991).

Stickiness of phytoplankton was investigated by Kiorboe et al. (1990) who found alpha values varying from 0.06 to 0.15. These values were obtained by counting numbers of particles after mixing water in a viscometer. Also investigating the stickiness of phytoplankton, the Sigma tank experiment grew a mesocosm of phytoplankton and many investigators studied it. These included Dam and Drapeau (1995) who used methods similar to Kiorboe's and found alpha to vary from 0.03 to 0.8. They found larger alpha values early in the experiment when plankton growth rates were higher.

Gibbs (1983a) determined alpha values for a variety of mostly clay sediments over a range of salinities. He removed organic coatings from particles and thus determined their effects on alpha. In most cases alpha was higher if the organic coatings were removed. At higher salinities the presence of organic coatings had less effect. Delaware Bay sediments at 17 ppt salinity had alpha values of 0.207 and 0.177 with and without organic coatings, respectively.

There is much variation in reported alpha values. However, 0.2 appears to be a reasonable value.

Breakup

If a system is mixed well enough to keep aggregates in suspension, the aggregate size distribution for that system results from a balance between aggregation and disaggregation. Therefore, the attention paid to disaggregation should be comparable to that devoted to aggregation. Unfortunately, aggregation theory is much further advanced than disaggregation theory.

One disaggregation problem that has been given consideration is breakup of drops of immiscible fluids. Hunt (1984) discussed this analysis drawing from Taylor (1932). The criteria for breakup is given by the Weber number. The Weber number is the nondimensional ratio of the drag force, which tends to tear an aggregate apart, and surface tension, which tries to hold the aggregate together.

$$We = \frac{\rho \langle U^2(d) \rangle d}{\sigma} \quad 2-30$$

In equation 2-30, $\langle U^2(d) \rangle$ is the mean square of the relative velocity fluctuations across a droplet of diameter d , and σ is the surface tension. The value of $\langle U^2(d) \rangle$ depends upon whether a particle is larger or smaller than the Kolmogorov scale. If it is larger

$$\langle U^2(d) \rangle \propto (\varepsilon d)^{2/3} \quad 2-31$$

and if it is smaller then

$$\langle U^2(d) \rangle = \frac{\varepsilon d^2}{\nu} \quad 2-32$$

Substitution, followed by some algebra, shows that for aggregates bigger than the Kolmogorov scale the maximum droplet diameter is proportional to $(\sigma^3/\rho^3\varepsilon^2)^{1/5}$ whereas for droplets smaller than the Kolmogorov scale the maximum droplet diameter is proportional to $(\nu\sigma/\varepsilon\rho)^{1/3}$. Note that these relationships require constants to give useful predictions.

This analysis does not translate directly to aggregates because the structure of the aggregate, not surface tension, holds aggregates together. This greatly complicates matters because strengths of similar sized aggregates can vary greatly. Also, when aggregates break apart, they break at weak points in the aggregate. The smaller

aggregates resulting when one aggregate breaks up can be of similar or very different sizes. This is one of the larger debates in the aggregation literature with Thomas (1964) proposing that flocs essentially split in half, whereas Argaman and Kaufman (1970) propose that primary particles are individually eroded off large aggregates. Both these researchers base their interest in aggregation on wastewater applications.

Thomas (1964) adapted the Weber number analysis to flocs. He estimated the yield stress, τ_y of a floc as

$$\tau_y \propto \frac{(1-e)^3}{d_0^2} \quad 2-33$$

Equation 2-33 is not dimensionally consistent. Stress is a force divided by a length squared and, although there is a length squared term in the denominator, the numerator is dimensionless. The yield stress can now be related to a pseudo surface-tension, σ , by

$$\sigma \propto \frac{\tau_y}{d} \quad 2-34$$

which is dimensionally consistent. Substituting equation 2-33 into 2-34 and combining the result with equations 2-31 and 2-30 gives an expression for maximum aggregate size.

$$d < \frac{1}{\varepsilon^{1/4}} \left[\frac{(1-e)^3}{\rho d_0^2} \right]^{3/8} \quad 2-35$$

Repeating this process but using equation 2-32 gives

$$d < \left[\frac{\nu(1-e)^3}{\rho \epsilon d_0^2} \right]^{1/4} \quad 2-36$$

Both equations 2-35 and 2-36 need to be multiplied by dimensional empirical constants to be useful. However, in both cases d is a function of $\epsilon^{-1/4}$ which agrees with the frequently used estimation that aggregates are limited by the Kolmagorov length scale. It is unknown if equations 2-33 and 2-34 were chosen to attain this result.

Thomas (1964) presented his analysis prior to adoption of the fractal view of aggregates. It is interesting to recast equations 2-35 and 2-36 using the fractal view of aggregates. Assuming a fractal dimension of 2, equation 2-35 becomes

$$d < \left[\frac{1}{\epsilon^{2/3} \rho d_0^{3f-7}} \right]^{\frac{35-9f}{3}} \quad 2-37$$

and equation 2-36 becomes

$$d < \left[\frac{\nu}{\rho \epsilon d_0^{3f-7}} \right]^{\frac{1}{13-3f}} \quad 2-38$$

When f , the fractal dimension, equals three, which represents the case of no porosity, equations 2-37 and 2-38 reduce to equations 2-35 and 2-36. When f equals two, typical for estuarine aggregates, they do not.

Parker et al. (1972) considered aggregation in the context of water treatment. They found there were two floc erosion modes. Flocs held together by filaments broke apart much as Thomas (1964) predicted while flocs held together by particle attraction broke up by erosion of surface particles. Surface erosion was treated by considering the equation of fluid motion near the aggregate. Parker et al. (1972) suggest that the maximum floc is the size at which erosion begins. This occurs when

$$d = \frac{1}{G} \left[\frac{1.5\tau_y}{(\rho_b - \rho_p)\delta} \right]^{1/2} \quad 2-39$$

In this equation G is the shear rate in the fluid and δ is a constant. Erosion and rupture are difficult to separate and this study concluded by stating that the Kolmogorov scale is roughly the upper size limit on flocs. Other marine science studies have supported this conclusion including Alldredge et al. (1990) and Eisma (1986).

LABORATORY STUDIES

Uses of Laboratory Aggregation Devices

This section describes applications of laboratory aggregation devices. Laboratory aggregation devices can be useful for investigating aggregation processes and also for obtaining fundamental relationships and constants required by modeling efforts. They are also useful for investigating biological and chemical processes including many not related to aggregation.

As the previous chapter demonstrates, aggregation is a complex process. Aggregation research becomes a challenge of determining which of the many independent variables cause an observed phenomena. Although field investigations are useful for aggregation studies, the only way an investigator can control aggregate forming conditions in the field is by appropriate choice of sampling time and location. For example, if one wants to study the effect of higher freshwater inflows in the field, he has to wait for a period of heavy rains. It is also often hard to separate out conditions in the field. For example, the high freshwater inflow may usually occur in the spring when biological activity is increasing. Which of these phenomena caused an observation? Another problem with field observations is that an aggregate may travel considerable distances

through a variety of conditions while forming. A comparison between aggregate characteristics and those of the location where it is observed may have little meaning. For example, an aggregate may mostly form in fresher, clearer, surface water then fall into the bottom water. Its characteristics would not be totally determined by the bottom water environment. A laboratory aggregation device enables the investigator to limit conditions and better identify causal factors.

Information needs in any modeling effort may be grouped into two general types: fundamental relationships and constants. Initially, research attempts to determine fundamental relationships that describe a process. For example, in a more energetic environment, aggregates form more rapidly but they can not grow as large as they can in quiescent conditions. Later, as needs arise for specific predictions for specific locations, constants for a model or relationship are required. An advanced model will have many free parameters so calibrating and verifying it requires many and varied data. Laboratory experiments can make this process easier because they allow closer control of conditions thereby limiting free parameters.

To date, much of the experimental efforts regarding aggregation have focused on determining fundamental relationships, although in determining these relationships constants for specific circumstances are obtained. Laboratory experiments using aggregation devices have looked for what controls aggregate porosity and what controls aggregation rates.

Klimpel and Hogg (1986) investigated what controls aggregate porosity by varying agitation intensity, polymer coagulant concentration, mixing time, solids concentration, and primary particle size. Being mineral processing engineers they did all experiments with quartz crystals. Tambo and Watanabe (1979), being wastewater engineers, did similar experiments using clay. Lick et al. (1993) used riverine sediments for similar experiments.

Aggregation rates, which are controlled by particle stickiness, were addressed early by wastewater engineers (Argaman and Kaufman 1970 and Hunt 1982). However, aggregating wastewater has less variability than estuarine water and determination of stickiness is an area in need of research in marine science. Evidence suggests that for aggregating plankton, stickiness varies species to species and varies with the nutrient levels in the water (Kiorboe and Hansen 1993 and Passow and Wassmann 1994). It is also an area well suited to the laboratory approach because a laboratory settling allows use of pure cultures of phytoplankton species in controlled nutrient environments. Considering the numerous nutrients and wide variety of microorganisms present in water, this avenue of research offers many research opportunities. The laboratory settling also allows investigation of other interesting questions such as the effect of temperature on aggregation. Hanson and Cleasby (1990) looked at this in the context of wastewater engineering. Another application for aggregation devices is determining aggregation constants for specific areas and materials such as Milligan and Hill (1998) did for drilling muds.

Devices suitable for aggregation studies may also be applied to other studies such as Shimeta et al. (1995) who studied feeding rates of ciliates and flagellates in a viscometer types device. They found more energetic flow increases feeding rates. These experiments were conducted in a viscometer type device but a grid turbulence device would add more realistic conditions.

The author originally built ROGTAC, the new aggregation device described in this chapter, and also a conventional viscometer type device to compare aggregation rates in the two devices and thereby investigate the equivalence of turbulent and laminar shear with respect to aggregation. Upon investigation of the devices, it was determined that the two devices could be compared over a limited range of shear conditions. Also, equipment available to observe and measure aggregates produced in the devices had severe limitations. The research focus of the author was therefore redirected to what appeared to be a more promising project, the two component computer model. However, upon consideration of the many potential uses of laboratory aggregation devices, which are described in this section, it was felt that a documentation of what was learned about the ROGTAC would be beneficial to the dissertation. Therefore, this chapter will describe the design of ROGTAC and an investigation of its hydrodynamic characteristics. Final sections will discuss how future investigators might collect data from it and finally how it might be used in the calibration and verification of the two-component model.

Device Types

Many investigators have created aggregates in the lab using a variety of devices. This section will describe many of the more important ones.

Batch Reactors

Much early work was done using batch reactors, and they are still commonly used in the water and wastewater industries. These are tanks or buckets of water outfitted with mixing devices such as paddles. Although batch reactors are effective at producing aggregates, the turbulent fields they produce vary spatially with much high shears at blade tips than elsewhere in the reactor (Stanley and Smith 1995). Batch reactors, although used in waste water treatment studies, have been rarely used in marine science research. They will not be discussed extensively herein. Researchers who have used batch reactors include: Hanson and Cleasby (1990), Al Ani et al. (1991), Weilenman et al.(1989), and Tambo and Watanabe (1979).

Grid Turbulence Generators

Studies which require homogeneous isotropic turbulence usually use grid turbulence generators (Figure 3-1). Many investigators have used such devices to create aggregates in the lab. Thompson and Turner (1975) determined basic information on such devices including the fact that turbulence decays linearly away from the grid. Although tank size, grid bar and grid spacing vary, the designs are essentially the same. Table 3-1 shows tank geometries for several grid turbulence generators.

Viscometers

Laminar shear conditions are more regular than turbulent flow and are often used. Laminar flow is typically created in a viscometer type device. These devices consist of two concentric cylinders with fluid in the gap between the cylinders. The outer cylinder turns and the inner cylinder is held fixed. Many such devices have been built with varying geometries. If the viscometer is operated at a fast enough speed the Reynolds number increases to where flow become turbulent. In most studies of aggregate formation viscometers have been set to avoid turbulent conditions.

Rolling Cylinder

Even simpler than a viscometer is the rolling cylinder device. It consists of a cylinder or even a bottle which is rolled by a roller table. The cylinder rotates about its cylindrical axis. Shanks and Edmondson (1989) first used this device. Aggregates that fall to the bottom of the cylinder are lifted as it rotates.

Rotating Oscillating Grid Turbulence Aggregation Chamber (ROGTAC): A New Device

Most experiments which require uniform turbulence create the turbulence by passing the fluid through a grid. Such setups have been used successfully in aggregation experiments with neutrally buoyant particles where particles did not settle (Hill et al. 1992). Alldredge et al (1990) used such a tank for aggregate breakup experiments where aggregates broke up as they fell through the grid. Van Leussen (1994) described a four meter high tube used in an attempt to model aggregation processes in a natural water body

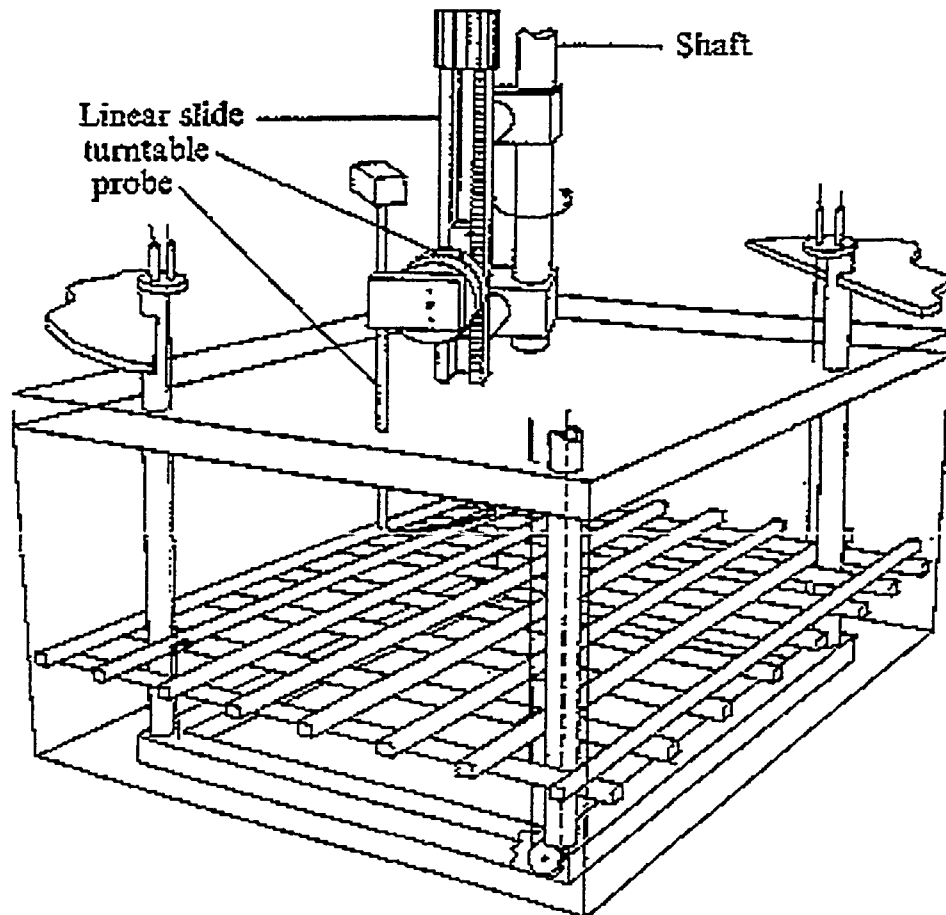


Figure 3-1 Oscillating Grid Turbulence Generator

A typical oscillating grid turbulence generator, Brumley and Jirka (1987). The grid at the bottom of the tank oscillates up and down to create turbulence.

Table 3-1. A Summary of Characteristics of Oscillating Grid Turbulence Devices

Authors	tank size (cm)	grid geometry (cm)	stroke freq and amplitude	use
Thompson and Turner 1975	25.4x25.4x4 6	5 space 1 sq bar	2 - 5 Hz 1 cm	mixing
Brumley and Jirka 1987	50 x 50 x40	6.35 ctc space 1.3 sq bar	.5 to 5 Hz 1.3 to 15 cm	interface gas transfer
Allredge, Granata, Gotschalk and Dickey 1990	62 x 62 x 76	5 space 1 cm tubes	2.4 to 4.9 Hz 6 cm	gas transfer/ aggregate breakup
Casson and Lawler 1990.	?	3.18 space .635 bars + mesh	0.25 - 0.75Hz 1.91 - 0.64cm	Flocculation
van Leussen 1994	425 x 29	7.5	7.5 cm 5 Hz max	estuarine sediment dynamics
Kiorboe Andersen Dam 1990	? beaker	round plate with holes	energy input calculated	phytoplankton stickiness
Hill Nowell Jumars 1992	50 x 50 x 40	6.35 space 1 cm	2.5 - 3.4 Hz 4 - 6 cm	Particle interaction
Chisholm 1999	28 x 10	2.5 space .64 grid	.38 - .75 Hz 7.5 cm	

Table 3-2 Viscometers

Author	dimension	speed	use
Van Duuren 1968	8.9 id 11.5 od 25 long	?	flocculation
Gibbs 1983	1 cm gap 900 ml vol	?	flocculation
Drapeau, Dam, and Greiner 1994	9.038 id 11.538 od 26 long	?	stickiness
Tsai, Iacobellis, and Lick 1987	2.3 id 2.5 od 25.4 long	<830 rpm	flocculation
Hunt 1982	7.5 id 8.13 od	shear 0.5 - 32 1 Hz	flocculation

Table 3-3 Rolling Cylinder Devices

Author	dimension	speed	use
Shanks and Edmondson 1989	15 ϕ x 8	2.6 to 30 rpm	aggregation
Passow and Wassmann 1994	6 ϕ	2.8 rpm	aggregation
Lick, Huang, and Jepsen 1993	20 ϕ 2.6 30 ϕ 2.8 100 ϕ 3.5	2 rpm	aggregation
Logan Kilps 1995.	4 ϕ 60 ml	7.5 rpm	aggregation

with stronger turbulence near the bottom. Aggregates broke up as they fell through the grid but reformed as the pieces were resuspended. None of these designs are well suited for studies where interaction between aggregates and the grid are undesirable.

To make a grid type turbulence generator useful, a method of keeping particles suspended but away from the grid must be developed. The most successful method of keeping aggregates in suspension was the rolling cylinder device developed by Shanks and Edmondson (1989). They placed water in a rotating cylinder so the particles could continually fall without hitting the bottom of the cylinder.

Combination of these two devices results in a rotating cylinder with an oscillating grid in one end, or rotating oscillating grid turbulent aggregation chamber - ROGTAC. This is a new design first presented herein. This design combines the superior turbulence generating capabilities of the oscillating grid design with the superior aggregate suspension characteristics of the rotating cylinder design. Aggregates should stay evenly distributed throughout the device due to turbulent mixing. Aggregates are carried into the grid by turbulent diffusion and residual currents, not by both turbulent diffusion and gravity as in conventional aggregation devices. Thus, the grid will interfere with the aggregation to a lesser extent. The device should quickly come up to solid body mean flow since momentum diffusion is governed by turbulent eddy viscosity instead of molecular viscosity.

An obvious question regarding a grid turbulence generator is whether the turbulence generator does indeed produce turbulent flow; that is, is its Reynolds number sufficiently large? Turbulent flow generally begins when the Reynolds number exceeds about 1500 (White 1979). A grid with 1 cm spacing must move at 15 cm sec⁻¹ to achieve this Reynolds number. Other researchers who have used "turbulence grid" generators such as Hill et al. (1992) and Brumley and Jirka (1987) actually had Reynolds numbers too small to generate turbulence. Hill et al. (1992) had a Reynolds number of about 100. If the Reynolds number for an oscillating grid is too low unsteady laminar flow results. It behaves much as turbulent flow and is acceptable for many applications but it is not truly turbulent in that it is not chaotic. (Dr. Robert Ash, personal communication). The flow characteristics of ROGTAC were investigated experimentally to determine the nature of the flow as a function of grid oscillation stroke frequency.

ROGTAC consists of a 10.2 cm diameter cylinder which is 28 cm long giving a volume of 2.2 l. The barrel is cast acrylic. The grid is constructed of 0.635 cm square acrylic with 2.54 cm center to center spacing. Power is transmitted to the grid by a 1.9 cm diameter acrylic rod. A double O-ring seal prevents leakage where the rod enters the barrel. The end of ROGTAC away from the grid is covered with a 3.2 mm thick glass plate. The glass has superior optical properties to acrylic. It is also removable to allow access for filling the device. A 1/8 Hp gear motor transmits power through a slider mechanism to the rod connected to the grid. The motor is a variable speed DC motor and can vary its speed between 0 and 60 rpm. At 60 rpm, the Reynolds number is about 1500. Rotation is driven by an AC motor which transmits its power through a chain drive to a

drive pulley. Rotation speed cannot be varied and is fixed at 3 rpm. Figures 3-3 through 3-5 show the plans for the device. The as-built device has a few deviations from the plans. The pulley which drives the barrel rotation mates with a 5 tooth per inch timing belt which is glued on the barrel. A second pulley on the top insures that the drive pulley and the timing belt stay in contact.

Analysis of ROGTAC

The ROGTAC is a new design so it is necessary to describe its hydraulic characteristics as accurately as possible. This was done using a Laser Doppler Velocimeter. The ROGTAC's characteristics of primary interest are the mean flow rate and the turbulent energy dissipation rate.

Laser Doppler Velocimetry

When faced with the challenge of determining flow velocities inside a container it is advantageous to obtain measurements without inserting anything into the container which disrupts the flow. Because light has virtually no effect on flow, the idea of looking at the flow is appealing. A Laser Doppler Velocimeter (LDV) measures flow velocities using a laser light and appropriate optics and electronics. The Doppler phenomena is well known; when waves bounce off moving objects their frequency changes. Measuring the frequency change allows determination of the velocity of the object. Although the concept is simple, making it work is more complicated. The frequency of light is on the order of 10^{15} Hz which is much faster than electronics operate. Furthermore, the Doppler shift is

ROGTAC - Chamber & Grid

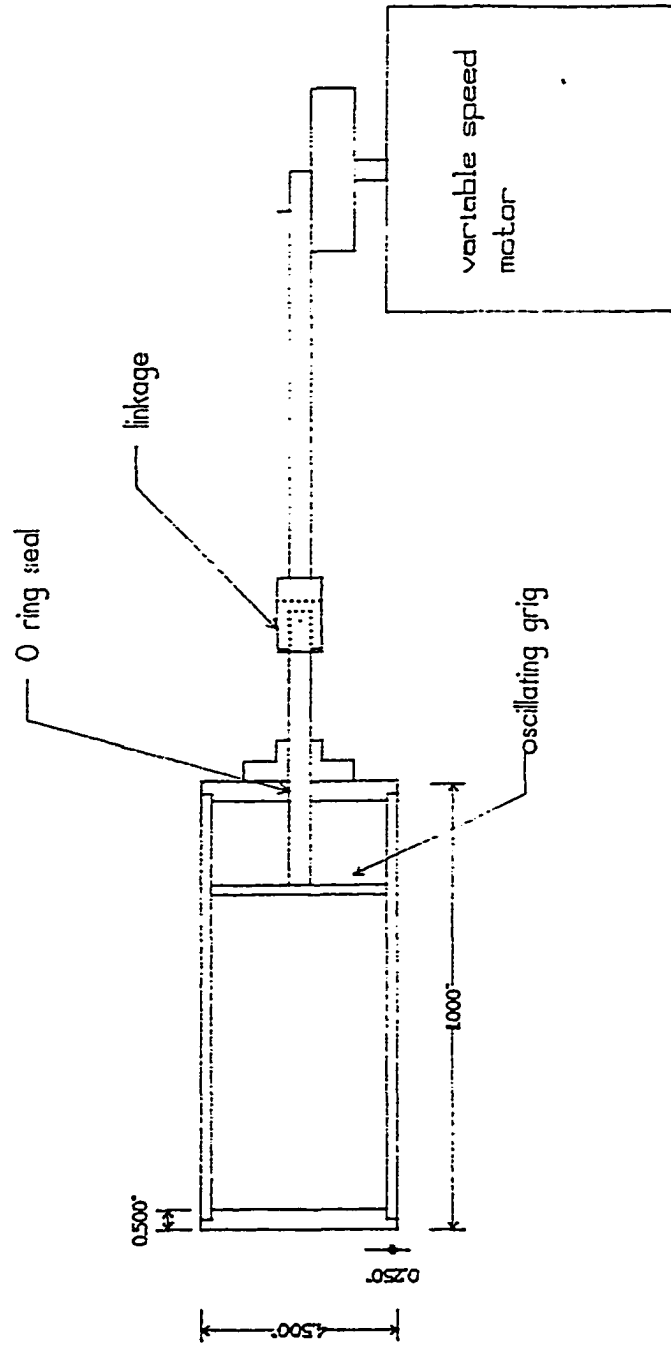


Figure 3-2 ROGTAC Chamber and Grid Side view.

Drum is supported by rolling table

ROGTAG End View

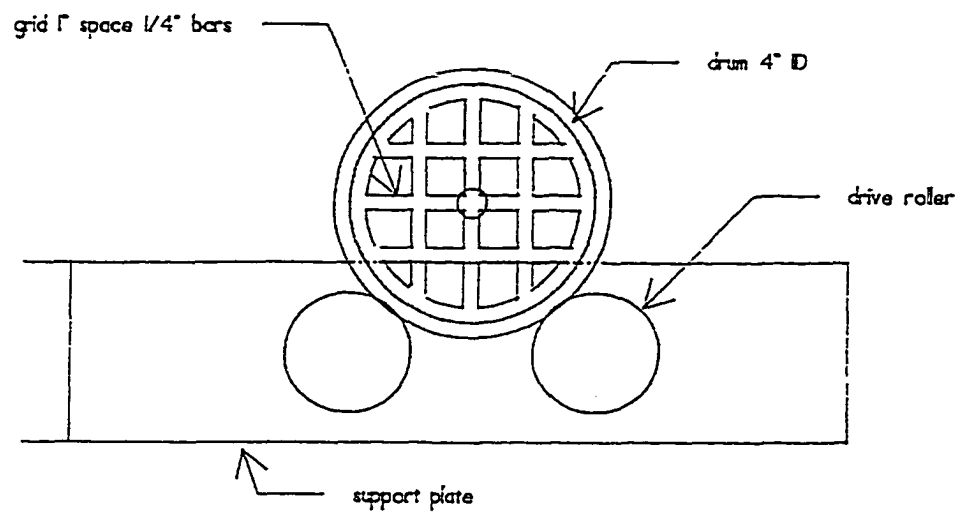


Figure 3-3 ROGTAC Chamber End View
ROGTAC chamber end view showing grid in barrel.

Support for rolling - grid turbulence Flocculator .

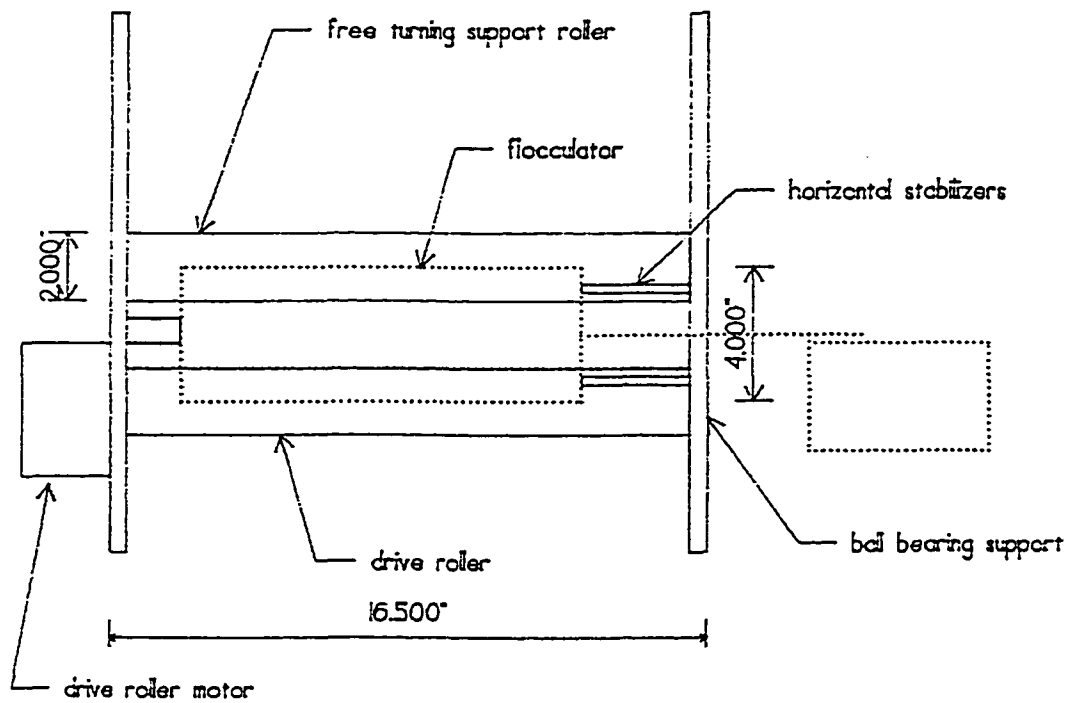


Figure 3-4 ROGTAC Support
ROGTAC chamber on its support.

usually less than 10^6 Hz, 9 orders of magnitude slower than the frequency of the light. To solve these problems light is broken into 2 beams; the frequency of one of the beams is shifted; and the beams are focused at a location where the two beams interfere. The shift frequency is selected by the LDV operator to be close to but larger than the expected Doppler shift. A pattern with alternating light and dark bands moving at the shift frequency develops. These are reflected or scattered and Doppler shifted. The bands move in the plane of the beams perpendicular to the bisector of the angle between the beams. Velocities are determined in the plane of the beams and in the direction the fringes move.

Experiments were run at the Flow Modeling and Control Branch of the NASA Langley Research Center. The LDV used included an Innova 70 Laser and a TSI LDV system. The LDV system consisted of a colorburst 9201 separator, IFA 750 correlator, and a colorlink 9230 multicolor receiver. Although the system can be configured for 3 axis work it was used in the two axis mode for this project. Light wavelengths used included green, 514.5 nm, and blue, 488.0 nm.

Measurement quality improves if laser beams are transmitted through higher quality optical surfaces. Generally, flat glass is required. High quality optical windows are preferred, but plate glass from a hardware store will work. Measurement is more difficult through acrylic and attempts to obtain measurement through the curved surfaces of the acrylic cylinder were not successful. A flat glass end made of hardware store glass was placed on the ROGTAC. Because measurements can only be made in the plane of the

beams, measurements could only be made perpendicular to the axis of the cylinder. No measurements could be made parallel to the axis of the cylinder.

The fundamental equation for LDV is $f_0 = |U|/d_f$ where f_0 is the Doppler frequency, U is the particle velocity, and d_f is the fringe spacing. Thus, to calculate the velocity we need the Doppler frequency and the fringe spacing. Fringe spacing depends on probe optics and the wavelength of the light used. In water the wavelength of light is shorter, and the velocity of light is slower for a given frequency than in air. The ratio of velocities between air and any substance is that substance's index of refraction; for water it is 1.33. A shorter wavelength results in a smaller fringe spacing. Thus for a given Doppler shift velocities in water are smaller than in air. The laser beams are focused on a very small location. The measurement volume for the NASA LDV system with green light is a cylinder 159 micron diameter by 2.29 mm long.

LDV systems determine speed by measuring the Doppler shift of light interacting with particles; hence, particles are necessary. Ideally the particle is smaller than the fringe spacing and highly reflective. The fringe spacing in these experiments was $3.72 / 1.33$ microns. Particles should also track the flow. This is best done if the particle is the same density as the fluid. Latex particles are often used because they are almost neutrally buoyant and can be made very small. Attempts at flow measurement using 1.9 micron latex spheres were not successful because the latex was not reflective enough for the LDV processing electronics. This resulted in unacceptably low data rates. Tests with 10 micron hollow metal spheres gave good data rates because of the high reflectivity of the

spheres. They also appeared to give good signatures on the oscilloscope, confirming that they were not unacceptably large. These particles were used for the measurements reported herein. However, these particles did settle and tended to stick to the cylinder walls and the grid. New particles were added each day prior to experiments. There were noticeable decreases in data rates as the day progressed and particles settle out and stuck to the ROGTAC's cylinder walls.

Verification

Before using any measurement device it is advisable to compare the measurements with known values. This is rather difficult in the ROGTAC because the flow is not known; it is what we are trying to determine. One possibility is to rotate the cylinder and keep the laser focused at a spot away from the center. Knowing the speed of rotation allows calculation of the velocity of the water at that location provided the flow is solid body rotation. However, for solid body rotation to occur the momentum must diffuse outward from the cylinder wall which can take a while (Jackson 1994). A simpler method is to move the LDV probe relative to the cylinder with the cylinder still and the water in it at rest. This is easily done because the LDV probe is mounted on a stage which can be programmed to move at selected rates. Figure 3-5 shows measured and programmed velocities. The agreement is quite good. However, the standard deviations are more than one would wish. It is uncertain if these were due to variations in the speed of the stage, which could be the case if it uses a stepper motor, variation in the instrument, or unobserved variation in the flow.

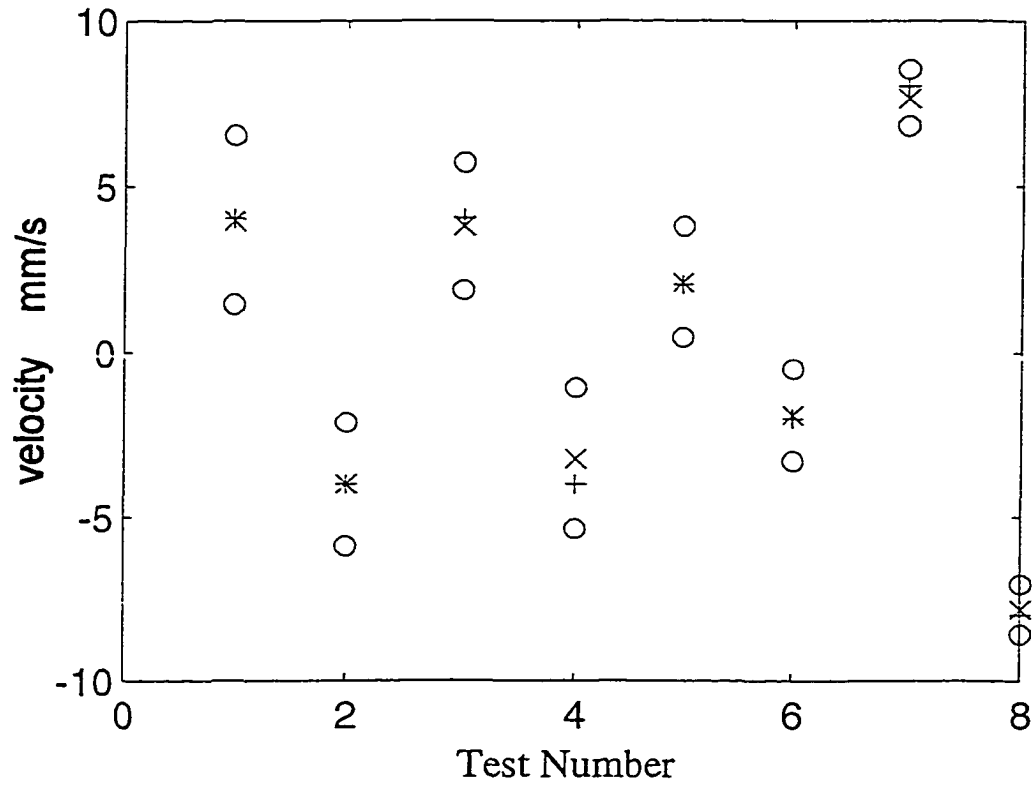


Figure 3-5 LDV Velocity Verification

Eight separate comparisons were made between programmed velocities of the moving stage and velocities measured by the LDV. The + symbol represents the velocity of the stage and the x represents the velocity measured by the LDV. The o's indicate the standard deviation of the LDV measurements.

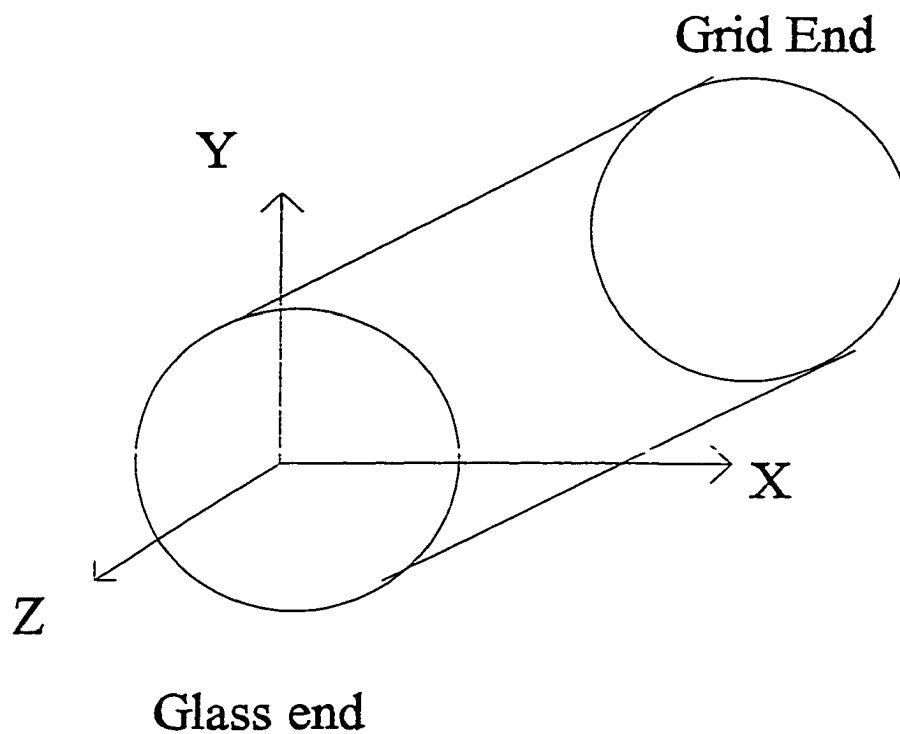


Figure 3-6 LDV Data Coordinate System

The coordinate system used in the LDV analysis of ROGTAC is shown. Facing the glass end and looking into ROGTAC, the x axis extends to the right, the y axis is vertical, and the z axis extends outward. This preserves a right hand coordinate system but all z coordinates in ROGTAC are negative.

Mean Flow

The first task of the LDV study was to determine mean flow patterns in the ROGTAC. This analysis was facilitated by first defining a right hand coordinate system with its origin at the center of the chamber at the window end. The y-axis was vertical and the x-axis extended to the right if one is looking into the chamber through the glass end plate. To maintain a right handed coordinate system, the z axis extended forward away from the chamber making all z values in the chamber negative.

Mean velocities were determined by a series of measurements spread over the y-z plane. Note that in Figure 3-7 the location of the measurements is shown by the base of the arrows which is in the y-z plane. This location is found from the graph axis. However, velocity magnitude and direction is shown by the length and direction of the arrows that are in the x-y plane. That is, the vertical component of the arrows shows radial motion and the horizontal component shows tangential motion. The plot shows what appear to be reasonable readings. Upon inspection several trends emerge. The flow at the bottom and ends is mostly tangential in the positive x direction and flow at the top is downward in the negative y direction. However, the mean velocity of these measurements is 3 mm sec^{-1} . An estimate of the time for circulation around the tank may be obtained by dividing the length of the perimeter of ROGTAC, $100\pi \text{ mm}$, by the mean velocity to obtain about 100 seconds. More importantly, if it is assumed that longitudinal flow equals tangential flow, the time for a particle to complete a circuit in the y-z plane would be about 250 seconds. In one early test run of ROGTAC a small jellyfish found its way into a water sample and thus into the device. It did a slow circulation in the y-z plane, taking

several minutes to complete a circuit. It was not swimming and appeared to be dead, although maybe it was just sleeping. However, the former is more likely because passing through the grid would probably wake it up. Knowledge of the circulation rate is important because it gives a measure of how quickly aggregates forming in the device pass from the more energetic grid end to the more quiescent end.

Standard deviations of the above data were also calculated and are plotted in Figure 3-8 in the same format as the mean velocities. Note that by their nature all standard deviations are positive. The lower left velocity in the grid is actually a missing value. The data appear regular. Note that the flow is much more energetic close to the grid and decays away from the grid. This effect will be treated in more detail with a later data set.

Measurements were made next across one square of the grid and varying distances in the z direction. These are plotted in Figure 3-9. The flow in front of a grid is a jet. Mean velocities at various distances away from a jet were calculated. Note that the measurements are close together. Neglecting the large velocities close to the grid, the mean velocity is 2.7 mm sec^{-1} , close to the value for the whole grid scan. As in Figure 3-8, standard deviations for the single grid cell measurements are plotted in Figure 3-10. It was hoped when collecting these data that a form to the jet would emerge. However, the variation in the flow is close to constant across a transect and decreases away from the grid.

Grid Turbulence

Grid turbulence has been used in many studies of mixing or gas transfer in addition to a few aggregation studies. Most of these studies, described in Table 3-1, characterized grid turbulence. Thompson and Turner (1975) used a hot wire anaemometer to measure turbulence at various distances above the grid. They found: "The flow produced by oscillating grids can be discussed in terms of three consecutive processes. First, there is the generation of a quasi-steady jet flow very close to each grid bar. The form and intensity of the motion in this region depends on the cross section of the bars and on the amplitude, and there may be an explicit dependence on viscosity. Second, the jets interact, and break down to give turbulence which is advected by the jets. Finally, this turbulence decays with distance away from the grid ..." The flow structure near oscillating grids is different than that downstream of a grid in the flow.

Thompson and Turner (1975) give the following expression for decay of turbulence which they credit to Batchelor (1953) $dU^2/dt = -AU^3/l$ where U and l are the velocity and length scales of the turbulence determined by autocovariance procedures and A is a constant of order 1. They adapted this expression to obtain $dU^3/dz = -B_c U^3/l$. If l varies linearly with z , the distance away from the grid, it can be expressed as $l=D_c z$. Substitution and solution of the differential equation gives $U=U_0(z/z_0)^{-B_c/3D_c}$ where U_0 is the velocity at z_0 . They found $U \sim z^{-1.5}$, $B_c=0.45$, $D_c=0.1$. Hypothesizing that $U_0=f_s s$ and $z_0=s$ and substituting into the equation for U gives $U=1.4 f_s^{2.5} z^{-1.5}$. This implies that turbulent velocities depend upon the stroke frequency, f_s , and the stroke length, s . Turbulent velocities decrease away from the grid at the -1.5 power.

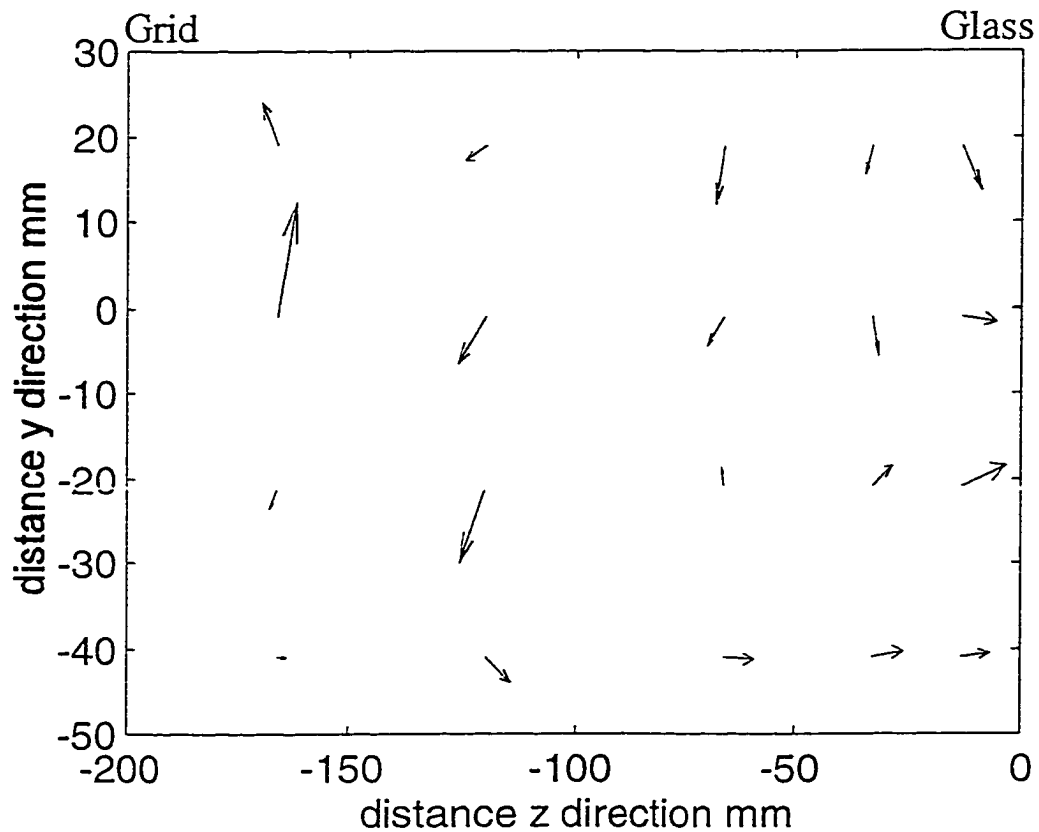


Figure 3-7 Mean Velocities in the XY Plane

Measurements were made in 20 locations spread over a vertical slice through the long axis of the chamber (the yz plane). The location of the base of each arrow depicts the measurement location. For example, the largest arrow in the leftmost column of arrows shows a measurement which was made at location $x=0$, $y=0$, and $z=-170$. In this location, the mean flow was mostly upward but slightly to the right when viewed through the glass end. To provide scale, the arrow in the upper left corner represents 4.4 mm sec^{-1} .

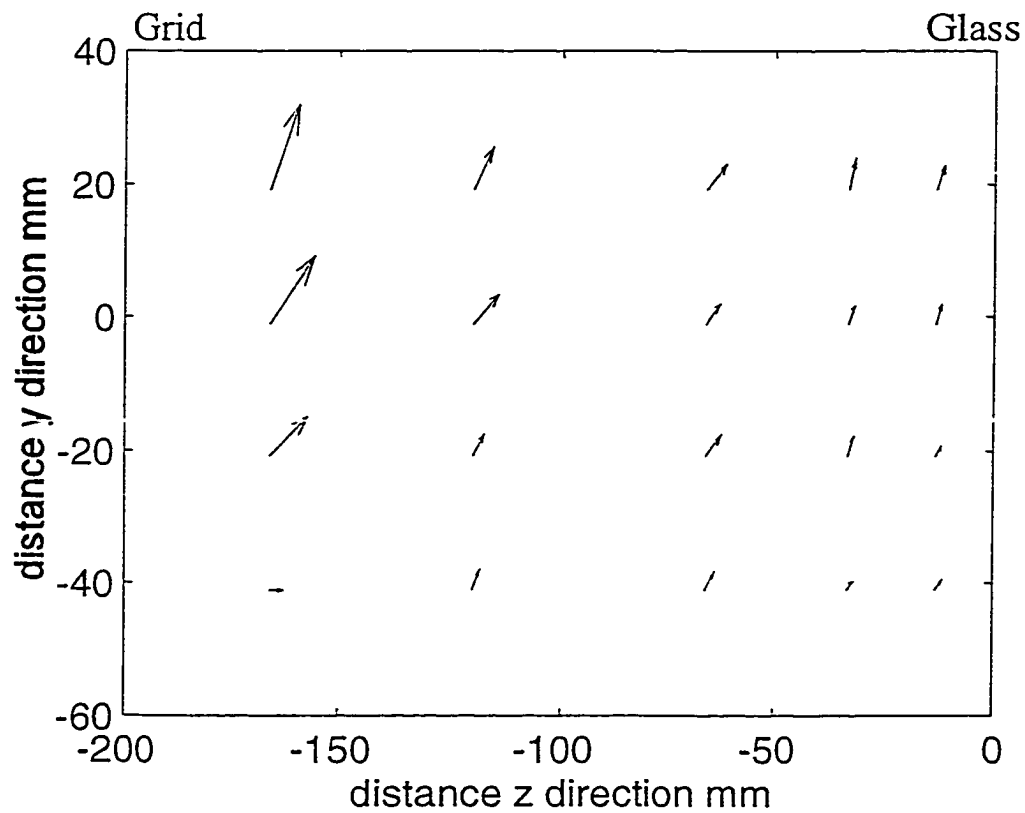


Figure 3-8 Standard Deviation of Velocity in XY Plane

Standard deviations of the mean values shown in figure 3-7 are given. The location of the base of each arrow depicts the measurement location. The arrows are vectors showing the standard deviation in the x and y directions. Note that flow is less energetic away from the grid. To provide scale, the arrow in the upper left corner represents 12.9 mm s^{-1} .

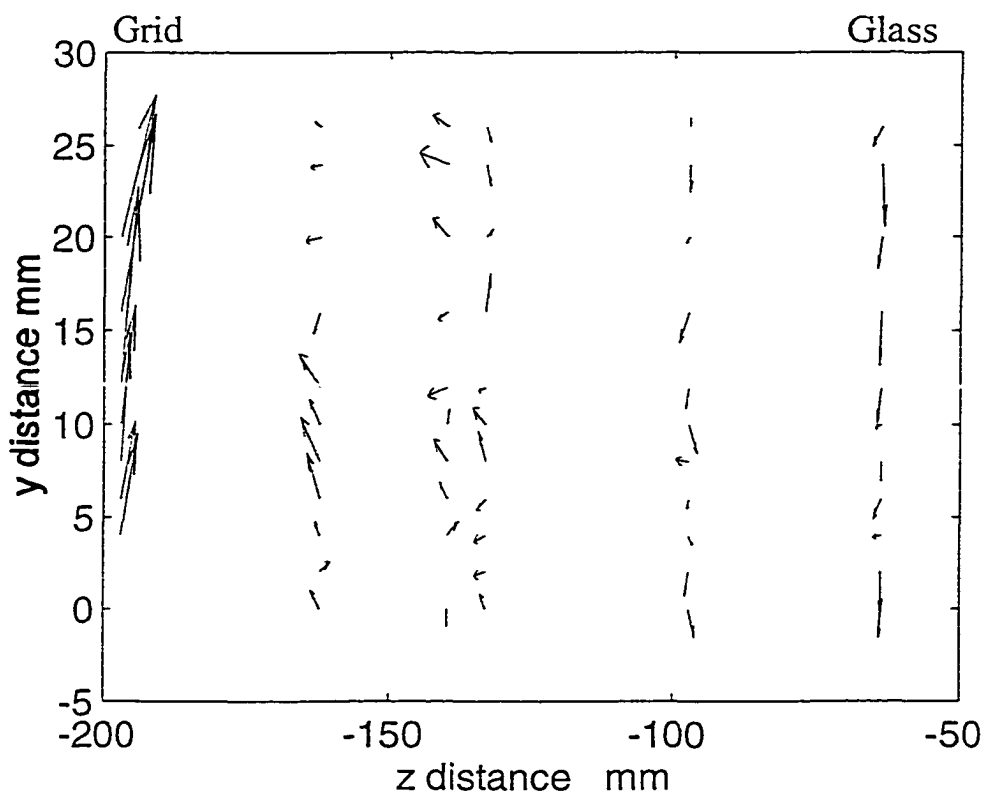


Figure 3-9 Mean Velocities in XY Plane Across a Grid Cell

Mean velocities in the jet leaving a grid cell were measured. The large velocities on the left are inside the grid stroke. The arrows are vectors showing the mean flow in the xy plane. Away from the grid, a weak rotary flow velocity is visible. The location of the base of each arrow depicts the measurement location in the yz plane. To provide scale, the arrow toward the upper left corner represents 15.8 mm s⁻¹.

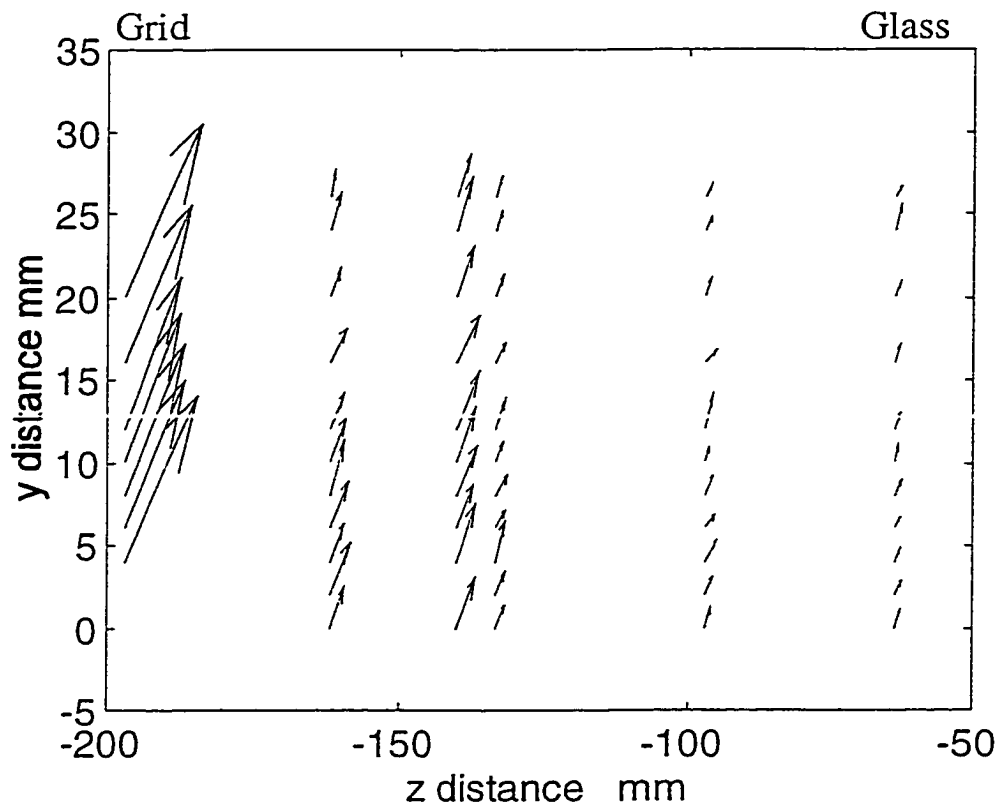


Figure 3-10 Standard Deviation in WY Plane Across a Grid Cell

The structure of the jet leaving a grid cell was determined. The large velocities on the left are inside the grid stroke. The arrows are vectors showing the standard deviation in the flow in the xy plane. This figure clearly shows the decrease in turbulent intensity away from the grid. The location of the base of each arrow depicts the measurement location in the yz plane. To provide scale, the arrow closest to the upper left corner of the figure represents 36 mm s^{-1} .

Stanley and Smith (1995) performed an LDV study of flow in a standard mixing jar used for wastewater treatment studies. A standard mixing jar is square and hold 2l. It is equipped with a 76mm diameter flat blade impeller. They again suggest that the turbulent energy dissipation, ϵ , equals AU^3/l and derive this by dividing the turbulent kinetic energy by a dissipation time. This time is considered to scale as the square root of the turbulent kinetic energy divided by the characteristic length scale of the turbulence. They state that it is commonly known that the length scale of grid turbulence is $\frac{1}{2}$ the grid spacing. Using this, the turbulent energy dissipation rate is readily calculated from the turbulent kinetic energy and the geometry of the grid.

Speed Variation

To assess the effect of varying plunger speed, fluid velocity measurements were made, by the author, on a line parallel to the direction of plunger motion at 3 speeds: 23, 32, and 45 rpm. Measurement locations are shown in Figure 3-11. These velocity measurements will be used to determine turbulent energy dissipation rates using the methods described earlier as presented by Stanley and Smith (1995).

Velocity measurements at a point lasted for 120 seconds and data rates were relatively high with at least one data point per second in almost all case and up to almost 30 data points per second. As one would expect, at higher grid speeds the flow is more energetic and more particles are advected through the measurement volume per unit time resulting in more points. However, this effect is counteracted by the number of particles

in the water decreasing with time because they settle out. The measurements were done in the order 32, 45, then 23 rpm.

Because more rapid flows carry more particles through the measurement volume per unit time, faster velocities are over-represented if one simply calculates statistics on all the measurements obtained. To investigate this effect, means and standard deviations were calculated for all the points, then calculated on only those points closest to each even half-second intervals and the results compared. These data are presented in Figure 3-13 for x measurements from the scan with the motor control set for 32 rpm. As expected both means and standard deviations decrease when evenly-spaced points are selected. Note that turbulent energy is usually quantified by the average of the square of the time varying velocities, that is the variance. However, using the standard deviation, which is the square root of the variance, improves the legibility of figure, because both the mean and the standard deviation have the same units and similar magnitudes.

As mentioned previously, the LDV obtains a velocity measurement whenever a particle passes through the measurement volume. When the flow is faster, more fluid, and therefore more particles, pass through the measurement volume. To avoid over representing these faster velocities, velocity measurement taken at evenly spaced time intervals may be selected. However, because velocity measurements are made at random times, velocity measurements won't be available precisely at the evenly spaced time intervals and velocity measurements which are "close" to the evenly spaced time intervals must be selected. If there are many more data points collected than needed to have

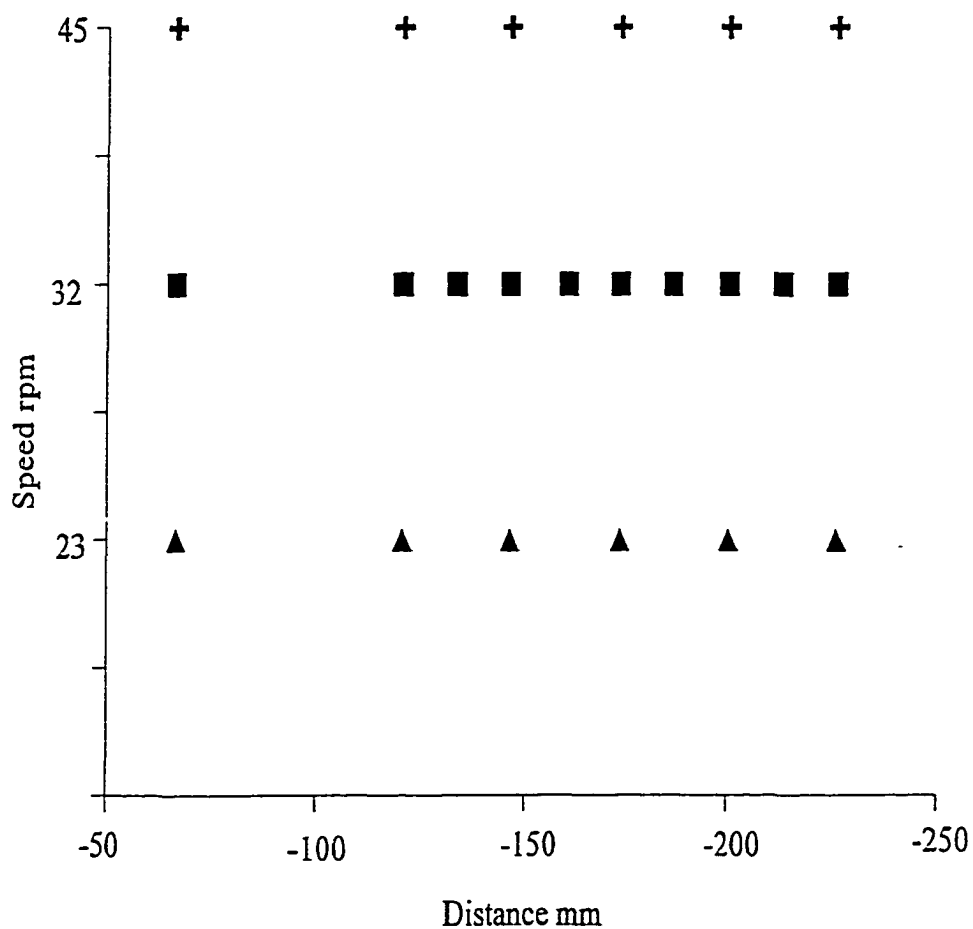


Figure 3-11 Measurement Locations

A graphical depiction of measurement locations used to calculate turbulent energy dissipation at 3 ROGTAC motor speeds is provided. All measurements were made at the same vertical location; they are shown at different vertical locations in this figure for clarity.

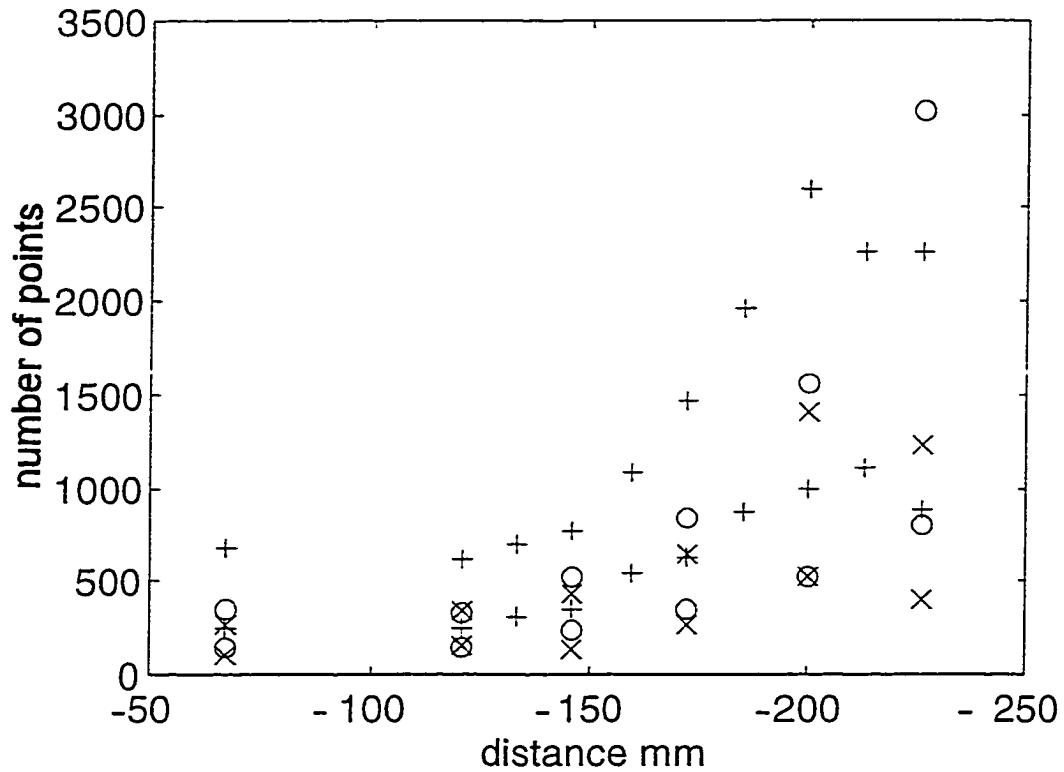


Figure 3-12 Velocity Measurements in 120 Seconds.

The number of velocity measurements collected during 120 seconds in the x and y directions are given. Motor settings of 23, 32, and 45 rpms are represented by x, o, and + respectively. The same symbol is used for both x and y measurements at a position and the y measurement is always the lower one. The LDV generates more x measurements than y measurements because it is more efficient at using green light.

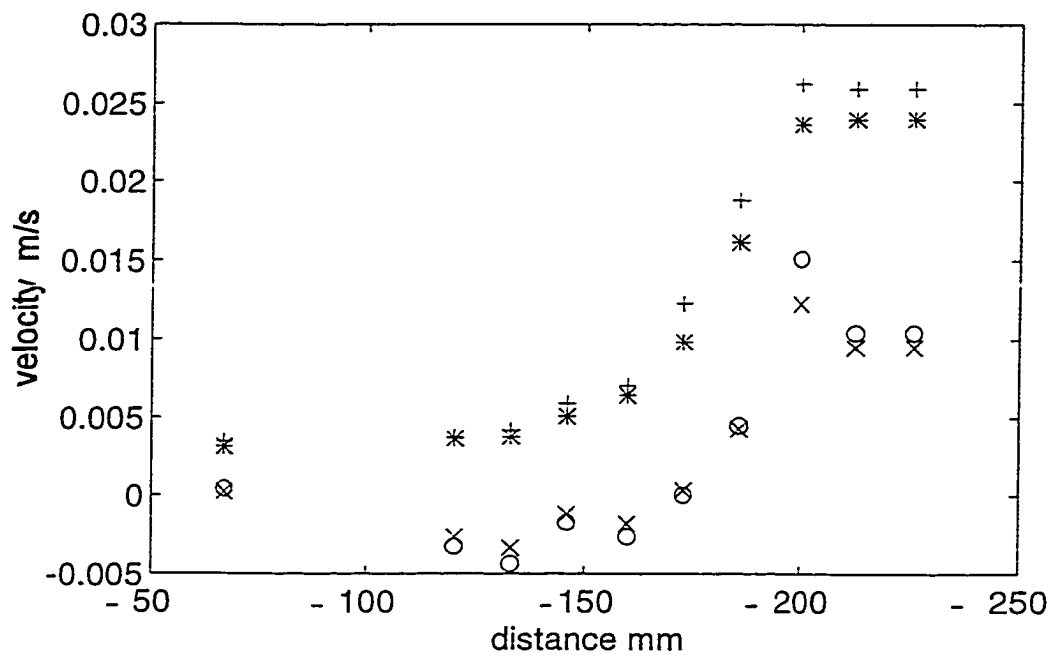


Figure 3-13 Effect of Selecting Evenly Spaced Points

The effect of selecting evenly spaced points on velocity measurements is shown. The symbols 'x' and 'o' represent mean velocities with and without the selection process, respectively. '*' and '+' represent standard deviations with and without the selection process, respectively.

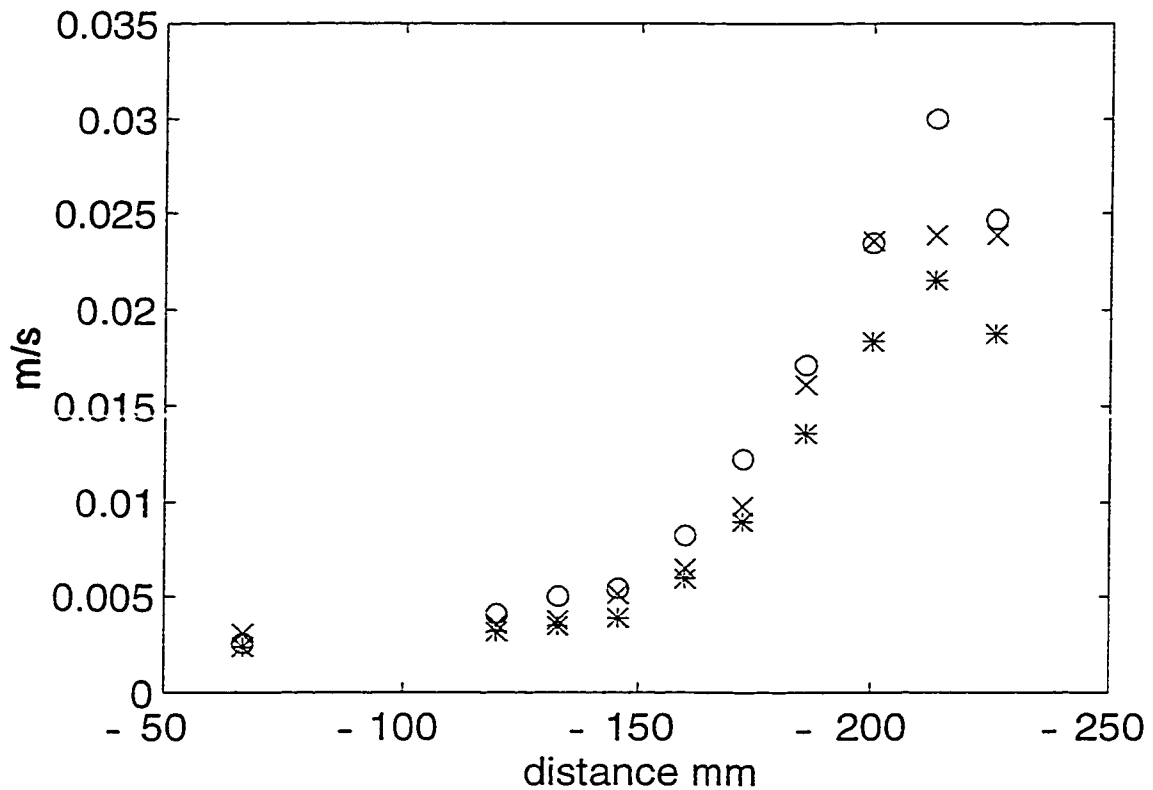


Figure 3-14 Comparison of Standard Deviation Between Axes

Standard deviations for the x, y axes and the covariance, $x*y$, are calculated. Symbolism includes x for the x axis, o for the y axis, and * for the product of the two axes. This plot indicates that the flow is reasonably isotropic. The product of the two directions is usually the lowest. This could be partly caused by velocity measurements for the two axes being made at slightly different times.

velocities at the evenly spaced time intervals, the selected velocity measurements will indeed be close to the evenly spaced time intervals. However, if there aren't a lot more point available than required, they won't be. The effect of selecting evenly spaced velocity measurements in the ROGTAC data set was not great, and statistics will be calculated from the raw data in the following analysis.

Figure 3-14 shows standard deviations for x and y directions and the covariance, $x*y$. This plot indicates that the flow is reasonably isotropic. The product of the two directions is usually the lowest. This could be partly caused by velocity measurements for the two axes being made at slightly different times.

Turbulent Energy Dissipation

Energy input to a fluid by mixing is dissipated by small scale viscous fluid motion. Turbulence transfers the motion imparted to the fluid by mixing to the small scales where it is dissipated. The energy input to the fluid by mixing equals that dissipated by viscosity at small scales. Turbulent energy dissipation in ROGTAC was calculated 2 ways: 1) from the LDV measurements using U^3/l and, 2) from the energy input to the fluid as calculated from the motion of the grid. The Reynolds number calculated using the maximum velocity of the grid with motor speed set to 32 rpm as the characteristic velocity and the grid spacing as the characteristic length is about 750. The onset of turbulent flow is generally considered to be between 1000 and 3000 so the flow in ROGTAC is unsteady laminar flow. However, the flow was assumed to be turbulent following the previously cited investigators of laboratory grid turbulence.

The LDV measures velocity over time at a point. Tennekes and Lumley (1972)

define dissipation as

$$\varepsilon = \frac{1}{2} \nu \left(\frac{\partial U_i}{\partial x_j} + \frac{\partial U_j}{\partial x_i} \right)^2 \quad 3-1$$

for isotropic flow where U is the turbulent velocity using indicial notation. Isotropic flow has no spacial orientation. Note that this equation requires spatial velocity gradients which are not readily obtainable from LDV's which provide point measurements. This problem is often treated by using the frozen turbulence hypothesis, which essentially states that time multiplied by the mean velocity of the flow gives spatial change. It converts time to distance, or, to look at it another way, it converts frequency to wave number. When the mean flow is too small, the root mean square velocity is used. In short, the ROGTAC does not conform well to the frozen turbulence hypothesis conditions. However, Tennekes and Lumley proposed the following scaling relationship for turbulent energy dissipation where λ_t is the Taylor microscale and U is the mean turbulent velocity

$$\varepsilon = 15 \nu \overline{U'^2} / \lambda_t^2, \quad 3-2$$

The Taylor microscale is the location where a parabola which matches the autocorrelation function at the origin intersects the x axis. The one shortcoming of this equation is that λ_t is not easily determined. Tennekes and Lumley (1972) describe how to obtain λ_t from autocorrelations but our data set is not well suited for autocorrelations. They provide additional equations which, after some manipulation, give

$$\lambda_t = \sqrt{15lv/\overline{U}^3}$$

3-3

Stanley and Smith begin their determination of ϵ , turbulent energy dissipation, by noting its definition, which is change in kinetic energy with time. Kinetic energy scales as U^2 , so kinetic energy divided by a suitable time scale gives ϵ . The time scale is U/l where l is the Eulerian length scale of the turbulence. Thus they give $\epsilon = \langle |U^3| \rangle / l$. They also state that for grid turbulence l equals one half the grid spacing. However, upon substitution of the Tennekes and Lumley equation for λ_t into their equation for ϵ , the two equations are similar since the T&L equation reduces to $\langle U^2 \rangle \langle U \rangle / l$. Both the Tennekes and Lumley, and Stanley and Smith equations will be used for analysis of the LDV data.

Figure 3-15 shows the variation in dissipation with speed using data from the x-axis. Dissipation is a clear function of motor speed. For comparison purposes, Figures 3-16 through 3-18 show the variation between calculation methods and axes for the three motor speeds. In general, the Stanley and Smith method gives slightly higher values. The x axis values are also slightly higher. This could be due to either some anisotropy in the flow or the higher data rates obtained from the x axis. After assuming the dissipation is symmetric and weighting each measurement by the volume near it, dissipations of $1.63 \text{ E-}4$, $4.04 \text{ E-}4$, and $10.0\text{E-}4 \text{ m}^2 \text{ s}^{-3}$ were calculated for the motor speeds of 23, 32, and 45 rpm respectively.

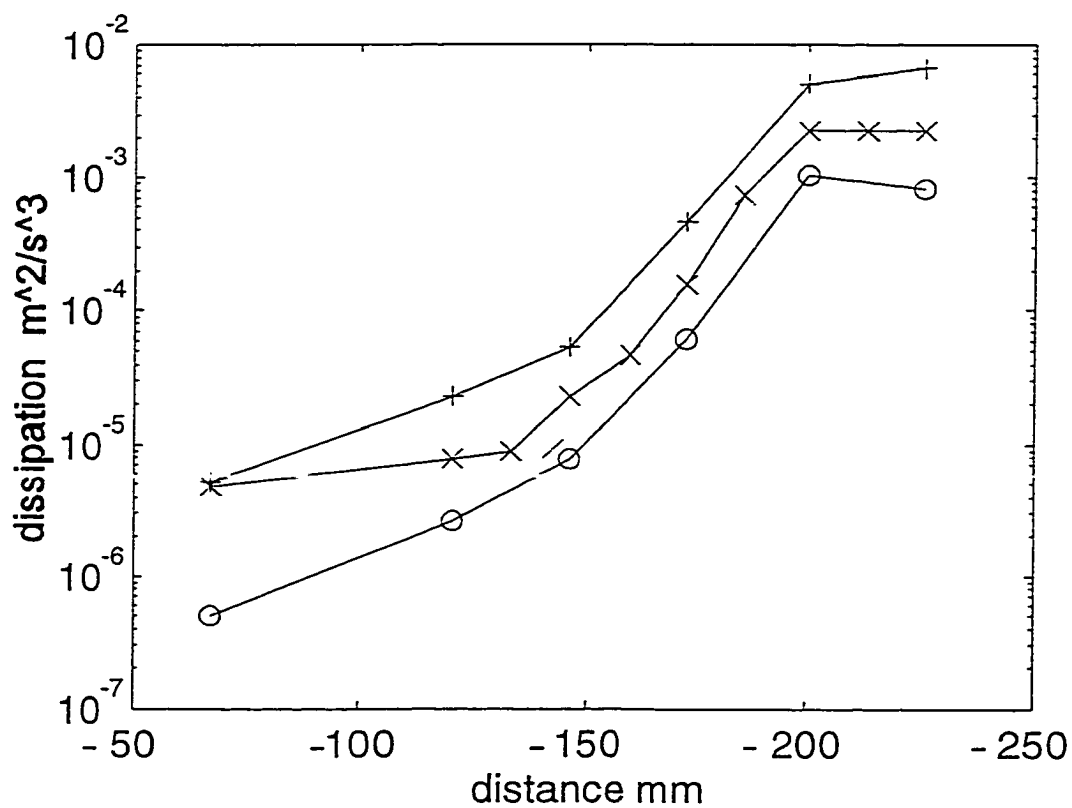


Figure 3-15 Dissipation for Three Motor Speeds

Dissipation was calculated by the Stanley and Smith method in the x axis. Motor speeds of 23, 32, 45 rpm are depicted by 'o', 'x', and '+' respectively.

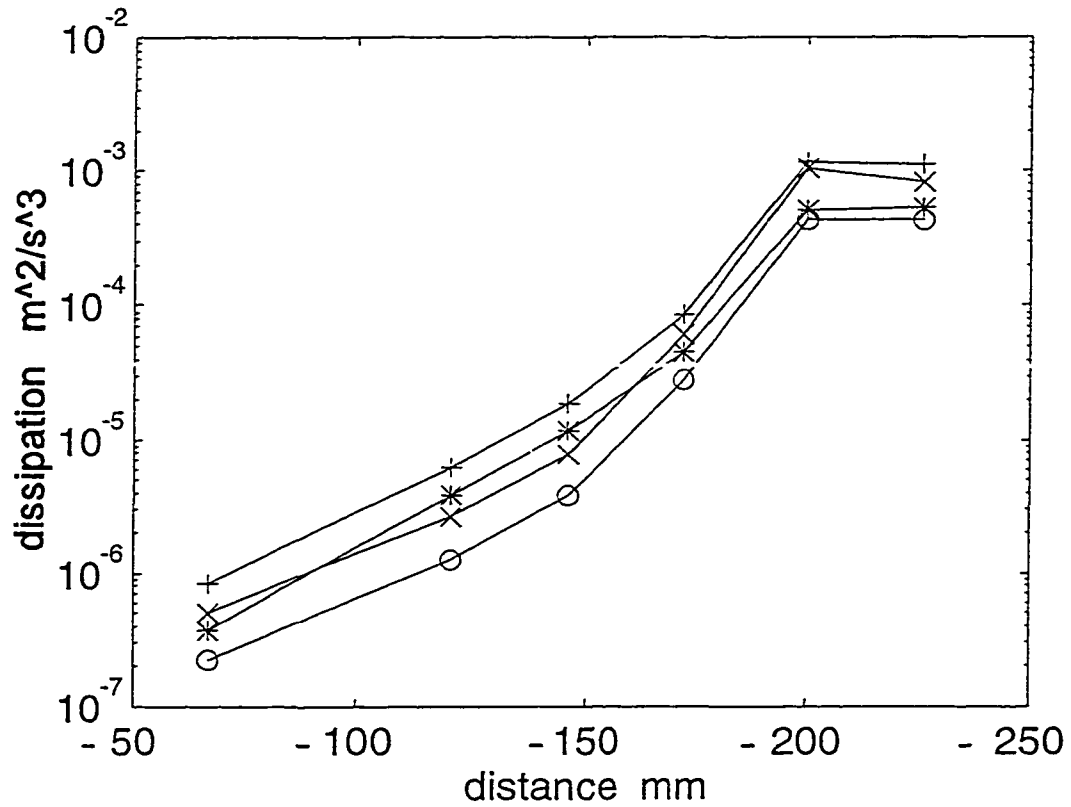


Figure 3-16 Dissipation for Motor Speed of 23 Rpm

Plotted are: x axis dissipation calculated by the Stanley and Smith method shown by a '+', y axis dissipation calculated by the Stanley and Smith method shown by a '*', x axis dissipation calculated by the Tennekes and Lumley method shown by a 'x', and y axis dissipation calculated by the Tennekes and Lumley method shown by a 'o'.

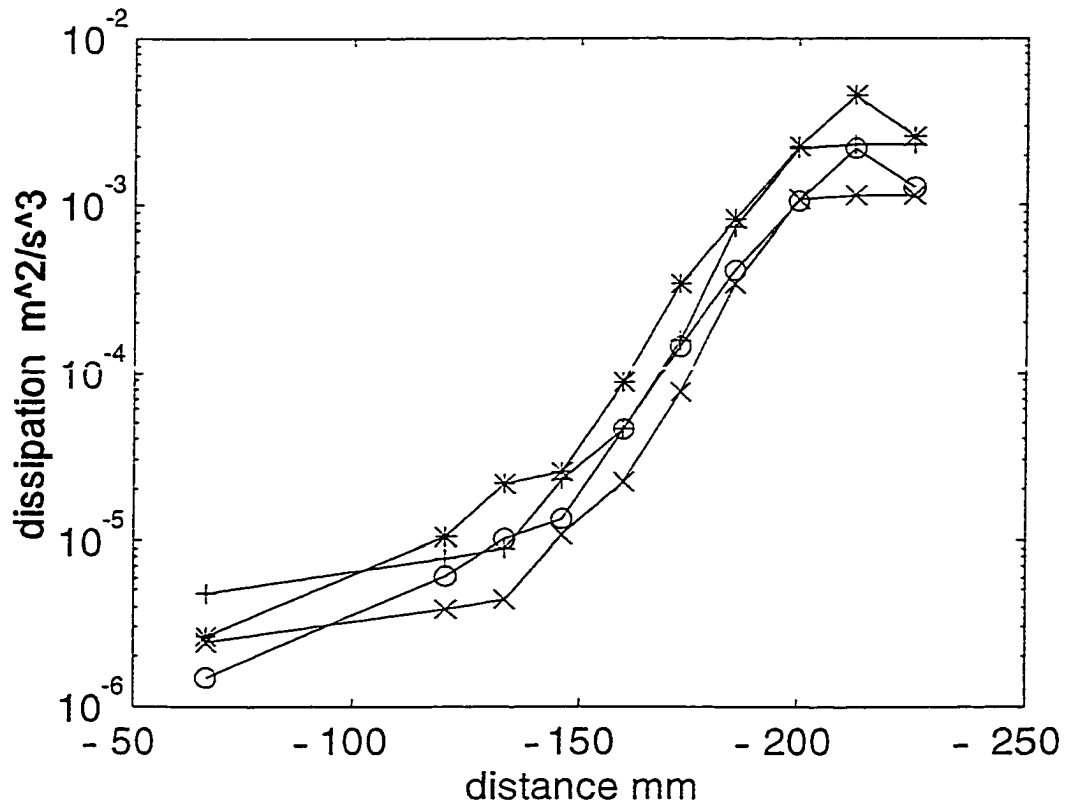


Figure 3-17 Dissipation for Motor Speed of 32 Rpm

Plotted are: x axis dissipation calculated by the Stanley and Smith method shown by a '+', y axis dissipation calculated by the Stanley and Smith method shown by a '*', x axis dissipation calculated by the Tennekes and Lumley method shown by a 'x', and y axis dissipation calculated by the Tennekes and Lumley method shown by an 'o'.

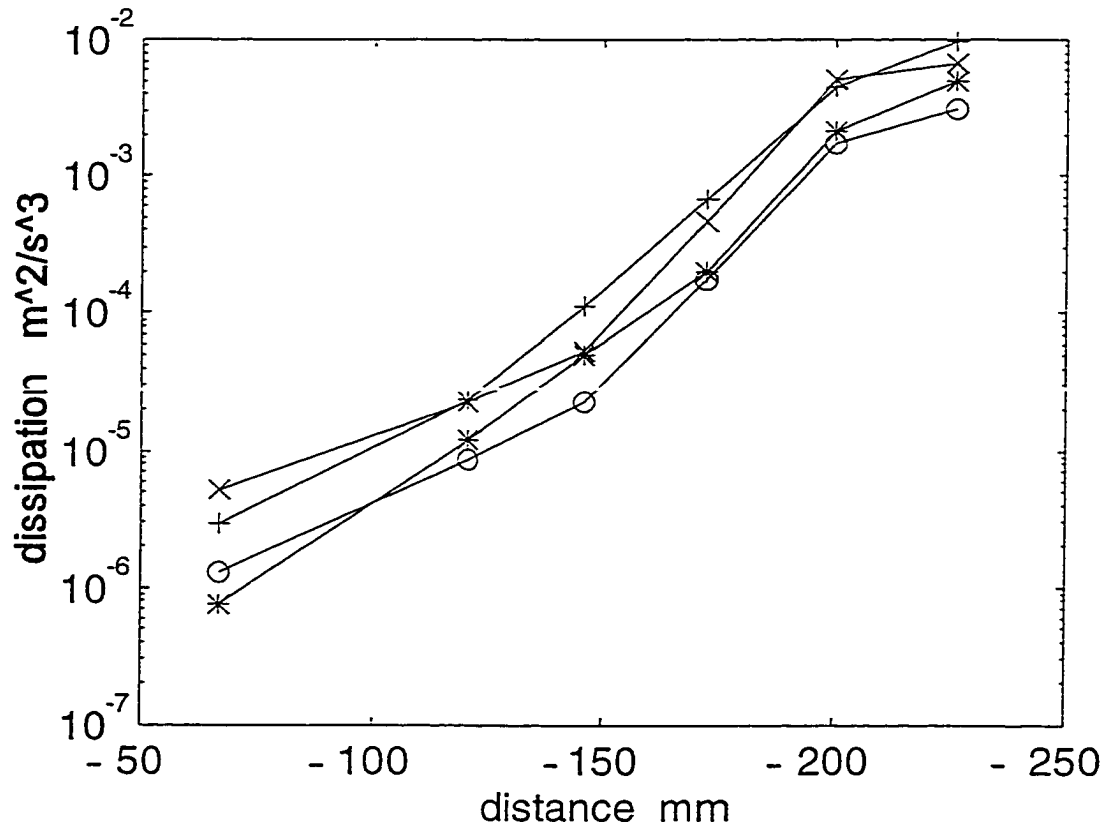


Figure 3-18 Dissipation for Motor Speed of 45 Rpm

Plotted are: x axis dissipation calculated by the Stanley and Smith method shown by a '+', y axis dissipation calculated by the Stanley and Smith method shown by a '*', x axis dissipation calculated by the Tennekes and Lumley method shown by a 'x', and y axis dissipation calculated by the Tennekes and Lumley method shown by an 'o'.

Drag Force Method

A simple, alternative method for determining energy dissipation involves direct calculation of the drag force on the grid and multiplication with the velocity of the grid (van Leussen 1994). Drag forces, F , are often calculated using the quadratic drag law, where C_D is the drag coefficient and ρ_f is the density of the fluid. Drag coefficients are empirically derived for steady flow. They are a function of object shape and Reynolds number (White 1979).

$$F = \frac{1}{2} \rho_f C_D A_a U^2 \quad 3-4$$

Where A_a is the cross-sectional area of the grid and U is its velocity. The grid mechanism is a slider mechanism so the motion can be expressed as:

$$x = B_a \cos \frac{t2\pi}{T_p} \quad 3-5$$

Where B_a is the amplitude of the motion, T_p is its period, x is distance, and t denotes time.

The instantaneous velocity is simply the derivative of equation 3-5.

$$U = \frac{B_a 2\pi}{T_p} \cos \frac{t2\pi}{T_p} \quad 3-6$$

Power, also called energy dissipation, equals force times velocity so

$$\frac{dE}{dt} = \frac{1}{2} \rho_f C_D A_a \left[\frac{B_a 2\pi}{T_p} \cos \frac{t 2\pi}{T_p} \right]^3 \quad 3-7$$

To determine the average power input, one must integrate over 1/4 of the period and divide by that time to get

$$\frac{dE}{dt} = \frac{16 \rho_f C_D A_a B_a^3 \pi^2}{3 T_p^3} \quad 3-8$$

For ROGTAC $A_a = 0.00316 \text{ m}^2$, $B_a = 0.022 \text{ m}$, and T_p depends upon motor speed but equals 2.61, 1.87 and, 1.32 seconds for motor speeds of 23, 32, and 45 rpm respectively. Thus for the 3 speeds energy dissipation equals $9.96\text{E-}5$, $2.71\text{E-}4$, and $7.70\text{E-}4 \text{ kg m}^2/\text{s}^3$.

Dissipation Comparison

Agreement between the LDV and drag law methods is quite satisfactory considering the assumption implicit in both methods.

Table 3-4 Energy Dissipation

motor speed rpm	LDV $\text{m}^2 \text{s}^{-3}$	Drag Law $\text{m}^2 \text{s}^{-3}$
23	0.000163	0.0000996
32	0.000404	0.000271
45	0.001	0.00077

Data Collection

The most challenging aspect of laboratory studies of aggregation is usually not forming the aggregates but collecting data about them. The most basic description of an aggregate is size. Several technologies have been developed to measure particle size. Notable among these are resistance measuring devices, commonly called Coulter Counters, and laser diffraction devices, called Malvern Particle Sizers. Coulter Counter have the disadvantage that the particle being measured must be drawn through a small orifice, that will break up aggregates (Gibbs 1982). A major drawback to both devices is aggregates must be transferred to the instrument which is likely to disrupt the aggregate (Gibbs and Konwar 1982).

The way to avoid damage to the aggregate by handling is to observe the aggregate where it was created without handling it. Although conceivably a laser sizing device could be integrated into an aggregation device, to date this has not been done. Measurements of aggregates in aggregation devices have been done optically. Optical methods are less suited to observing the smallest particles than the techniques described in the previous paragraph. ROGTAC is built with a glass end and its frame is designed so a dissecting (low power) microscope can look in this end. Microscopes are well suited for observation of aggregates in the lab because they can resolve small objects, have narrow depths of field, and can be fitted with cameras. The challenge in using microscopy is in the lighting. As the magnification increases, the microscope is collecting and focusing light from a smaller and smaller area. In the case of aggregates, only the small part of the viewing area filled with aggregates is reflecting light. The water is not. However, there may be

considerable amounts of stray light reflecting from objects in the field of view but out of focus. The human eye is pretty good at dealing with this situations. Cameras are generally not as good.

Attempts were made at viewing aggregates using a video camera which fed its signal to a Silicon Graphics Indy computer via an American Video Equipment time stamp device. The time stamp device imprinted the time precise to 1/100 th of a second so each frame could be individually identified. After the computer digitized each frame, they were transferred to a Macintosh computer for image processing. The computer used NIH Image image processing software. Although the process was somewhat successful, it suffered from lack of contrast in the video. Despite considerable experimentation with the image enhancement features of NIH Image data obtained was of questionable quality. Both the video camera and frame grabber were more than 5 years old. The smallest particle resolvable with this system was estimated to be about 50 micron diameter.

Later, size measurements were made using a Laser in-situ Scattering Transmissometer (LISST). The LISST is similar to the Malvern Particle Sizer but is designed for field deployment and uses different algorithms for processing the scattered light. Although the LISST is designed for use in the field, it can be adapted for laboratory use by fitting it with a calibration chamber then placing a cubicle in its measurement volume. The cubicle holds about 100 ml. The ROGTAC was fitted with a 10 mm diameter port into which screwed a plug. Water was withdrawn from ROGTAC using a syringe after removing the plug. Damage to aggregates was minimized in the withdrawal

process by boring out the end of the 30 ml syringe to about 8mm. Withdrawals were made slowly, again to minimize shear. Although the LISST requires 100 ml of sample volume, only 10 ml was collected from ROGTAC in each sample to avoid drastically decreasing the water level in ROGTAC. The 10ml sample was gently mixed in with 100 ml of particle free water before being placed in the LISST. This resulted in less than ideal but acceptable particle concentrations. Initial tests were done using filtered sea water as the particle free water, but later tests used distilled deionized water because it is more readily available. This change had no noticeable effect on the results. It is unlikely that cells appreciably changed their volume by up taking fresh water because LISST measurements were made immediately after mixing the ROGTAC sample with the distilled water.

Particle Aggregation

Limited tests were performed to verify that ROGTAC does indeed foster aggregation. Four runs were conducted using a mix of clay and phytoplankton *Thalassiosira weissflogii*, *TW*, particles. A mix was made so that the concentrations of the two components was approximately equal at about 100 ul l^{-1} total suspended concentration. In four runs, particles were mixed in the ROGTAC for 60 minutes. At the initiation of the experiments and at 15 minute intervals, 10ml samples were withdrawn from the barrel. A syringe with its end bored out to about 8 mm diameter was used for sample collection. This large bore was designed to prevent large shear stresses from affecting aggregates as they were drawn into the syringe. The 10 ml of suspension was

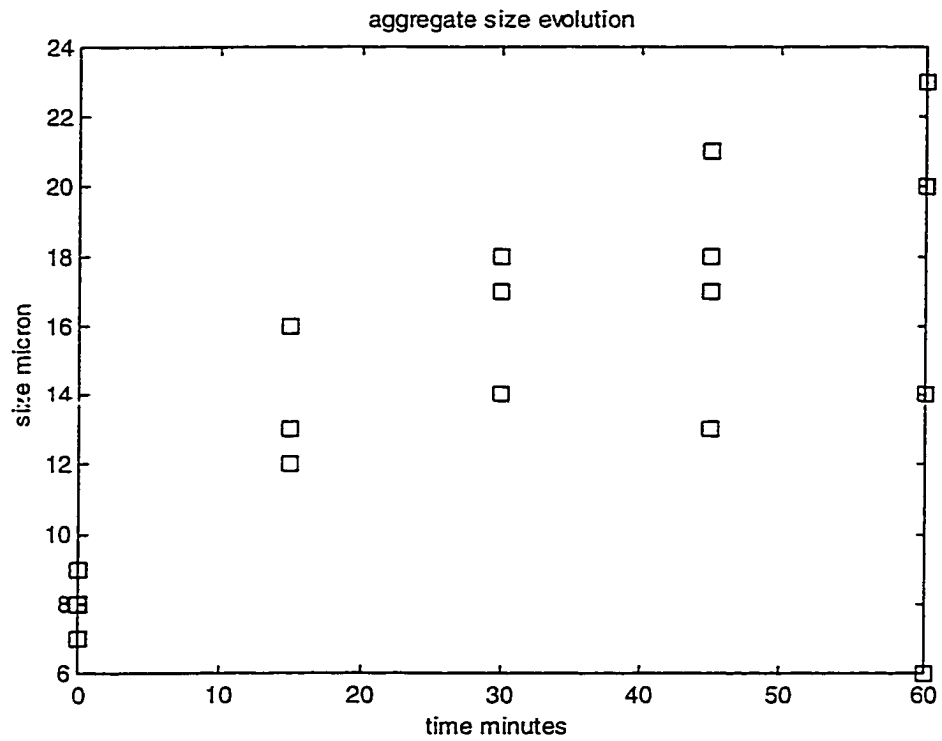


Figure 3-19 ROGTAC Aggregation

Representative aggregate sizes as measured by LISST as a function of time are provided. Four model runs were completed.

then injected into a cubicle which contained 100 ml of deionized water. This cubicle was immediately placed in a LISST to obtain size measurements. Calculating the first moment of aggregate size gave a characteristic aggregate size at each time. Figure 3-19 shows these increasing with time. A linear regression of the data reinforces this conclusion by giving a positive slope of 0.13 with a standard error of 0.04.

Proposed Two Component Model Calibration and Verification

This section discusses how ROGTAC might be used in calibration and verification of the two component model. Free parameters in the two component model include particle densities, primary particle sizes, stickiness, fractal dimensions, and the turbulent energy dissipation rates. Materials can be selected with known primary particle sizes and densities which are within the detection limits of the size measurement device chosen. Turbulent energy dissipation rates were reported earlier in this chapter. This leaves stickiness and fractal dimension to determine. These are calculated using data on aggregate size, composition, and fall velocity.

Size is the easiest to measure. The LISST has been somewhat successful. The smallest particle the LISST can observe is 5 micron and the largest is 500 micron, although size bins greater than 100 micron are sensitive to background scattering and frequently give erroneous results. Thus, if the LISST is used for size measurement, it is advantageous to choose particles with diameters greater than 10 microns. The phytoplankton species *Thalassiosira weissflogii*, has worked well. Its nominal diameter is 20 microns although LISST measurements have shown its actual size to be closer to 15

microns. Clay may be used as the inorganic fraction. Although some clay may show up in the LISST's smallest size class, much of it is not seen by the LISST until aggregation proceeds. A larger inorganic primary particle, possibly very fine quartz, would be better. With hardware improvements, the video system described in the previous paragraph would likely provide data on aggregate sizes for the larger aggregates.

Composition is not so easy to measure. Some estimate can be obtained by collecting aggregates which settle out and using standard laboratory techniques to determine their ratio of fixed and total solids. However, settling is an imperfect way to sort by size. The material collected from the bottom of a settling container at a given time will contain both small aggregates which were close to the bottom and large aggregates which fell from higher up in the column. Also, aggregates composed of heavier materials fall faster and will be over represented in the material which has sunk to the bottom. One possible method to determine aggregate composition is by epifluorescent microscopy. Holloway and Cowen (1997) used fluorescent technology to observe marine snow collected near Hawaii. A material stained with epifluorescent dye responds to light of a certain frequency by reradiating light at another characteristic frequency. In this manner material which accepts the stain will appear bright and other materials will not but will still be visible. The challenge would be transporting an aggregate to the microscope without destroying it or adapting the technique to observing aggregates in ROGTAC. Phytoplankton are sometimes observed by allowing them to settle then observing them through the bottom of a container using an inverted epifluorescent microscope. It is also uncertain if organic coatings on inorganic particles will make them also fluoresce like the

organic particles. There are a variety of stains for various applications but proflavin might be good for aggregates because it stains almost all organic matter including detritus. An even better but more challenging method would be to observe the aggregates directly in ROGTAC using epifluorescent technology. It is likely that individual particles would not be observable because in this configuration high magnification leads to limited depth of field making it difficult for the microscope to see into ROGTAC.

Fractal dimension is calculated from a series of porosity measurements. Porosity is calculated from fall velocity, aggregate composition, and size. Composition and size determination has already been discussed in the previous paragraphs so the only new piece of information needed is fall velocity. Fall velocity measurements are made by particle tracking. Many computer implemented image analysis programs have routines to do this. These routines use two images of the same area which were taken at a known and closely space time interval. The routines determine how far a particle has moved in the time between images by finding the particle on both images, calculating the distance between them, then dividing by the time elapsed between images. It sounds simple. It is actually a difficult problem because aggregates change their orientation in the flow and as they do this their appearance changes. It can be difficult to determine which blob in the first image corresponds to which blob in the second image. The methods have been explored by researches doing particle image velocimetry (Adrian 1991) and used by several marine scientists (Sternberg et al. 1996, Syvitski and Hutton 1995). Previous measurements of aggregate velocity have used stilling wells. Fall velocity is not readily measured in the ROGTAC because particle velocity due to gravitational settling is relatively small

compared with turbulent and rotational flow. This is necessary to keep particles in suspension. If ROGTAC's motors are turned off, the turbulence will die out, but by the time it does larger aggregates have already settled out. With care aggregates might be removed and placed in a settling column.

Another possible way to measure fall velocity of aggregates in ROGTAC without removing them is to analyze motion of aggregates with respect to nearby very small particles. The small particles can be assumed to have zero fall velocity. To my knowledge no such system has been built and it would require high resolution video equipment. Lighting is necessary to observe falling particles but lighting usually introduces heat to the water. Heat causes thermally driven current in the fluid which can corrupt fall velocity measurements.

Techniques exist, using state of the art video equipment, to obtain the data on aggregate size and fall velocity needed to verify and calibrate a one component aggregation model. Obtaining data on aggregate composition needed to verify and calibrate a two component model remains a technical challenge. This challenge might be partially solved if a method was found to measure aggregate fall velocities without handling and disrupting the aggregates.

NUMERICAL MODELING

A new numerical model has been written to predict the development of aggregates. This model incorporates practices from existing aggregation models and adds several new features, notably the ability to treat two types of primary particles.

Previous models have considered aggregates to be composed of one type of primary particle with a fixed size and density. Furthermore, these particles all combine to form aggregates with a constant fractal dimension. Obviously this is unrealistic, and measurements of fall velocities of aggregates of a given size show large variations. It is well known that naturally occurring aggregates found in estuaries contain a variety of materials including clay, plankton, bacteria, and detritus. Considering that the specific gravity of clay is close to 3 times that of water whereas the specific gravity of most organic matter is only slightly higher, failure to consider differences in the composition of aggregates may lead to large errors in predicting fall velocities. Furthermore, it is logical to assume that some materials preferentially attach to certain other materials more strongly. Because aggregation is a dynamic process, in which aggregates are continually being broken up, aggregates consisting of materials which bond more strongly can be more open and thus have lower densities than aggregates whose primary particles bond less strongly. An advancement in aggregation modeling is to create a model which

considers aggregates to be formed from 2 types of primary particles, each with their own characteristics. The characteristics of aggregates would depend upon the fractional composition of the particle from which they are composed.

Existing Models

Aggregation equations have been known since the early 1900's but were not useful until the advent of the computer. With the availability of computers investigators in many disciplines including atmospheric sciences, wastewater treatment, and oceanography have attempted to model particle aggregation. The models are quite similar in structure. This section will discuss the more notable aggregation modeling efforts.

Possibly the first aggregation model was produced by Fair and Gemmell (1963). Although the paper is somewhat scant on details, it appears they used Smoluchowski's (1917) equation, described in chapter one, for shear and assumed aggregated particles had no porosity. Size bins were not log spaced so the maximum size aggregate the model could treat had 20 primary particles. Upon reaching this maximum size aggregates broke up. Although the authors appeared to realize the model was too crude for useful application, they noted that chemical floc growth studies provided the incentive for their research. In another early work, Vold (1963) wrote a computer model of the growth of an aggregate by random addition of primary particles. Her model predicted the decrease in density of larger aggregates. Again, limitations in computer power limited maximum aggregate sizes to about 100 primary particles.

Valioulis and List (1984) modeled a settling basin of a wastewater treatment plant. The model was the end product of a series of studies on aggregation led by List. This model has the features of a modern model with 15 log spaced size bins. Curvilinear kernels were used to calculate particle interaction, and when calculating aggregate density, porosity was considered. Their model divided the settling basin which they modeled into 5 horizontal and 3 vertical sections for a total of 15 sections. They also relied on the work of Gelbard et al. (1980) who formally investigated log spaced size bins and called their use sectional representation. In summary, Valioulis and List's model can be considered the first modern aggregation model.

Much of the aggregation work in marine science has concentrated on modeling the aggregation of phytoplankton in the ocean. This application has assumed more importance as interest in the transfer of carbon to the seafloor by sinking phytoplankton has increased due to concerns about global climate change. Jackson may be the first oceanographer to model aggregation. His first paper on the subject (Jackson 1990) used the rectilinear model without sectional representation. The model is essentially similar to the Fair and Gemmel (1963) model, but with the benefit of 1980's computers and a simulation package. The Jackson model could support aggregates with up to 1600 primary particles. Jackson soon improved on this simple initial model. Jackson and Lochmann (1993) included the curvilinear corrections to the kernels, sectional representation (23 sections) , and variable porosity described using fractals. Jackson (1995) compared the model with results from the SIGMA mesocosm experiment (Alldredge and Jackson 1995).

Conclusions from this work include the finding that curvilinear kernels are superior and disaggregation is important. Material from disaggregating aggregates is spread over all smaller sized bins. Jackson's most recent effort (Burd and Jackson 1997) took a new direction and added curvilinear effects and fractal representation to the aggregation model of Farley and Morel (1986). Farley and Morel developed a polynomial expression for the rate mass removal by sedimentation of colloids.

Few investigators have attempted to model estuarine aggregation. Lick and coworkers wrote the most advanced existing model of aggregation applied to estuaries (Lick et al. 1992) referred to as LLZ. Although a modeling effort by Hill and Nowell (1990), referred to as H&N, was developed to model particle dynamics on the continental shelf benthic boundary layer it probably has applicability to estuaries. H&N developed two models, one treating vertical variations in aggregate concentration and one depth integrated. The objective was to determine under what conditions the simpler depth-integrated model could be used in larger scale circulation models. The following will discuss the models created by LLZ and H&N.

Both models solve the conservation equation. The change in concentration of particles of size class i at a location in the water column is determined by turbulent diffusion through the water column, settling of these particles, and movement of particles into other size classes by aggregation. This process is described by the one dimensional sediment conservation equation

$$\frac{\partial C_i}{\partial t} - \frac{\partial}{\partial z} \left(v_i \frac{\partial C_i}{\partial z} \right) - \frac{\partial}{\partial z} (WC_i) + b_i = 0 \quad 4-1$$

This is a one dimensional formulation that only considers changes in particle concentration in the vertical dimension. The one dimensional formulation frees computational resources which would be devoted to multidimensional hydrodynamic modeling for more elaborate modeling of aggregation processes. In doing this, the one dimensional formulation assumes a spatially homogenous study area.

LLZ compared models with 3, 5, and 10 size classes. They reduced the number of size classes by reducing the range of aggregate sizes treated and also increasing the size of each size class. H&N use 24 size classes. Both models have turbulent eddy viscosity vanishing at the bed and increases away from it. LLZ ran their model in 10m water depth with 11 depth bins and the turbulent eddy viscosity, v_t , varying from 0.8 to 4 cm² s⁻¹ from bottom to top. H&N use v_t equal to $\kappa u_* z$ close to the bottom and a constant value above that.

Both models calculate fall velocity using Stokes Law (equation 2-2). Both models also acknowledge that aggregates have high porosities and that porosity increases with aggregate size. H&N considered aggregates to be fractals while LLZ considered fall velocity to be related to size by a power law. As was demonstrated in chapter two, the end result of both approaches is the same. However, LLZ related the constants in the

power law to shear rates and suspended sediment concentrations where the aggregates formed.

The two models both use rectilinear kernels. H&N justify the use of the rectilinear approach by noting that some fluid flows through the porous aggregate. It is doubtful if the flow through an aggregate accounts for the huge difference between the rectilinear and, generally accepted as more accurate, curvilinear. LLZ discuss stickiness values between 0.002 and 0.5 and appear to use 0.15 in calculations. H&N use stickiness values of 1 and 0.1 in their runs.

Description of the Model

This section describes a new model which considers aggregation of two types of primary particles. Size, density, and fractal dimension for the two primary particle types may be specified. The model treats aggregation by turbulent shear and differential settling. No existing models in the literature consider two types of primary particles, all are limited to one type of primary particle. Written in Matlab, the model's code appears in Appendix A.

Governing Equation

Virtually all studies of aggregation have concerned themselves with the interaction of aggregates of varying sizes all composed of identical primary particles. Equation 4-2 forms the basis for models which incorporate only one type of primary particle. If the

numerical scheme assigns aggregates to size classes based on the number primary particles each contains, the change in number of particles in each size class is expressed as

$$\frac{dN_i}{dt} = -\sum_{j=1}^N \alpha \beta_{ij} N_i N_j + \sum_{j=1}^{i-1} \alpha \beta_{j,i-j} N_j N_{i-j} - B N_i + \sum_{j=i+1}^N K_j B N_j - \frac{W_i N_i}{H} + Q_i \quad 4-2$$

The right side of equation 4-2 consists of 6 terms. In order, they describe the following:

1) The loss of aggregates from a size class as they combine to form larger aggregates. β considers the probability of two aggregates colliding and α considers the probability of them sticking after a collision. 2) Gain of aggregates in a size class from smaller aggregates merging. Note that the two size classes which join to form an aggregate with i particles are j and $i-j$. 3) Loss of aggregates of a size class from them breaking up to form smaller aggregates. 4) Gain of aggregates in a size class from breakup of larger aggregates. This is a function of the number of aggregates in the larger size class, N_j , multiplied by the probability of the aggregate breaking up, B , multiplied by the likelihood of the broken aggregate forming aggregates of size N_i , which is represented by K_i . 5) Loss of aggregates by settling. 6) Spontaneous formation or introduction of aggregates.

When two types of primary particles are considered, equations retain the same form and same six terms. However, they expand from one dimensional to two dimensional. In equation 4-3 the first subscript indicates the number of primary particles in the aggregate and the second subscript indicates what fraction of those primary particles are of type a. By default the remainder must be of type b. A few added complexities arise

in that the interaction coefficients, α (the stickiness coefficient) and β (the encounter rate coefficient), depend on aggregate composition. Aggregates with i particles and f composition are formed from aggregates with j particles and g composition and $i-j$ particles and $(if-jg)/(i-j)$ composition.

$$\begin{aligned} \frac{dN_{if}}{dt} = & - \sum_{j=1}^N \sum_{g=1}^F \alpha_{f,g} \beta_{ifjg} N_{if} N_{jg} + \\ & \sum_{j=1}^{i-1} \sum_{g=1}^F \alpha_{f,g} \beta_{jg:i-j,(if-jg)/(i-j)} N_{jg} N_{i-j,(if-jg)/(i-j)} - BN_{if} + \\ & \sum_{j=i+1}^N \sum_{g=1}^F K_{ifjg} B_{jg} N_{jg} - \frac{W_{if}}{H} + Q_{if} \end{aligned} \quad 4-3$$

Size Classes

The previous equations account for aggregates with a given number of primary particles. If a primary particle is 1 micron and the largest aggregates are 1 mm, basic arithmetic shows that 10^9 particles can fit in the 1 mm aggregate with perfect packing. In practice aggregates do not have perfect packing, and the high porosities of aggregates decrease this by several orders of magnitude. In any case, a computer cannot treat anywhere close to 10^9 size classes, 10^2 is a challenge.

To make aggregation modeling computationally feasible, aggregates are grouped into size classes. Any aggregation model must have enough size classes to represent the

process but few enough to be computationally feasible. Size classes can be by volume, mass, or number of particles. The model described herein groups size classes by the number of primary particles in the aggregate. Aggregates in each size class have twice as many particles as those in the next smaller size class. Because the two types of primary particles are different sizes and have different fractal dimensions, the size of aggregates with a given number of primary particles will vary with the relative amount of each primary particle type it contains. There are 6 bins for fractional composition, linearly spaced. The choice of 6 bins was made in an effort to balance resolution and computational efficiency.

Aggregate Characteristics

For each of the two types of primary particles, size, density, stickiness, and fractal dimension are specified. Prior to model operation, several values that will be used repeatedly during model operation are calculated. The size of aggregates in each size class is used in other parts of the model, so it is calculated once at the beginning of the model run and stored for future reference. Aggregates are considered to be fractal, which implies larger aggregates are less dense than smaller aggregates. The basic fractal equation, equation 2-14, is extended to two particle types. If we assume both the primary particles and the aggregate have the same shape, the left hand side of equation 2-14 reduces to n , the number of primary particles in the aggregate. If the aggregate is composed of fraction h of particle type a and fraction g of particle type b, where $h+g=1$, the equation for aggregate size becomes

$$d = (hd_{0a} + gd_{0b})n^{1/(hf_a + gf_b)} \quad 4-4$$

This assumes that the size of the primary particle and the fractal dimension vary linearly with aggregate composition. Knowing the aggregate size and the number and density of the primary particles allows calculation of aggregate bulk density.

Bulk density, ρ_b , is useful in calculating fall velocity, W . In sediment transport modeling, particle fall velocity is an important parameter. It is calculated by assuming a balance between drag forces and buoyancy forces. Assuming a quadratic drag law results in the following expression:

$$(\rho_b - \rho_f)g \frac{\pi d^3}{6} = \frac{1}{2} \rho_f \pi \frac{d^2}{4} C_D W^2 \quad 4-5$$

The problem is reduced to determining the drag coefficient, C_D . If the Reynolds number, Re , is less than 1, advective terms in the equation of motion can be ignored and the drag coefficient can be solved for analytically assuming a smooth sphere and steady flow. The solution results in $C_D = 24/Re$ and is called Stokes Law, which has been previously discussed. Stokes Law can be extended for higher Reynolds numbers by including advective terms in one direction. This extension is called the Oseen solution and in this case $C_D = 24/Re + 9/2$. Comparison of these solutions with experimental data shows that for Reynolds numbers slightly greater than one, Stokes Law under-predicts C_D , and the Oseen

solution over-predicts C_D . It is also obvious that for high Reynolds numbers the Stokes Law C_D will become very small and the Oseen solution C_D will equal $9/2$, which is unrealistically large. If a C_D of the form $C_D=24/Re+K_c$ is substituted into the force balance equation, fall velocity is calculated by

$$W = \frac{-12\nu}{K_c d} + \sqrt{\left(\frac{12\nu}{K_c d}\right)^2 + \frac{4\rho g d}{3K_c}} \quad 4-6$$

where $\rho = (\rho_b - \rho_f) / \rho_f$. A K_c value of 0.6 leads to a reasonable C_D value when the Reynolds Number is near 10^2 . When the Reynolds number is small, the value of K_c is unimportant. Alldredge and Gotschalk (1988) use a variation of this approach. Note that equation 4-6 is derived using the quadratic formula. Therefore, if K_c equals zero the conditions of the derivation are invalid.

The probability of two particles adhering upon impact is denoted by α in equation 4-7. When there is only one type of particle, there is one alpha value. However, when two types of primary particles are present there are three possible values: 1) type "a" particles interacting with themselves 2) type "b" particles interacting with themselves and 3) type a particles interacting with type b particles. When two aggregates collide the probability of adhesion is proportional to the surface areas of the aggregates experiencing each of the three α values. If primary particles are the same size, and the fractional composition of the first aggregate is f "a" particles and g "b" particles and of the second h "a" particles and k "b" particles then.

$$\alpha = \alpha_1(fh) + \alpha_2(gh + fk) + \alpha_3(gk) \quad 4-7$$

This equation is only valid if all primary particles are the same size. If the primary particle size varies, the surface area of an aggregate will depend upon the square of the characteristic dimension of the primary particles, l_a and l_b . Equation 4-7 can be modified to account for this effect by substituting the primed variables from equation 4-8 for the unprimed variables in equation 4-7.

$$\begin{aligned} f' &= l_a^2 f / (l_a^2 f + l_b^2 g) \\ g' &= l_b^2 g / (l_a^2 f + l_b^2 g) \\ h' &= l_a^2 h / (l_a^2 h + l_b^2 k) \\ k' &= l_b^2 k / (l_a^2 h + l_b^2 k) \end{aligned} \quad 4-8$$

Aggregation Kernels

Considering that size bins are log spaced with each bin having twice the number of particles as the next smaller, there are three ways a bin can increase in number of particles. The next size smaller bin can interact with itself or with the bin one size smaller than itself, or the bin under consideration can interact with bins 2 or more sizes smaller. Interaction between a bin and other bins with 1/8 or fewer as many particles as that will not drive that bin out of its prescribed limits. Therefore, interactions between a larger aggregate and aggregates more than two bin sizes smaller can be treated as the interaction of the larger aggregate and a matrix of the characteristics of the smaller aggregates. Interaction of

aggregates which are within two bin sizes of that aggregate require the model to place the product aggregate in the proper bin, which may not be the bin of either of the two aggregates which interacted.

Differential settling and shear are the two aggregation mechanisms considered. Curvilinear kernels are used. A turbulent relative motion kernel proposed by Saffman and Turner (1956) is used. Hill (1992) presents an approximation to equation 2-11

$$\frac{7.5p^2}{(1+2p)^2} \quad 4-9$$

where p is the ratio of diameters of the smaller and larger interacting aggregates. Two further changes are made to the Hill (1992) curvilinear kernels, equation 2-10 and 2-11. The kernel for differential settling is multiplied by 2 to make some attempt at treating unsteadiness in the boundary layer and chemical interaction between particles. The factor of 2 multiplied by p in equation 4-9 is deleted. Because p is usually much smaller than one this increases the kernel only slightly. The resulting equation is

$$\beta_{ij} = \frac{\pi}{2} d_i^2 \left[\frac{1}{2} |W_i - W_j| + 7.5(d_i + d_j)(\epsilon/30\pi\nu)^{1/2} \right] \quad 4-10$$

The interaction kernel, β , contains information on how likely it is that two particles will interact. Differential settling is the mechanism by which aggregates with higher fall velocities impact aggregates with slower fall velocities. This mechanism is thus a function

of aggregate size and fall velocity. The fall velocity of an aggregate containing a given number of primary particles is thus a function of density of the primary particles, packing of the primary particles, which is also called fractal dimension, and size of the primary particles.

Turbulent aggregation for an aggregate with a given number of primary particles is a function of the turbulent energy dissipation rate, and the size of the aggregate which is a function of the size of the primary particles and the fractal dimension.

The form of the kernels for the two mechanisms and their ratio may be viewed in Figures 4-1 through 4-3. In these cases, particles are 1 micron diameter, fractal dimension is 1.8, and density of particles is 2.65 g ml^{-1} . Plots show β on the vertical axis for interaction of 2 sizes of particles on the 2 horizontal axes. The bins are log spaced. In these cases turbulent aggregation, which is $0.01 \text{ cm}^2 \text{ sec}^{-3}$, dominates differential settling. These plots are shown to illustrate the characteristic shapes of the kernels.

Breakup

After a sufficient amount of time, the resulting size distribution of aggregates is a balance between formation and breakup of aggregates. Breakup occurs because turbulent variations in flow impose stresses on the aggregates. As discussed in chapter two, there is debate as to whether breakup occurs by aggregates fracturing approximately in half or by primary particles being stripped off the outside of aggregates. This debate is not resolved

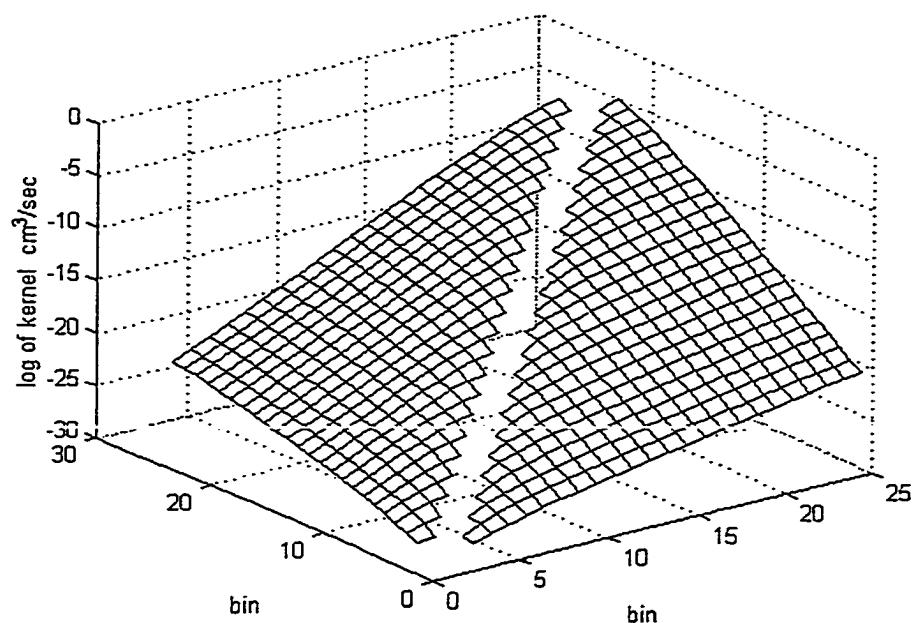


Figure 4-1 Differential Settling Kernel

The natural log of the differential settling kernel is plotted as a function of interacting bins. Aggregates in the smallest bin are 1 micron in diameter and in the largest bin, about 8 mm in diameter. Primary particles are 1 micron in diameter and have densities of 2.65 g ml^{-1} . The fractal dimension is 1.8. The gap in the middle occurs because for aggregates which have the same fall velocities, the kernel equals zero. The log of zero is undefined.

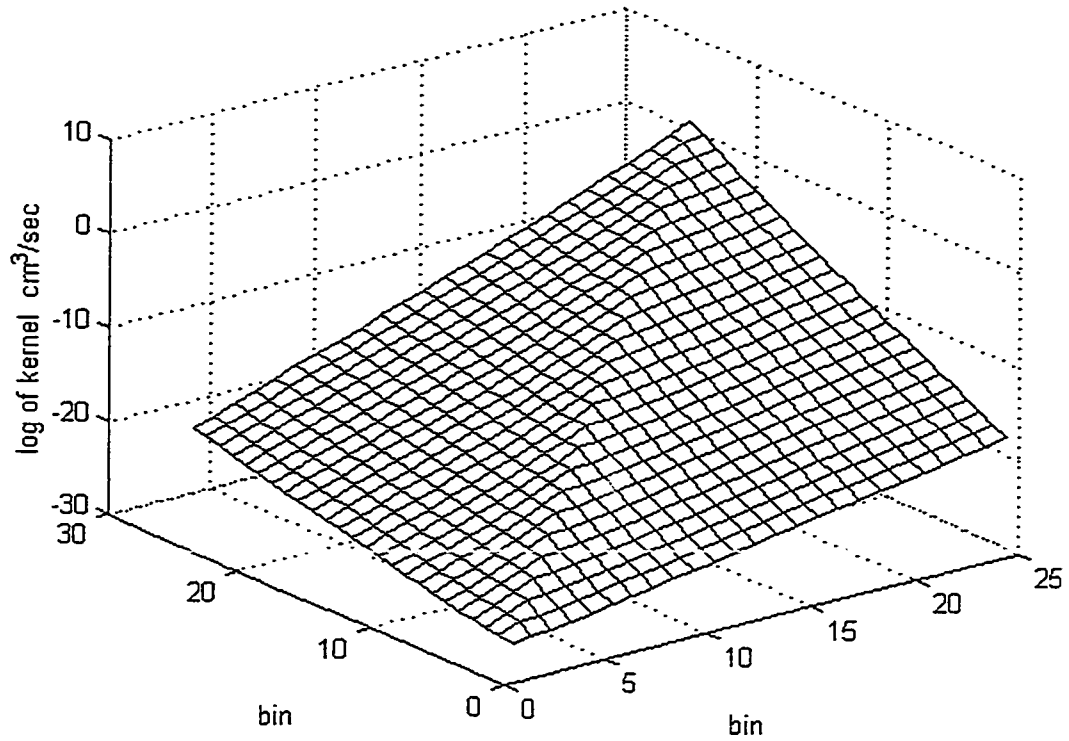


Figure 4-2 Turbulent Aggregation Kernel

The natural log of the turbulent aggregation kernel is plotted as a function of interacting bins. Aggregates in the smallest bin are 1 micron in diameter and in the largest bin, about 8 mm in diameter. Primary particles are 1 micron in diameter with a density of 2.65 g ml^{-1} . The fractal dimension is 1.8. Turbulent aggregation is $0.01 \text{ cm}^2 \text{ sec}^{-3}$.

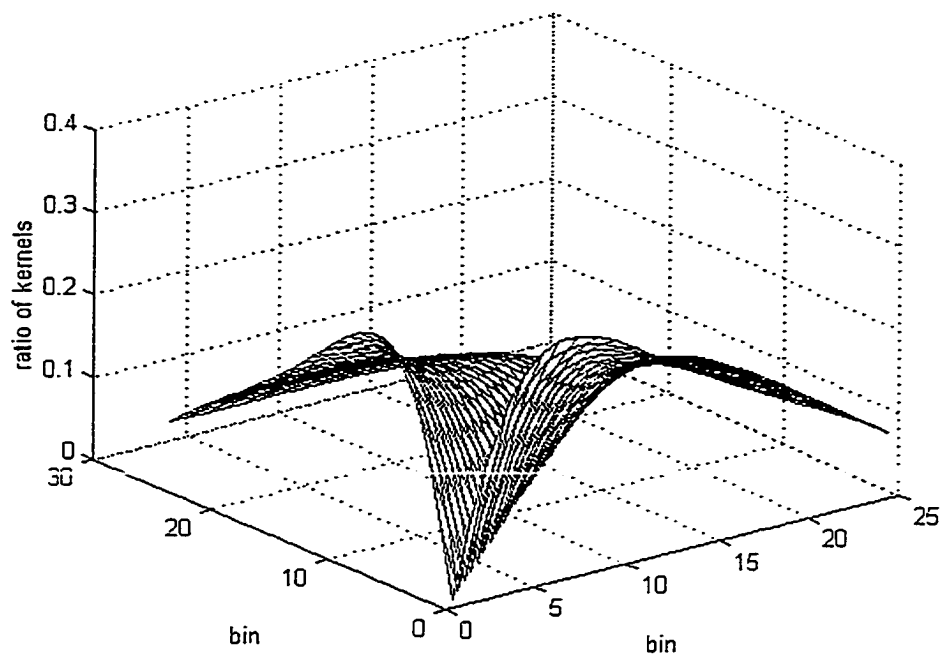


Figure 4-3 Ratio of Kernels

The ratio of the differential settling kernel to the turbulent aggregation kernel is plotted as a function of interacting bins. Aggregates in the smallest bin are 1 micron in diameter and in the largest bin, about 8 mm in diameter. Primary particles are 1 micron in diameter with densities of 2.65 g ml^{-1} . The fractal dimension is 1.8. Note that in this case, the turbulent aggregation kernel dominates.

so the computational method used in this model will be a compromise. Material from broken aggregates is spread evenly with respect to aggregate size to smaller bins. The Kolmogorov microscale, the size of the smallest eddies, is calculated as $\lambda=(\nu^3/\epsilon)^{1/4}$, where ν is kinematic viscosity and ϵ is turbulent energy dissipation. In each time cycle, all aggregates one size bin larger than λ are broken up. Fifty percent of those the same size as λ are broken and twenty five percent of those one bin smaller than λ are broken.

Recentering Bins

As particles are added and subtracted from a bin, the size of the aggregate in a bin will "walk" away from the center of the bin. To keep the model functioning, the aggregate size for the bin must be brought back to the center of the bin. Thus, if the size of the aggregates in a bin are larger than they should be for that bin, some particles will be placed in the next larger bin. The model remembers the number of "a" primary particles, the number of "b" primary particles, and the number of aggregates in each bin. For this discussion, particle and aggregate counts for a bin are contained in variables a_0 , b_0 , and n_0 . Information for adjacent bins is contained in similar variables subscripted 1 and 2. Determining how many particles are shifted from a bin gives rise to 6 unknowns; a, b, and n for each of the two bins. Determining 6 unknowns requires 6 equations. These equations are conservation of a and b particles, conservation of aggregates, the sizes of the two bins receiving reapportioned aggregates, and maintaining fractions of a and b particles in the bins. After some algebraic manipulation, the equations in Table 4-1 result. Equations are slightly different if a_0 equals zero to avoid a zero division error.

Once the entire aggregate matrix has been distributed to the proper sizes a similar process must be done for fractional composition. The inputs are again the numbers of each particle type, a_0 b_0 ; number of aggregates, n_0 ; and the fractional composition of the bins to which the aggregates will be distributed, ϵ_1 , ϵ_2 . Again this leads to 6 equations and 6 unknowns. The equations are conservation of primary particles a and b, conservation of aggregates, specified fractions of the two end members and insuring aggregates in the two end members have the specified size. After some algebra the equations in Table 4-2 are formed.

Table 4-1 Size Re-Center Code

```

if a0==0
  a1=0;
  a2=0;
  b1=(x1*x2*n0-b0*x1)/(x2-x1);
  b2=b0-b1;
  n1=n0-b2/x2;
  n2=n0-n1;
else
  a1=(x1*x2*n0-x1*(b0+a0))/((x2-
x1)*(1+b0/a0));
  b1=a1*b0/a0;
  a2=a0-a1;
  b2=b0-b1;
  n1=(a1+b1)/x1;
  n2=n0-n1;

```

Matlab computer code used to redistribute aggregates to center bins with respect to size.

Table 4-2 Fractional Composition Re-Center Code

```

b2=(f1*(a0+b0)-a0)*(1-f2)/(f1-f2);
a2=f2*(a0*(f1-1)+f1*b0)/(f1-f2);
a1=a0-a2;
b1=b0-b2;
if (a0+b0)==0
    n1=0;
else
    n1=n0*(a1+b1)/(a0+b0);
end
n2=n0-n1;

```

Matlab computer code used to redistribute aggregates to center bins with respect to fractional composition

Step Size

A bin having a small number of aggregates may interact strongly with bins with many aggregates. When this occurs, the bin may be left with a negative number of aggregates at the end of an iteration, which, of course, is physically impossible. If this occurs the time step is reduced and the iteration rerun. If the model runs for several time steps without this error occurring the time step is increased up to a maximum value, usually 30 seconds. In some cases, successive reduction of the time step may leave it very small. In order to alleviate this problem, if the negative number of particles in a bin is fewer than 1×10^{-10} , the bin is set to zero and the time step is not further reduced. This insures stability of the model but causes a very small violation of conservation of mass. Therefore, the amount of mass lost in the operation is displayed so the operator can insure it is negligible. If the aggregates in a bin become outside the size or composition range of

that bin they are placed in the correct bin. This prevents the repositioning algorithm from calculating negative numbers of aggregates in bins.

Discretization Tests

To make modeling of aggregation feasible, aggregates of similar sizes must be grouped into log spaced bins. The number of bins used is a tradeoff between computation time and resolution. This section will explore how to optimize the tradeoff.

Previous models have arbitrarily chosen bin size, although some have tried various numbers of bins to determine minimum acceptable resolution. As the number of bins decreases and bin size increases, the number of particles in each bin must increase to insure conservation of mass.

A preliminary analysis of this situation compares interaction of 2 bins and the case where the two bins are split into 3 bins each for a total of 6 bins. In this case the equation 2-1 becomes:

$$c_{ij} = \sum_{i=1}^3 \sum_{j=1}^3 \alpha \beta N_i N_j \quad 4-11$$

where the N 's equal one third of the N 's in equation 2-1. If α and β do not vary, the above equation simplifies to $9N/3 = N/3$. In this simplified analysis, the number of bins has no effect on the result of the aggregation model.

A one component aggregation model was written such that α and β were held constant, but bin size could be varied. It was used to see whether there is a maximum bin size above which model performance degrades. The model was run for 200 iterations with an initial number of primary particles. The aggregate size spectrum varied from 1 to 16777216 particles and was log spaced into the required number of bins. Figure 4-4 shows results for 5, 10, 25, and 50 bins. It appears that above 25 bins the number of bins does not matter, but having fewer bins introduces an artificially fast aggregation rate.

The alternate test of an aggregation model is to set the smallest bin at a fixed number of particles and remove the particles in the largest bin by setting it to zero. Figure 4-5 shows the calculated number of particles in bins after 10000 iterations for a five bin and a twenty five bin model. The agreement appears to be pretty good. The peak is $1.9e7$ for the 5 bin model but $2.28e7$ for the 25 bin model. However, when the number of particles in each system is totaled, the 25 bin model has 4 times as many particles as the 5 bin model.

The test was run again to compare the cumulative number of particles if 5, 15, 25, and 40 bins are used and the results are shown in Figure 4-6. Again 25 bins are required to obtain consistent answers. In conclusion, it appears that both the calculated aggregation rate and steady state particle concentrations can be affected if bin sizes are too large. It appears each bin should not have more than twice the number of particles in the next size smaller bin.

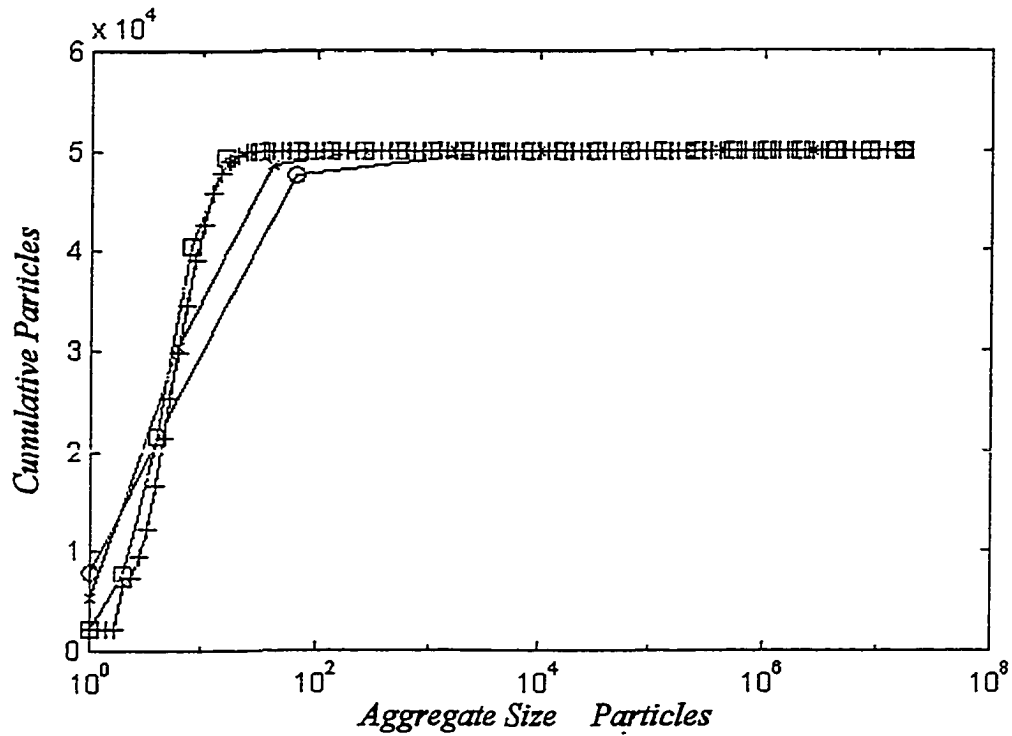


Figure 4-4 Cumulative Number of Particles Conserved - Binsize

The cumulative number of particles from smallest to largest bins is shown. An initial number of 50,000 particles was modeled for 200 iterations. The number of bins was varied and is denoted by the following symbols: \circ 5 bins; $*$ 10 bins; \square 25 bins; $+$ 50 bins.

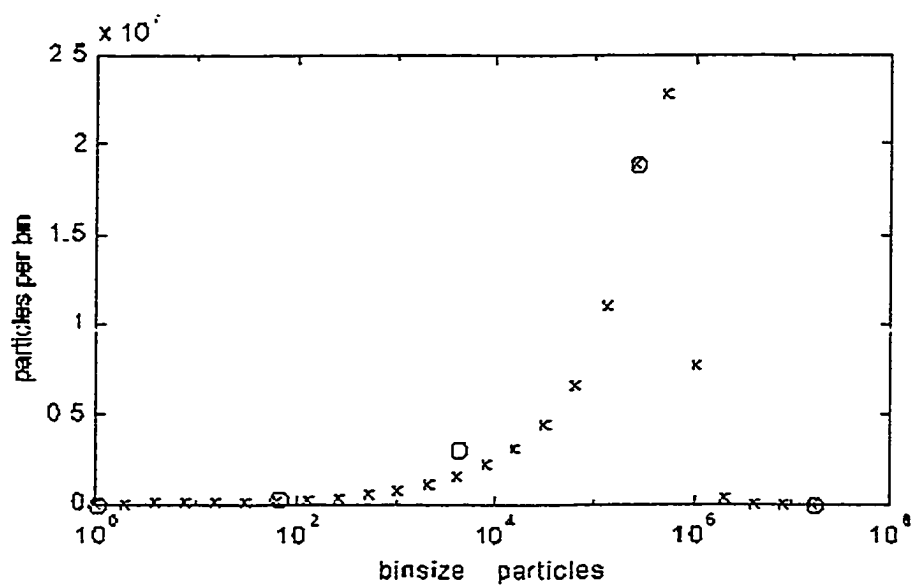


Figure 4-5 Number of Particles Per Bin at Steady State - Binsize

The number of particles per bin is plotted as a function of bin size as the model approaches steady state conditions after 10,000 iterations. The model was run twice, once with five bins and once with 25 bins. Five bins is denoted by o and 25 bins is denoted by x.

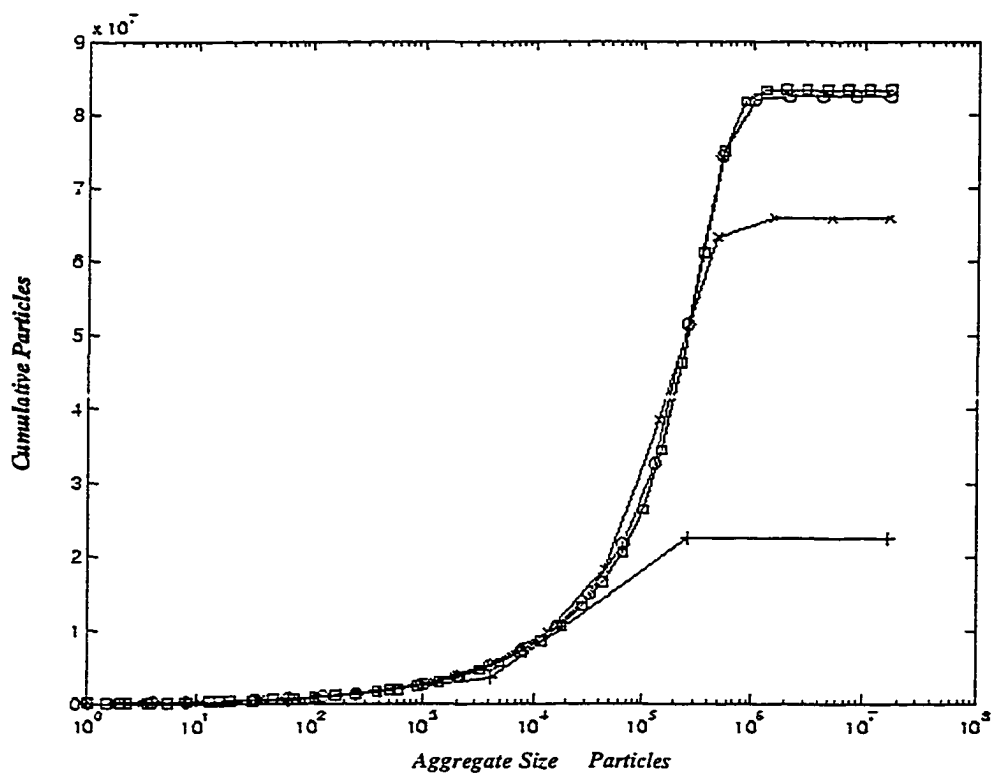


Figure 4-6 Cumulative Number of Particles at Steady State - Binsize

The cumulative numbers of particles in existence when the model approaches steady state conditions after 10,000 iterations is shown. The number of primary particles is set to 10^5 and the number of the largest aggregates is set to zero. The model was run four times with 5, 15, 25, and 40 bins. Symbolism is: + 5 bins; x 15 bins; o 25 bins; and □ 40 bins.

Model Testing

Any new model must be tested to insure that it works properly. Models can fail to represent reality for many reasons including: 1) algorithms included in the model do not adequately represent reality, 2) algorithms are not properly translated into computer code, and 3) incorrect constants are used. Although it might seem logical to test the model by comparing its output with a data set, this approach has limitations. It requires that constants be known fairly accurately. In aggregation studies, this is not the case. Even if a given data set can be matched by appropriate selection of constants, it does not allow one to say with confidence either that the model or the constants are correct. It is quite conceivable that an incorrect model with carefully selected, albeit incorrect, constants may agree with a small number of data sets. Therefore, it is important to test a model to see that it behaves in a reasonable manner. That is; it conserves mass, gives symmetric results given symmetric inputs, and converges to a steady state at long times. Symmetric results given symmetric inputs means that if initial conditions are equal numbers of identical primary particles, at the end of the run the plot of number of aggregates as a function of size and composition will look symmetric as a function of composition. Essential tests are summarized as follows.

1. Tests with one type of particle

A Is mass conserved for one type of particle? (repeat for a and b particles)

B With a constant number of primary particles and removal of large particles is steady state achieved for both types of particles?

2. Tests with 2 types of particles

A Is mass conserved?

B Is steady state achieved?

C Are results symmetric?

Mass conservation is tested by giving initial conditions of all single particles, modeling their aggregation, and confirming that the same number of particles are present at the end of the run. Figure 4-7 shows the evolution of the number of primary particles in each bin. With time the particles move to the largest bin until they are almost all there. The 36 lines are spaced every 100 seconds for 1 hour. Evolution speed is a function of particle concentration and particle stickiness. In these tests, it is intentionally set for fast aggregation to make testing expeditious. At the beginning there are 10^6 particles. At the end of the run there are 1.0009×10^6 particles. This 0.09% error is likely due to rounding and various assumptions in the model but is small. An identical test for b particles was also conducted. The results are identical to Figure 4-7, as they should be. Mass is conserved for one type of particle in tests of both a and b particles.

The test for steady state is a test for convergence. For this case the concentration of primary particles is held constant and concentration of the largest particles is set to zero. After a sufficient amount of time the plot of number of particles as a function of bin size, Figure 4-8, stabilizes. The model was run for 10,000 sec and Figure 4-9 shows the

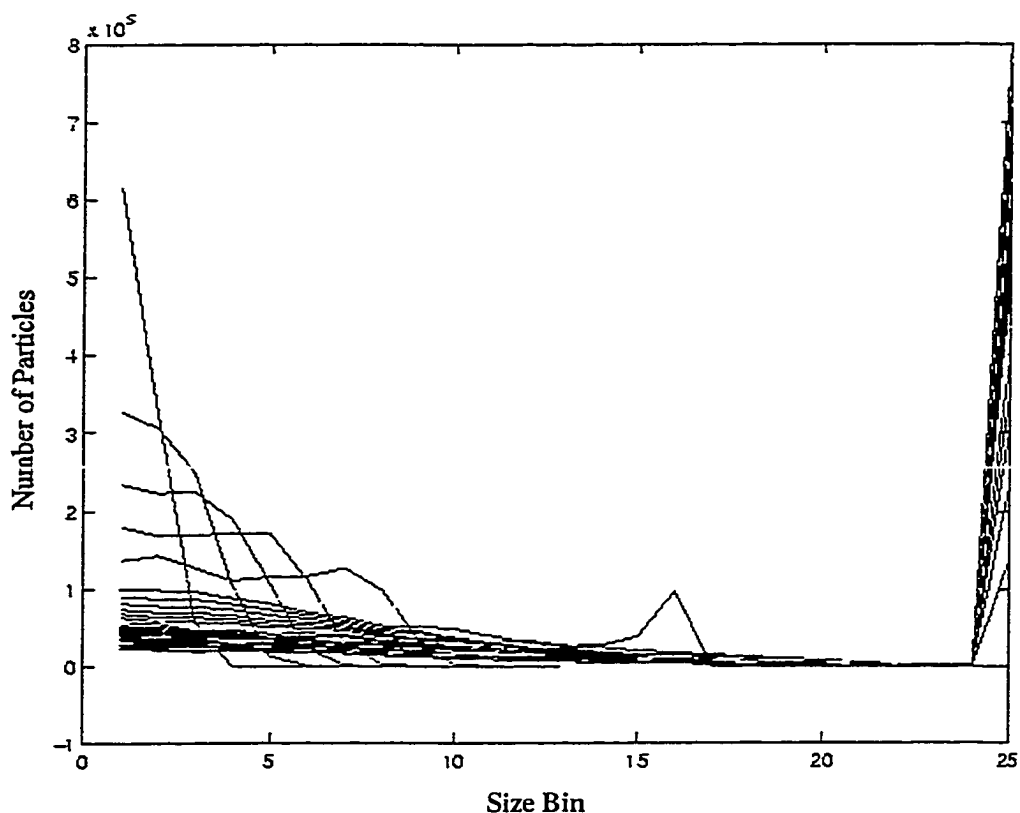


Figure 4-7 Profile Evolution, One Component

The number of primary particles in each bin is shown. Each line represents a time. At time zero all particles are in bin 1. As the model run progresses, particles move into the larger bins which are to the right and the mass in bin 1 decreases. When particles reach bin 25, they interact strongly with bins close to the same size removing mass from them. This verification version of the model does not include aggregate breakup. If it did, particles in bin 25 would be redistributed to smaller bins and the sharp discontinuity between bins 24 and 25 would be removed.

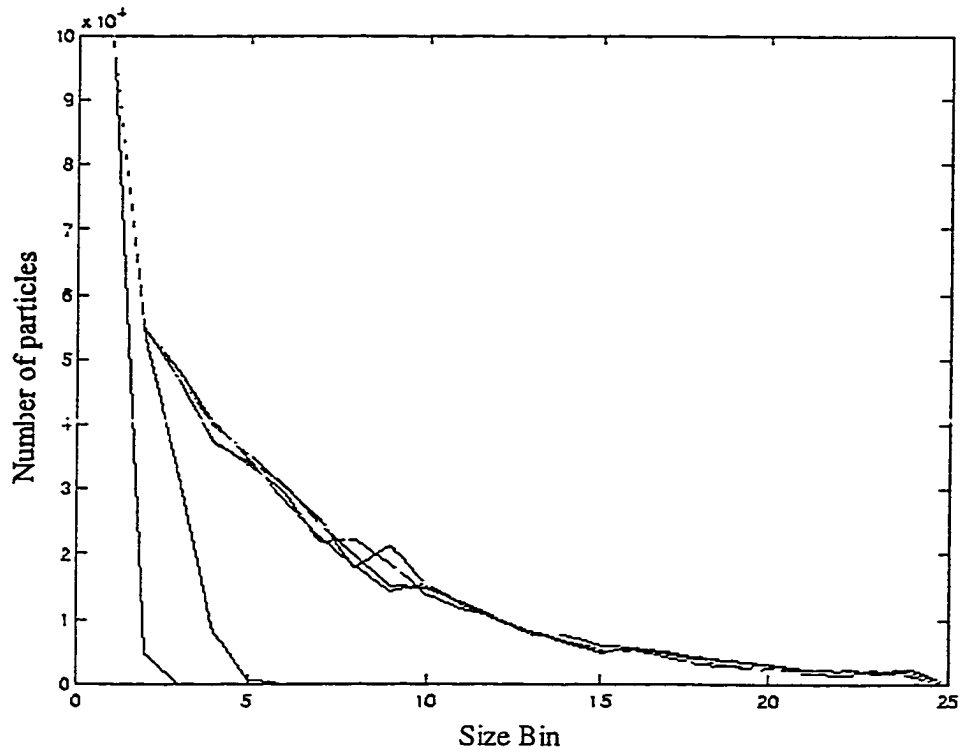


Figure 4-8 Steady State Convergence Profile, One Component

This plot shows the number of primary particles in each bin as steady state is approached. Each line depicts conditions at a time. The number of particles in bin one is held constant at 10^5 and the number of particles in bin 25 is held constant at zero. At the start of the run, all bins other than bin one have no particles. As the run progresses and particles aggregate, they move to larger bins and the smooth curve shown in this figure develops.

total number of particles in the system. Again, it stabilizes with small oscillations which do not materially affect results.

Convinced that model output is reasonable for one type of particle, we repeat tests with two types of particles. The particles are given identical characteristics and are present in the same quantities. In conservation of mass test, after 1 hour there are 1.2002×10^6 particles instead of 1.2×10^6 particles. The mass has mostly gone to the largest aggregate size as Figure 4-10 shows. Note that as the aggregates grow their composition become uniform. There is no bin centered at fraction 0.5 so the largest aggregates are split between the 0.4 and 0.6 fractional bins. Mass is conserved when two particles interact in the model.

The second test is for steady state and symmetry. The procedure is similar to that which produced Figure 4-8 but because the two component features of the model are used, a two dimensional figure (Figure 4-11) results. The steady state result is symmetric and behaves qualitatively correctly. At steady state there are small oscillations in both the total number of particles and the number in each bin. It is uncertain if these are due to the system or its mathematical representation. In any case they are small enough they do not materially affect results.

The model thus passed all the essential tests.

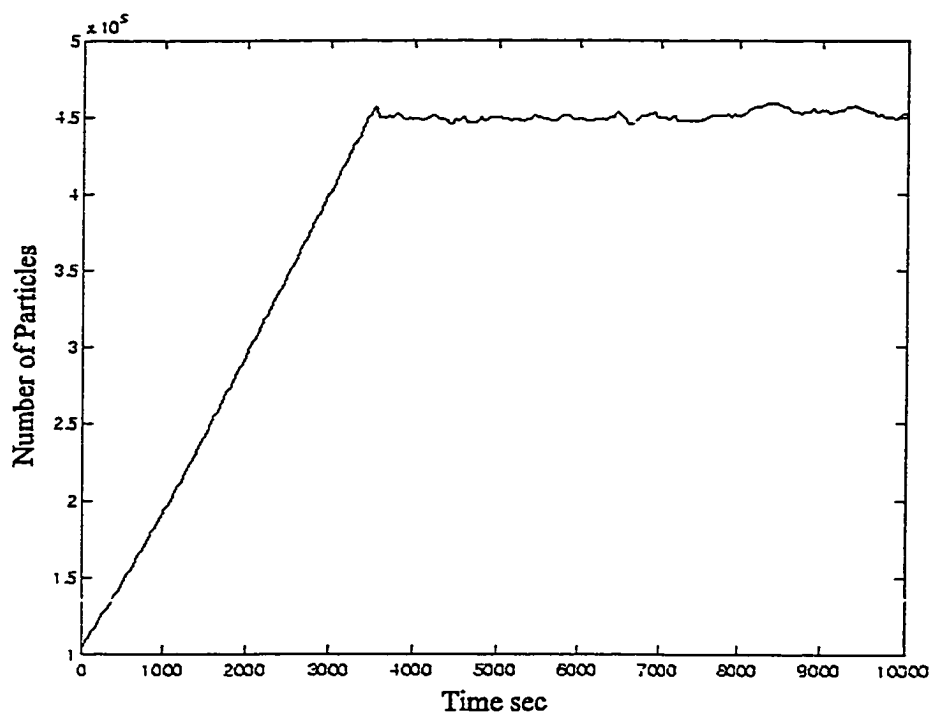


Figure 4-9 Steady State Total Number of Particles, One Component

The total number of particles in all bins as steady state is approached is shown. In this case, the number of particles in the smallest bin is held constant and the number in the largest bin is held at zero. After enough time has elapsed, the number of particles stabilizes with mild oscillations.

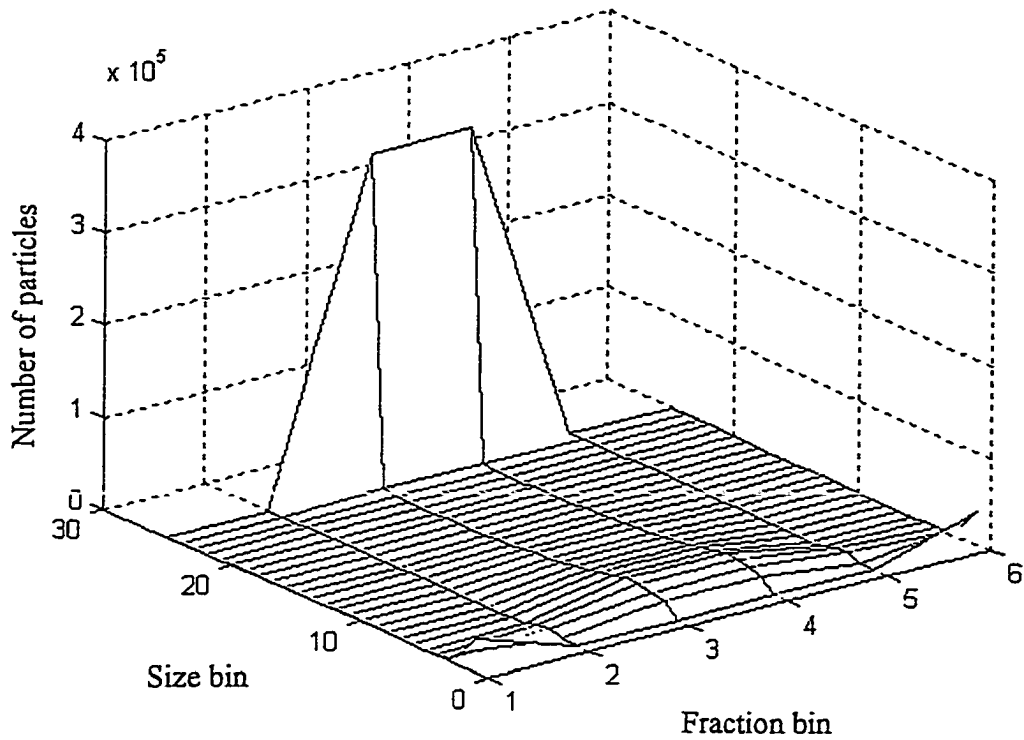


Figure 4-10 Particle Conservation, Two Components

This plot shows the number of particles present in each bin after aggregation is simulated for 33 hours. Initially, all particles were primary particles located in the smallest bins, the forward left and right corners of the plot. Both particle types were the same with densities of 2 g ml^{-1} , size of 5 microns, and fractal dimensions of 1.8. Particles were conserved in this run and there was no breakup of aggregates.

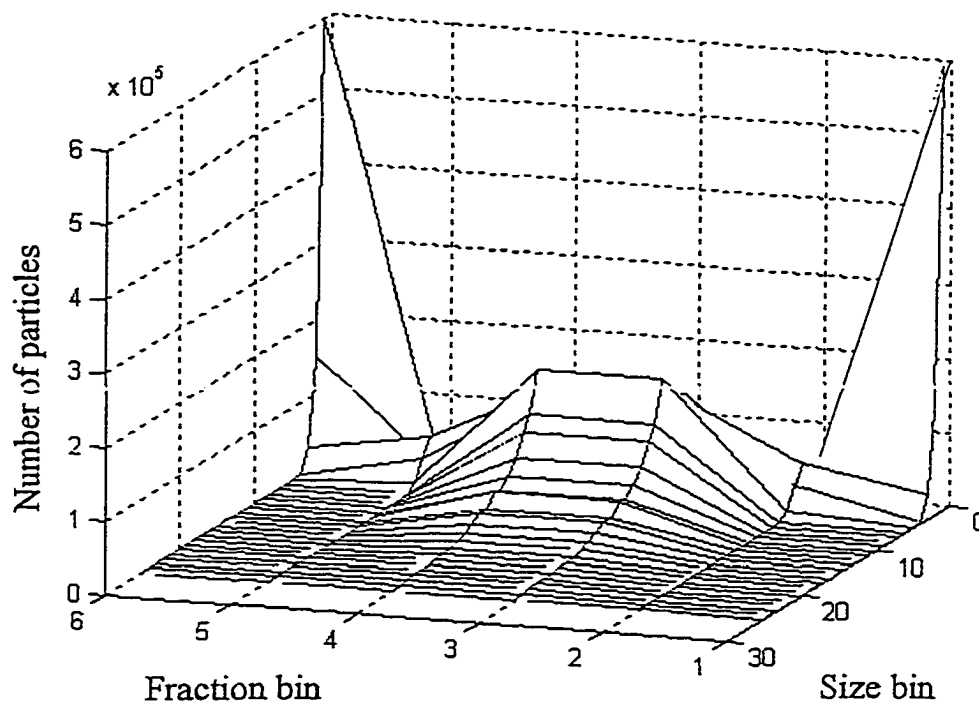


Figure 4-11 Steady State, Two Components

In this simulation, the number of primary particles is held constant at 6×10^5 a particles and 6×10^5 b particles. The number of aggregates in the largest bin is held constant at zero. The plot shows the steady state condition. Both particle types are the same with densities of 2 g ml^{-1} , size of 5 microns, and fractal dimensions of 1.8.

Effect of Stickiness

Initial modeling efforts investigated effects of the stickiness parameter. This was done by modeling an initial concentration of primary particles aggregating and settling. Aggregate breakup was not considered. The layer modeled is 100 cm thick, so the fraction of particles in a bin removed during a time step, dt , is given as $1-W/100*dt$ where W is the settling rate. Size and fractal dimension are held constant at 5μ and 2, respectively. Particles of type “a” have a density of 2.65 g ml^{-1} while those of type “b” have a density of 1.1 g ml^{-1} . Stickiness coefficients varied. Three coefficients describes how likely particles stick together if they encounter one another. The symbol α_1 represents the ability of a particles to stick to themselves; α_2 represents a particles sticking to b particles; and α_3 describes b particles sticking to each other.

Table 4-3 contains the total number of particles after 3500 seconds of simulation time and the ratio of a particles to b particles. Initially there are 12×10^5 particles which are half a and half b. They are evenly distributed across the size fractions. Table 4-3 demonstrates the obvious and expected result that sticky materials aggregate more rapidly and settle out. After the modeled period there is over 6 times more material remaining in the water if all the stickiness coefficients are 0.1 instead of 1. When α_1 is large, “a” particles are more easily removed and the ratio of a to b is small, whereas when α_3 is large, b particles are more easily removed and the ratio of a to b particles is large. The stickiness between particle types, α_2 does not have a great effect on the ratio. However, it is very important to the removal of particles and the total number of particles is smaller if α_2 is

larger. Note that when all α values are the same the ratio is close to one. This indicates that variations in the stickiness of particles to themselves, not the relative densities, dominate the ratio of particle types found in aggregation dominated particulate processes.

Table 4-3 Effect of Stickiness

run	α_1	α_2	α_3	total particles	ratio a / b
L1	1	1	1	1.78e5	0.983
L2	1	0.1	1	3.25e5	0.976
L8	1	0.1	0.1	6.12e5	0.626
L9	1	1	0.1	2.57e5	0.650
L10	0.1	1	1	2.53e5	1.49
L11	0.1	0.1	1	6.12e5	1.49
L12	0.1	0.1	0.1	11.1e5	0.978
L13	0.1	1	0.1	3.18e5	0.977

Ratio a/b is the ratio of the number of a particles to the number of b particles present.

Variation of Fall Velocity

This section investigates the ability of the two component model to explain variation in aggregate fall velocity. If the flux of suspended material is mostly in aggregated form as those who have observed aggregates have reported, it seems likely the variation in fall velocity can be explained in term of aggregation processes. Model inputs which affect fall velocity are primary particle density, size, and fractal dimension. Note that fractal dimension and primary particle size control aggregate porosity.

Experimental Results

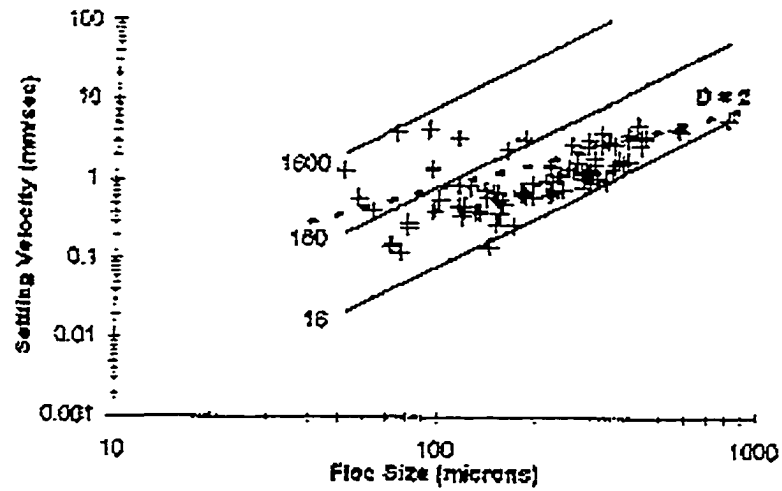
Figure 4-12 shows field measured fall velocity data from Dyer and Manning (1999), and Figure 4-13 shows similar data from Hawley's (1982) presentation of Chase's (1979) data. Data from any of several other investigators would be similar. It is illustrative to note that Hawley used a linear scale whereas Dyer and Manning used log plots. Log scales obscure increases in scatter of fall velocity with aggregate size. Although the three plots are different, variation in fall velocity increases or stays constant as aggregate size increase. Fall velocities of similarly sized aggregates typically vary by a factor of 10.

Analytical Results

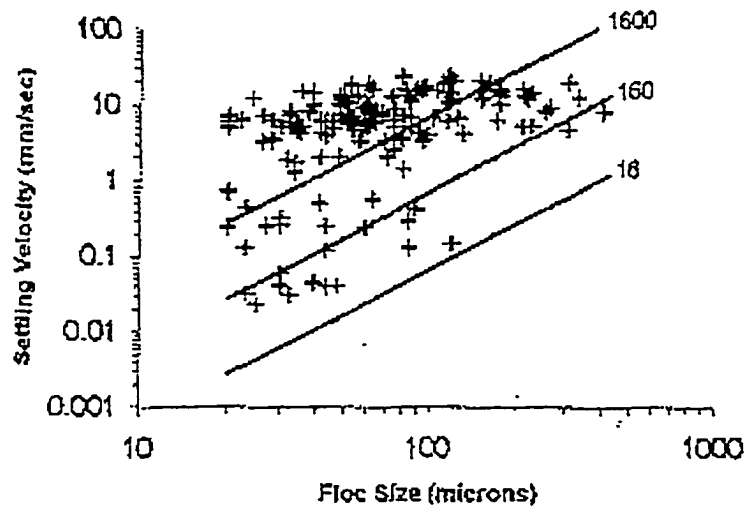
First, we will consider how variation in primary particle characteristics accounts for variation in aggregate fall velocity using the fractal equation and Stokes Law, not the model. To achieve this a fall velocity formula was derived by integrating the fractal view of aggregates into equation 4-6 to obtain equation 4-12.

$$W = \frac{-12\nu}{K_c d} + \sqrt{\left(\frac{12\nu}{K_c d}\right)^2 + \frac{4\rho g d^{f-2}}{3K_c d_0^{f-3}}} \quad 4-12$$

The behavior of this equation was investigated. First, primary particle density was varied while primary particle size and fractal dimension were held constant. For particles



Fall velocities in the Elbe Estuary, from Dyer and Manning (1999).



Fall velocities in the Tamar Estuary, from Dyer and Manning (1999).

Figure 4-12 Fall Velocity Measurements
The horizontal lines represent densities in kg m^{-3} .

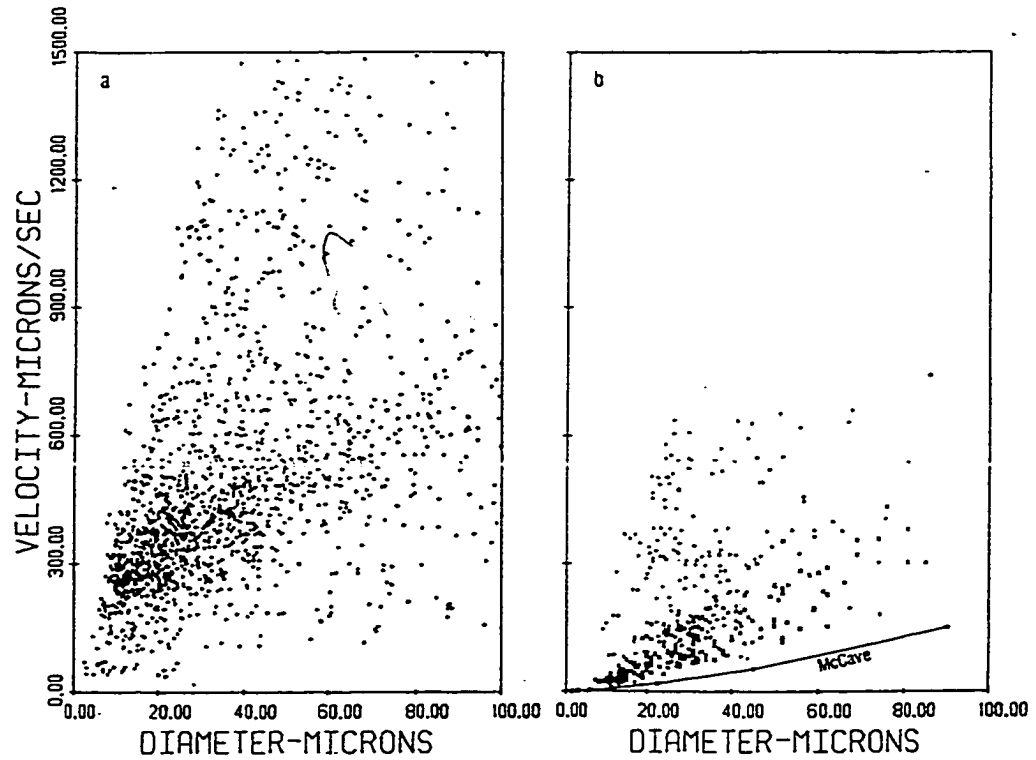


Fig. 1. (a) Lacustrine aggregate settling velocities of Chase [1977, 1979]. The bulk of the particles are concentrated in a band between about $300 \mu\text{m/s}$ at $15 \mu\text{m}$ and $700 \mu\text{m/s}$ at $100 \mu\text{m}$; a secondary concentration exists between $300 \mu\text{m/s}$ at $15 \mu\text{m}$ and $1500 \mu\text{m/s}$ at $50 \mu\text{m}$. (b) Marine aggregate settling velocities of Chase [1977, 1979] (pluses) and Kawana and Tanimoto [1976, 1979] (crosses). Two populations with trends similar to those of the lacustrine aggregates are evident. The line shows the settling velocities predicted by McCave [1975]. Note that the velocities are much less than the lacustrine ones.

Figure 4-13 Fall Velocity Measurements

Fall velocity measurements for natural aggregates made by Chase (1979), taken from Hawley (1982).

with densities of 2.65 and 1.1 g ml⁻¹, fall velocities were found to differ by somewhat more than 1 order of magnitude as Figure 4-14 shows.

Second, primary particle size was varied while fractal dimension and density were held constant. It is somewhat uncertain how primary particle size and fractal dimension relate in real aggregates. However, with a constant fractal dimension of 2 and density of 2.65, particle diameters of 1 and 10 microns give fall velocities shown in Figure 4-15. The aggregate with the larger primary particles has the larger fall velocity.

Third, fractal dimension was varied while primary particle density and size were held constant. Holding density at 2.65 g ml⁻¹ and primary particle size at 5 micron but varying fractal dimension from 1.5 to 2.5 generates Figure 4-16. The fractal dimension of 2.5 gives the faster fall velocities. Variation in fractal dimension causes variation in fall velocity to increase strongly with aggregate size.

Finally, both density and fractal dimension were varied. In this instance, a particle density of 2.65 g ml⁻¹ and fractal dimension of 2.5 is compared with a particle density of 1.1 g ml⁻¹ and fractal dimension of 1.5 in Figure 4-17. Particle diameter was held at 5 microns. The variation in fall velocity for a 1 mm aggregate in this scenario is greater than 3 orders of magnitude.

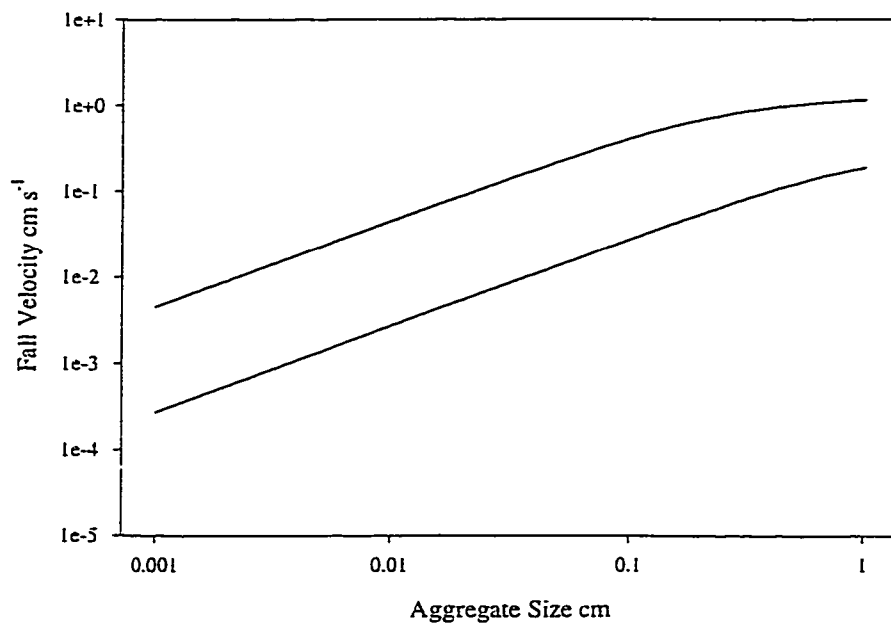


Figure 4-14 Particle Density - Fall Velocity Relationship

The effect of particle density on fall velocity is shown. The upper line plots fall velocities of aggregates containing primary particle with a density of 2.65 while the lower line is for aggregates whose primary particles have a density of 1.1. Fractal dimension is held at 2 and the particle size is held at 5 microns.

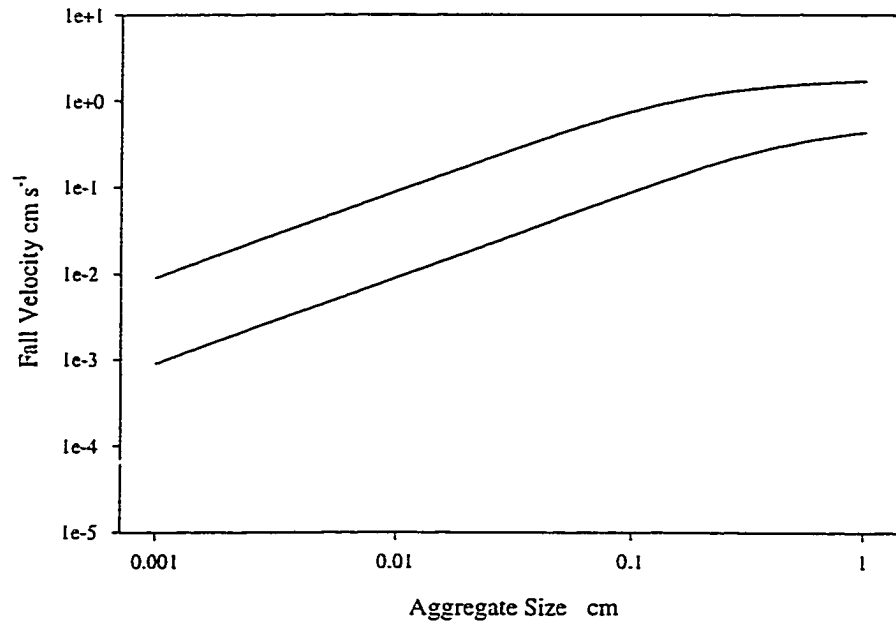


Figure 4-15 Particle Size - Fall Velocity Relationship

The effect of particle size on fall velocity is shown. The upper line represents aggregates containing 10 micron particles while the lower line represents aggregates containing one micron particles. Fractal dimension is held at 2 and density at 2.65.

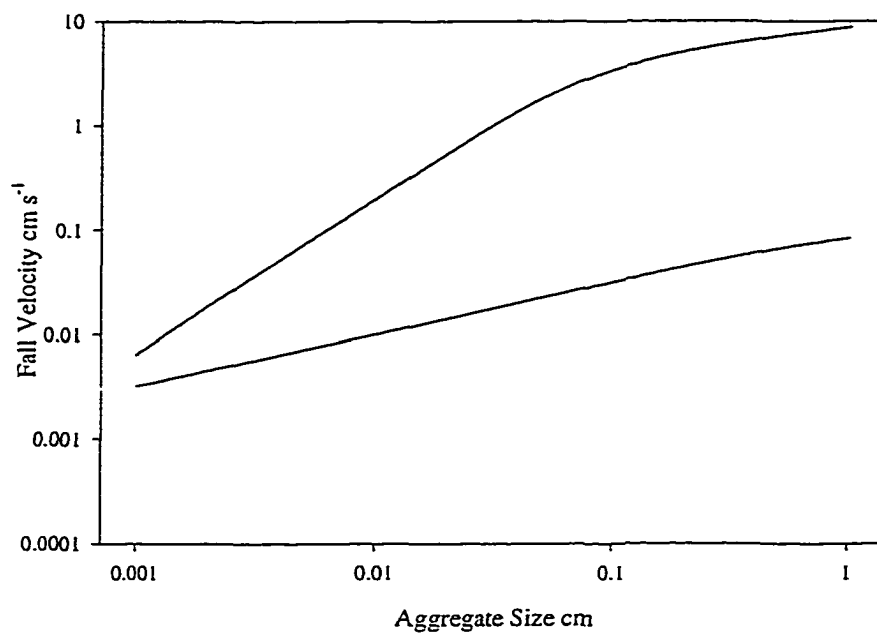


Figure 4-16 Fractal Dimension - Fall Velocity Relationship

The effect of aggregate fractal dimension on aggregate fall velocity is shown. Fall velocities depicted by the upper line are for aggregates with fractal dimensions of 2.5 whereas the lower line is for aggregates with fractal dimensions of 1.5. Density is held constant at 2.65 g ml^{-1} and primary particle size is held constant at 5 microns.

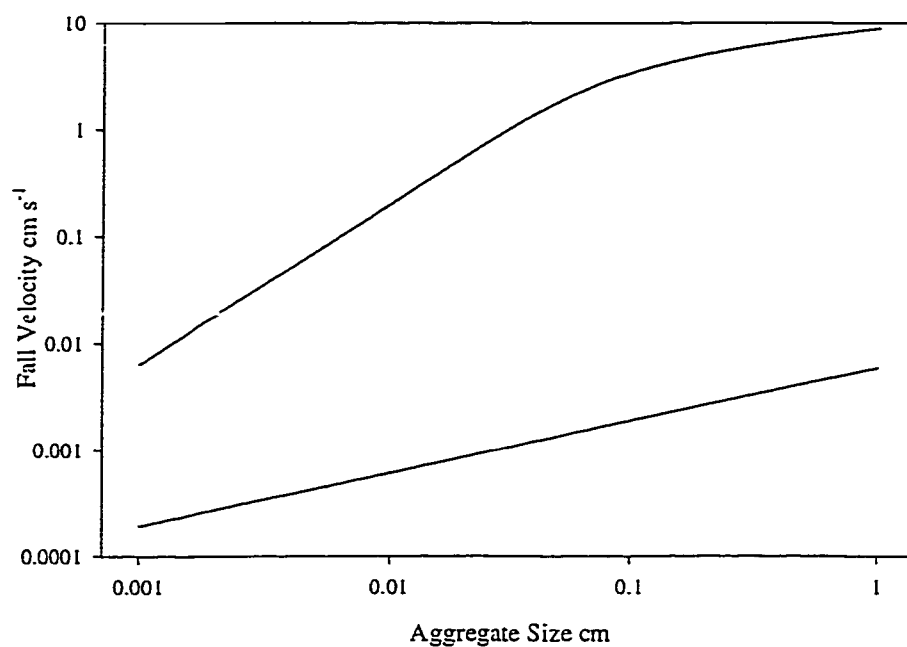


Figure 4-17 Fractal Dimension and Density - Fall Velocity Relationship
The effect of both aggregate fractal dimension and particle density on fall velocity is shown. The upper line represents a fractal dimension of 2.5 and density of 2.65 g ml⁻¹ while the lower line represents a fractal dimension of 1.5 and density of 1.1 g ml.

These cases demonstrate that the variation in primary particle characteristics may explain the variation in fall velocity that has been found in field measurements. Variations in primary particle size and density increase variation in fall velocity such that the variation appears constant in a log-log plot. Variation in fractal dimension increases fall velocity such that the variation appears to increase in a log-log plot. Thus, variation in fractal dimension has a powerful effect on variations in fall velocity.

Although Figures 4-14 through 4-17 show that appropriate mixing of varying primary particles could cause large scatter in fall velocities of aquatic aggregates, it is necessary to do some runs with the model to see if the model represents this. The cases presented in Table 4-4 were run in a model configured such that the numbers of primary particles were held constant and aggregates are removed by settling, assuming a 1 m thick mixed layer.

Figures 4-18 through 4-23 show the number of primary particles in each size bin. The numbers shown on the plots are the base 10 log of the number of primary particles in that bin with the constant 13 added to them. The constant 13 was arbitrarily chosen to result in mostly single digit positive integers. Location of the numbers indicates the size and fall velocity of that bin.

Inspection of the plots indicates that for a two component model to give variation in fall velocity for reasonably sized particles, the inter-particle stickiness values must be 3-

4 orders of magnitude smaller than between like particles. If they are not, most aggregates, even those only a little larger than primary particles, have uniform composition and aggregate fall velocity is solely a function of aggregate size. Analysis of the plots shows how variation of model parameters affects the fall velocity size relationships. The model generates a fall velocity - aggregate size plot with a characteristic shape. The shape has a bimodal fall velocity distribution for aggregates similar in size to the primary particles. This distribution merges to a broad scatter of fall velocities. As aggregate size increases the scatter decreases to approach a single value because all larger aggregates have similar compositions. Figures 4-18 through 4-23 show the effect of variation in the parameters on this distribution. As the two components are more likely to stick together the shape shifts to smaller particle sizes. If stickiness between particle types is close to that of particles to themselves, all aggregates of a given size have the same composition and therefore the same fall velocity. A greater variation in primary particle density increases the difference in fall velocity between the two nodes at the smallest sizes. If the primary particle sizes differ the variation in fall velocity increases at the size of the second particle. Variation in fractal dimension causes scatter in fall velocity to extend to larger aggregate sizes. Figure 4-24 graphically depicts this summary.

Does the model qualitatively agree with the field data presented in Figure 4-13? The answer is somewhat ambiguous. Even considering that the Chase (1979) data are on a linear plot, it appears there is not convergence in fall velocity with increasing aggregate size. The Dyer and Manning (1999) data appear to show less scatter at larger aggregate

Table 4-4 Fall Velocity Cases

	ρ_a	ρ_b	l_a	l_b	f_a	f_b	α_1	α_2	α_3
b1	2.65	1.01	5	5	1.8	1.8	1	0.0001	1
b2	2.65	1.01	5	5	1.8	1.8	1	0.001	1
b3	2.65	1.1	5	100	1.8	1.8	1	0.0001	1
b4	2.65	1.1	5	100	1.8	1.8	1	0.001	1
b5	2.65	1.1	5	5	2	1.6	1	0.0001	1
b6	2.65	1.1	5	5	2	1.6	1	0.001	1

This table contains primary particle characteristics for type a and b particles.

Captions for Figures 19 - 25

Figures 18 - 23 show the results of the model runs described in Table 4-4. Number on the plots represent the number of aggregates in a bin and the location at which the number is plotted denotes the size and fall velocities of the aggregates in that bin. The numbers are the log based ten of the number of aggregates in that bin with the constant 13 subtracted. This constant was arbitrarily chosen so number displayed on the figures would be mainly single digit positive integers.

Figures are interpreted by observing the change in variation in fall velocity with aggregate size. For the smallest aggregates, the numbers with the largest variation in fall velocity are largest. At larger aggregate sizes, the number of all aggregates sizes is similar. For the largest aggregates, the number at a fall velocity between two extremes will be the largest. Comparison of the figures reveals how rapidly the transition occurs. Note scale varies between figures to enhance readability.

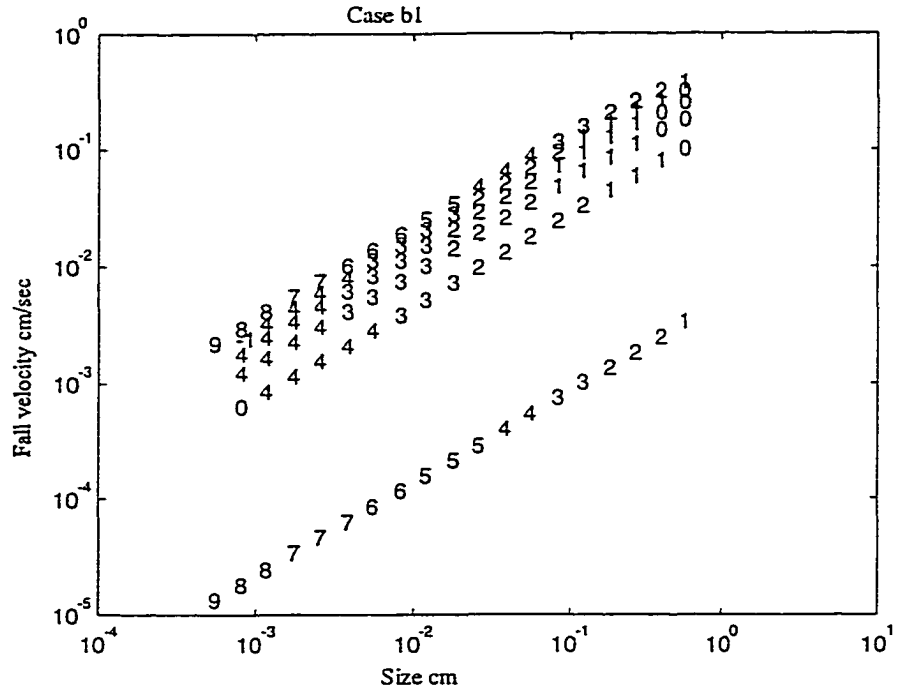


Figure 4-18

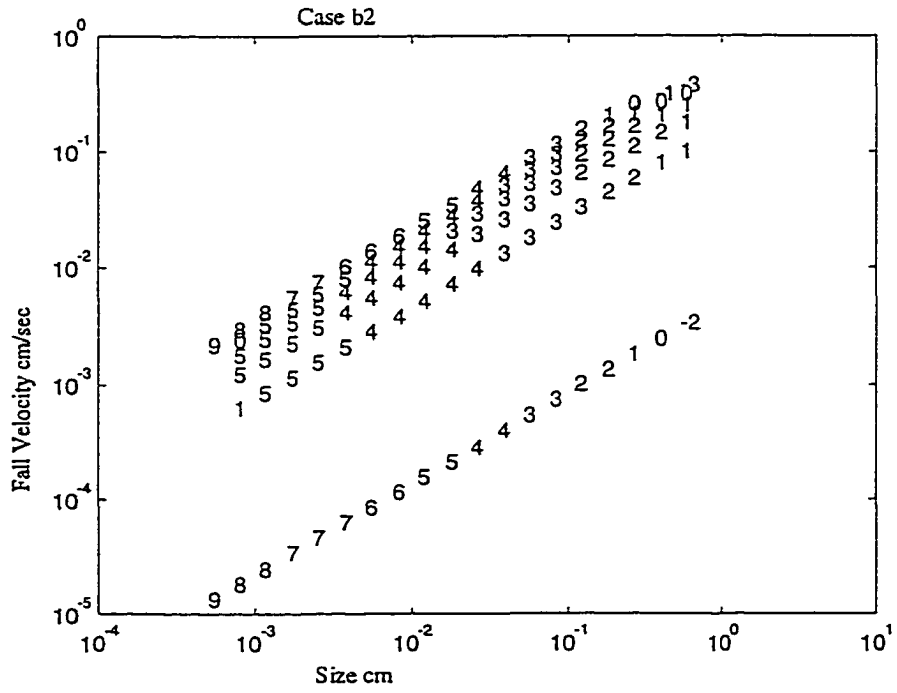


Figure 4-19

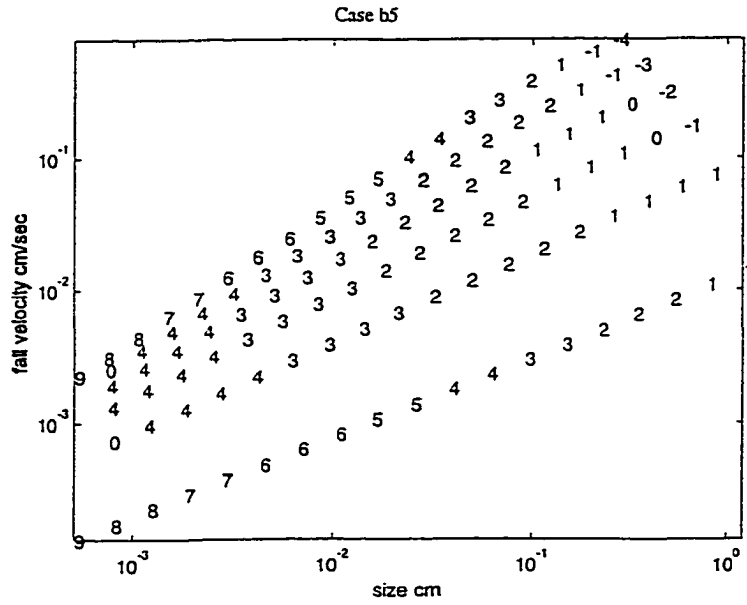


Figure 4-22

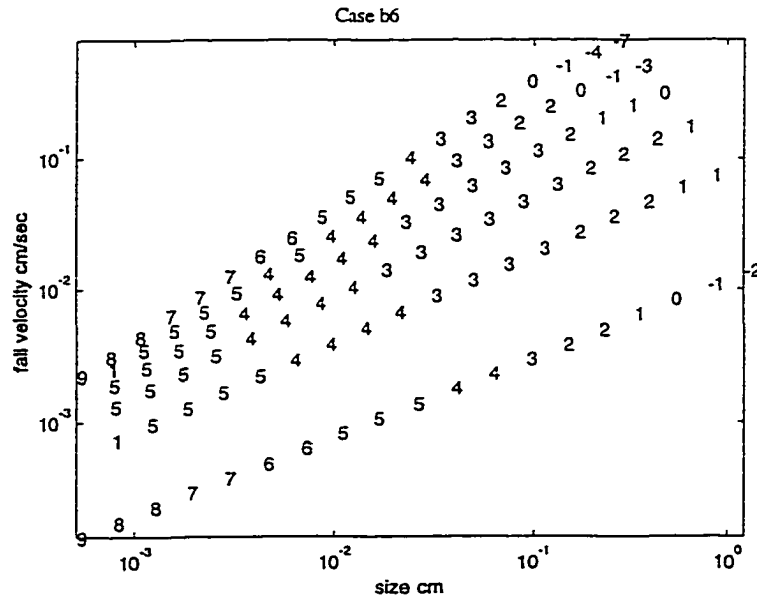


Figure 4-23

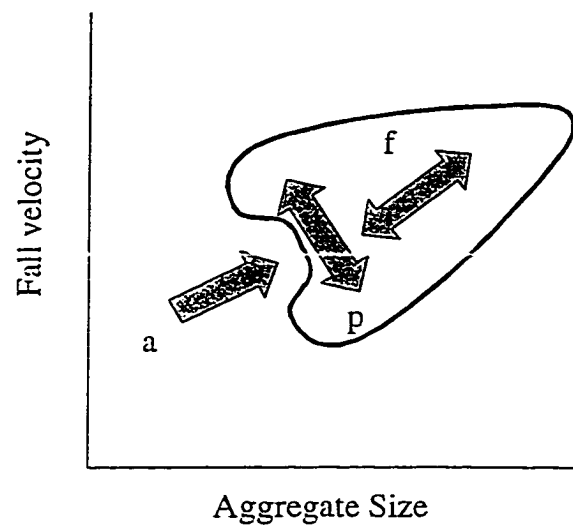


Figure 4-24 Fall Velocity Variation Summary

The effect of primary particle characteristics on fall velocity-size relationship is shown. Increased density differences, p , widen the spread of fall velocities close to the primary particle size. Increased stickiness, a , makes aggregates of uniform composition form at smaller sizes. Increased differences in fractal dimension, f , make differences in fall velocity exist for larger aggregates.

sizes. These data might generally support the two component model. It is likely that most of the variation in fall velocity comes from variation in particle packing - fractal dimension.

Composition Variation

This section will present data to show that the fraction of total suspended solids which are organic is higher closer to the surface of the water column. This effect will be investigated by considering particulate behavior as an aggregation process.

Data

Bay Monitoring Program Data as presented on CD ROM by Rennie and Nielsen (1993) allows calculation of ratios of particulate organic carbon to total suspended solids. Table 4-5 presents ratios calculated over 7 separate years at station WE4.3 (76.37° W 37.18° N) which is close to the mouth of the Poquoson River in 5 to 6 m water depth. This location was selected because the shallow depth is suited for later modeling efforts. Surface samples were from a depth of 1 m whereas bottom samples were collected at a depth of about 4 to 5 m. Total suspended solids, TSS, was determined by filtering then drying and weighing the filters. Particulate organic carbon, POC, was determined by filtering followed by analysis using a carbon nitrogen analyzer POM can be estimated as twice POC values. The last columns of Table 4-3 are most useful in addressing the effect of aggregation because taking the ratio removes the influence of relative bottom concentration of materials and also uncertainty in POC - POM conversion. To illustrate this, consider that the distribution of each material in the water column may be described

by an exponential decay, $C=C_0 e^{-Az}$ where A is a constant and C_0 is the reference concentration. In taking the ratio of the ratios from surface and bottom measurements the C_0 values for both materials cancel. This ratio is calculated with and without data from 1987. Data from 1987 is more than two standard deviations larger than the mean and may have undue influence on the mean.

Table 4-5 Ratio of mass concentrations of particulate organic carbon and total suspended solids

Year	Top			Bottom			Ratios	
	POC	TSS	P/T	POC	TSS	P/T	T/B	T/B
1985	0.66	13.12	0.05	0.83	16.94	0.05	1.02	1.02
1986	0.50	13.00	0.04	0.71	18.94	0.04	1.04	1.04
1987	0.78	7.00	0.11	0.80	13.94	0.06	1.94	
1988	0.72	17.89	0.04	0.75	20.63	0.04	1.11	1.11
1989	0.88	19.65	0.04	0.89	22.44	0.04	1.12	1.12
1990	1.14	26.23	0.04	0.97	30.85	0.03	1.38	1.38
1991	1.07	17.62	0.06	1.12	20.98	0.05	1.14	1.14
						averages	1.25	1.14
						std. dev.	0.30	0.12

Data from WE4.3 from Rennie and Nielsen (1993).

POC particulate organic carbon mg/l

TSS total suspended solids mg/l

P/T ratio of POC/TSS

T/B ratio P/T top to bottom

Water Column Model

The aggregation model will be extended to model suspension and aggregation of particles in the water column. Modeling of sediment suspension and aggregation in the water column is achieved by combining a module which calculates suspended sediment and a module which calculates aggregation. The module that calculates aggregation has been the topic of this chapter so far. The suspended sediment module is discussed in this section. These two modules operate on a series of matrices, one for each elevation modeled. This scheme is depicted in figure 4-25. Each matrix contains one element for each aggregate size and composition bin. The implementation used in this section had three elevations each with 25 sizes and 6 compositions for a total of 150 bins at each of the three elevations. The modules operate iteratively: the suspended sediment model calculates the change in vertical distribution of suspended material over the three elevations. It does this 150 times, once for each size - composition class. The module calculates the change over a time step which was chosen to be 100 sec. After the suspended sediment module completes its action, the aggregation that occurred during the suspended sediment module time step is modeled by the aggregation module. Several time steps of the aggregation module are required because the aggregation module requires a shorter time step. The aggregation module operates on each elevation sequentially. In summary, calculation of aggregation at each elevation alternates with calculation of suspension for each size-composition class.

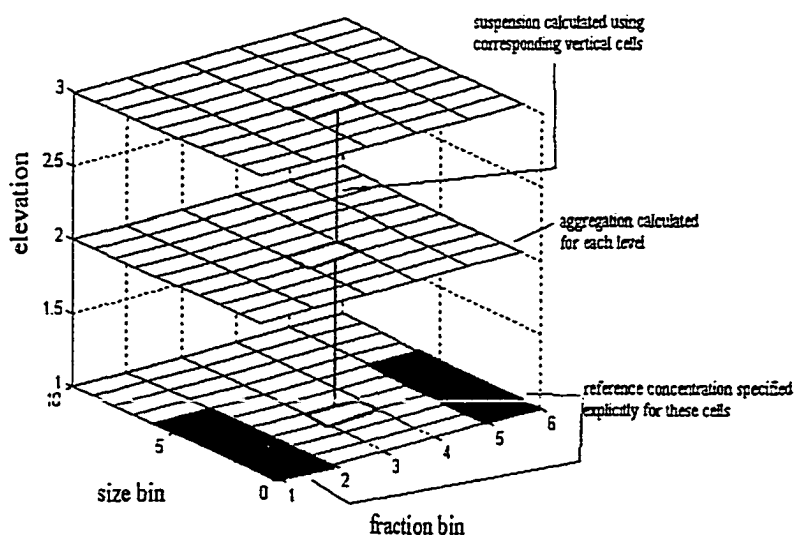


Figure 4-25 Module Interaction

This figure depicts interaction of the suspended sediment module and the aggregation module. The suspended sediment module operates on corresponding bins of the layers. One operation of the module is shown in the figure. It would operate on the 60 bins shown above sequentially. The aggregation module operates on the 60 bins shown for each level but does not cause any interaction between levels. The two modules operate sequentially, first the suspended sediment module then the aggregation module, etc. The bottom level is the reference concentration level. In this case reference concentration are specified explicitly for the dark squares, the other squares have the no diffusion boundary condition. The figure shows only 10 size classes and 3 elevations for clarity, but the model as written has 4 layers and 25 size classes.

The modeling of suspended sediment concentrations is done by considering that concentration results from a balance between upward turbulent diffusion and gravitational settling. The governing equation is

$$\frac{\partial C}{\partial t} = \frac{\partial}{\partial z} (WC + v_t \frac{\partial C}{\partial z}) \quad 4-13$$

where C is concentration, W is fall velocity, and v_t is vertical turbulent diffusivity. The bottom boundary condition is a reference concentration.

$$C_1 = C_a \quad 4-14$$

And the top boundary condition is no flux through the surface.

$$WC + v_t \frac{\partial C}{\partial z} = 0 \quad 4-15$$

In an aggregation model a reference concentration of large aggregates is unreasonable, because high shears in the boundary layer break up aggregates. Therefore, the reference concentration is given for small aggregates or primary particles and a no diffusion boundary condition, equation 4-16, is given for larger aggregates.

$$\frac{\partial C}{\partial t} = W \frac{\partial C}{\partial z} \quad 4-16$$

In practice, a no diffusion boundary condition is specified by setting the concentration at the reference concentration level equal to the concentration at the level above the reference concentration level. The question of which bins are given reference concentrations and which are given no diffusion boundary conditions is addressed in a later sections.

The governing equation is solved numerically. When long time steps are used, a fully implicit numerical scheme avoids stability problems. The modeled 5 m deep water column is broken into 4 evenly spaced cells with grid centers at 0.625, 1.875, 3.125 and 4.375 m above the bed. The concentration at the 0.625 m elevation is held constant as the reference concentration for the aggregate sizes which use a reference concentration and held equal to the concentration at the 1.875 m elevation for aggregate sizes which use a no diffusion bottom boundary condition. This is a case of the common practice in numerical modeling of eliminating diffusion by setting a concentration gradient to zero. Having the reference concentration 0.625 m above the bed complexities of very near bottom processes. The discretization scheme away from boundaries scheme is

$$\frac{C_j^{t+1} - C_j^t}{\Delta t} = W \frac{C_{j+1}^{t+1} - C_j^{t+1}}{\Delta z} + v_t \frac{C_{j+1}^{t+1} - 2C_j^{t+1} + C_{j-1}^{t+1}}{\Delta z^2} \quad 4-17$$

and for the top boundary condition

$$\frac{W}{2}(C_{N+1}^{t+1} + C_N^{t+1}) + v_t \frac{C_{N+1}^{t+1} - C_N^{t+1}}{\Delta z} = 0 \quad 4-18$$

Being implicit, this results in a series of simultaneous equations. However, with only 3 points to solve for in this simple formulation, matrix inversion can be used.

then modeling particulates in an area shallow enough that bed interaction is important, the interaction is represented mathematically as a reference concentration. This reference concentration is the concentration at a point a given distance above the bed. Most previous sediment transport models dealt with only one type of sediment so one number specified the reference concentration. A few more advanced models (Madsen et al.1994) used more than one size class and therefore required a reference concentration for each size class.

The model described herein includes 150 size- composition cells. However, they do not all need to be specified. From considerations of boundary layer flow it could be presumed that aggregates fall into the lower boundary layer where they encounter high shear stresses which break them up. Under this scenario, the reference concentration of large aggregates, those approaching the size of the Kolmagorov scale, close to the bottom is zero. However, when the reference concentration for these aggregates is set to zero, aggregates are being removed by two strong processes, settling and diffusion. Not only does this result in unrealistically fast aggregate removal, it also results in the

physically unrealistic situation of more large aggregates at the surface than at the bottom. Therefore, for large aggregates, the model assumes that aggregates pass through the bottom of the bottom layer only by settling. This eliminates the need to specify a reference concentration for these sizes because the no diffusion condition sets it automatically.

There are minimal data available for use in specifying reference concentrations as a function of aggregate size and composition. However, upon reflection it is obvious that two end member compositions should be specified. To illustrate this concept, assume that the two aggregate types introduced as reference concentration are 1) 80% type "a" primary particle and 20% type "b" primary particle and 2) 20% "a" and 80% "b", as aggregation proceeds an aggregate whose composition is 50% "a" and 50% "b" will eventually form. There is no mechanism in an aggregation model for a 100% "a" and 0% "b" aggregate to form. Therefore, the 100% "a" and 0% "b" bin in the model will never be used and are deadwood in the model. To effectively use the capabilities of the model one should redefine a primary particle which is 80% "a" and 20% "b" and has appropriate attributes.

Reference Concentration

There are two methods for introducing particles. One has all particles enter the system as primary particles. That is, there are reference concentrations only for bins (1,1) and (1,6). The second method specifies one reference concentration for bins which should contain aggregates at the reference elevation. In this case concentration is specified for

bins up to 2 size bins smaller than the Kolmogorov scale at 1m above the bed.

In most suspended sediment concentration models specifying the reference concentration involves merely specifying a concentration at one level. In this model it is slightly more complicated. The volume concentration at the reference concentration level is specified then the fraction of this concentration which is “a” and “b” particles is specified. However, it must be remembered that the reference concentration is only explicitly specified for some bins. Other bins have the settling but no diffusion boundary condition so the concentration at the reference concentration level for these bins is part of the solution. For these bins the reference concentration is assumed to be the same as at the first level. Therefore, when specifying the reference concentration for the bins which have it explicitly specified, the amount of material in the bins for which there is the no diffusion boundary condition is subtracted from the reference concentration for the level and the result is distributed over the bins for which reference concentrations are specified.

Total numbers of particles in a system modeled using the two types of boundary conditions are shown in Figures 4-26 and 4-27. The three lines are the three elevations modeled. The reference concentration specified the particles as 90% by volume “a” material with a specific gravity of 2.65 and the remainder “b” material having a specific gravity of 1.1. They both converge but to different values. However, the values only differ by a factor of 2. As expected, the distributed reference concentration has a lower total number of primary particles. This is because the distributed reference concentration

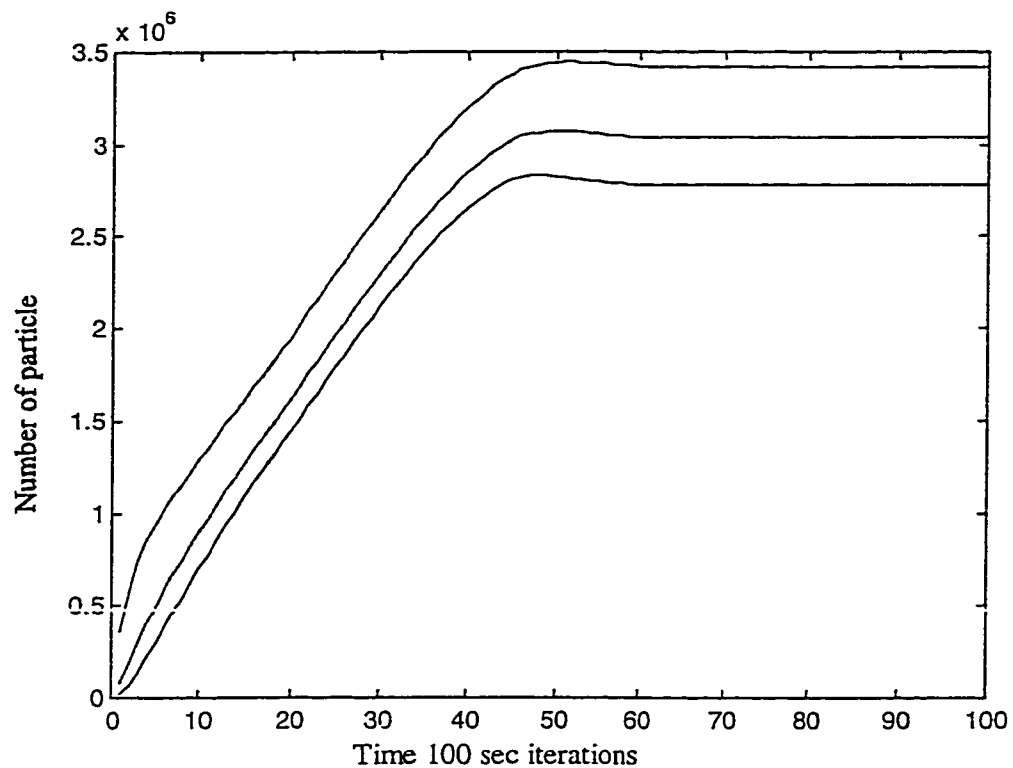


Figure 4-26 Model Convergence with Primary Particle Reference Concentration
 The total number of particles present when the reference concentration is all primary particles is shown. The reference concentration specified the particles as 90% by volume "a" material with a specific gravity of 2.65 and the remainder "b" material having a specific gravity of 1.1. The fractal dimension of all particles is 1.8 and the size is 5 microns. The bottom elevation, as expected, has the highest particle concentration and is represented by the top line. Conversely, the bottom line is the top elevation.

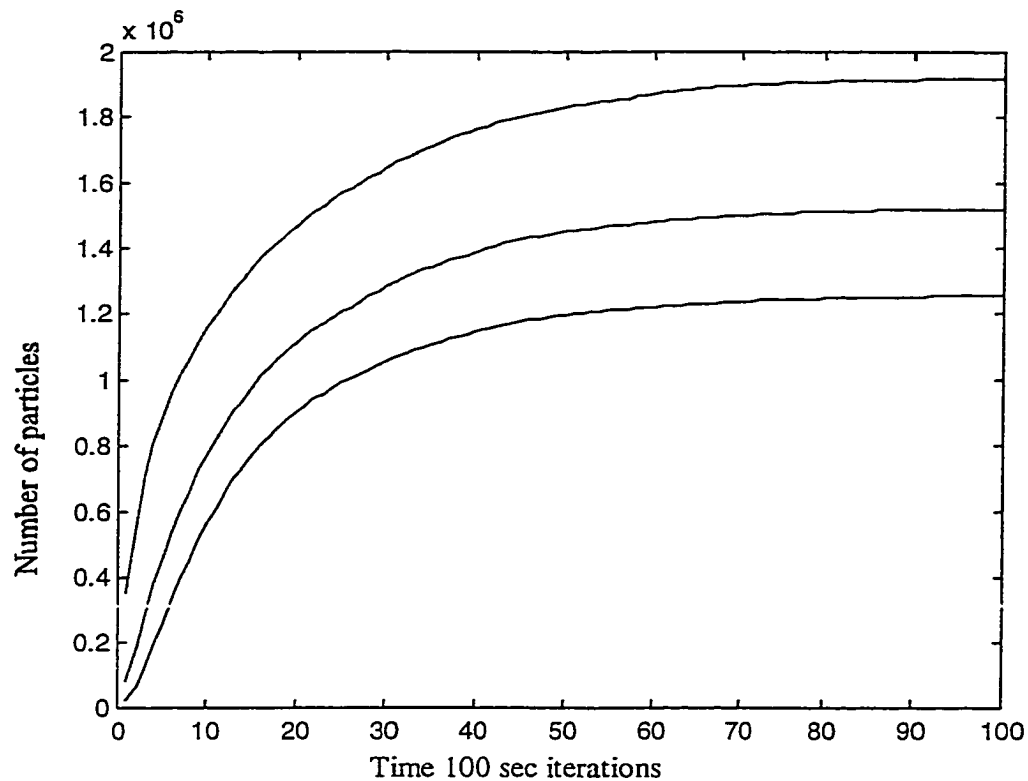


Figure 4-27 Model Convergence with Distributed Reference Concentration
 The total number of particles present as the system approaches steady state is shown. The reference concentration specified the particles as 90% by volume “a” material with a specific gravity of 2.65 and the remainder “b” material having a specific gravity of 1.1. The fractal dimension of all particles is 1.8 and the size is 5 microns. Reference concentration is distributed over aggregates of pure composition from primary particle size to 2 bins smaller than the Kolmogorov scale. The bottom elevation, as expected, has the highest particle concentration and is represented by the top line. Conversely, the bottom line is the top elevation.

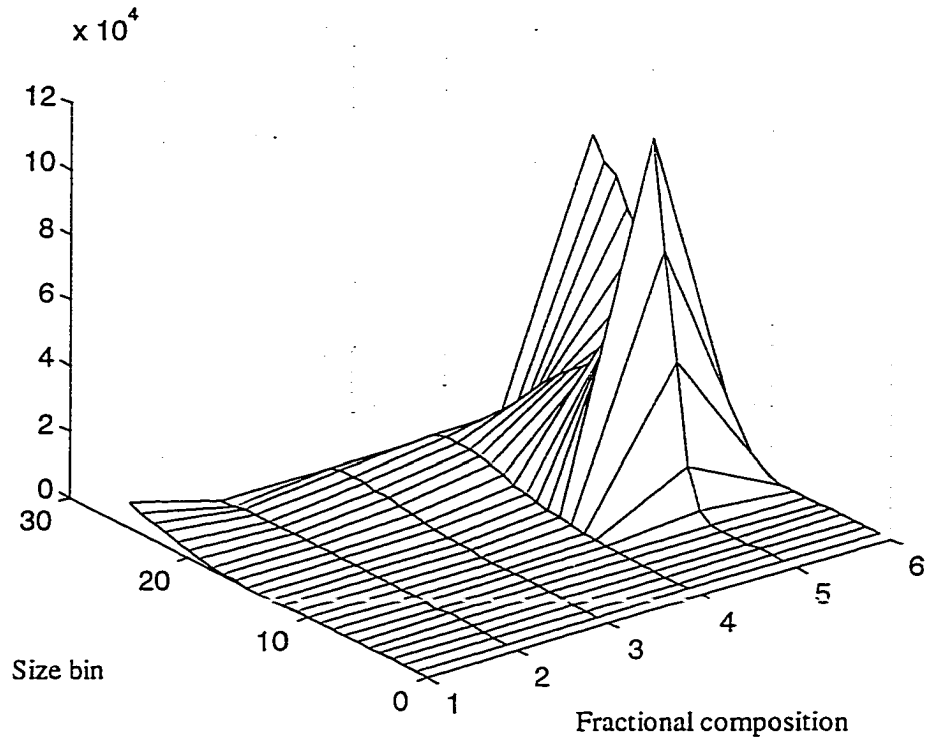


Figure 4-28 Profile - Distributed Reference Concentration

Distribution of primary particles at steady state when a distributed reference concentration is used is shown. The reference concentration specified the particles as 90% by volume "a" material with a specific gravity of 2.65 and the remainder "b" material having a specific gravity of 1.1. The fractal dimension of all particles is 1.8 and the size is 5 microns. The reference concentration is specified for fractional bins 1 and 6 (aggregates composed of pure b and a respectively) and size bins 1 through 11. Thus, it is explicitly given for 22 bins.

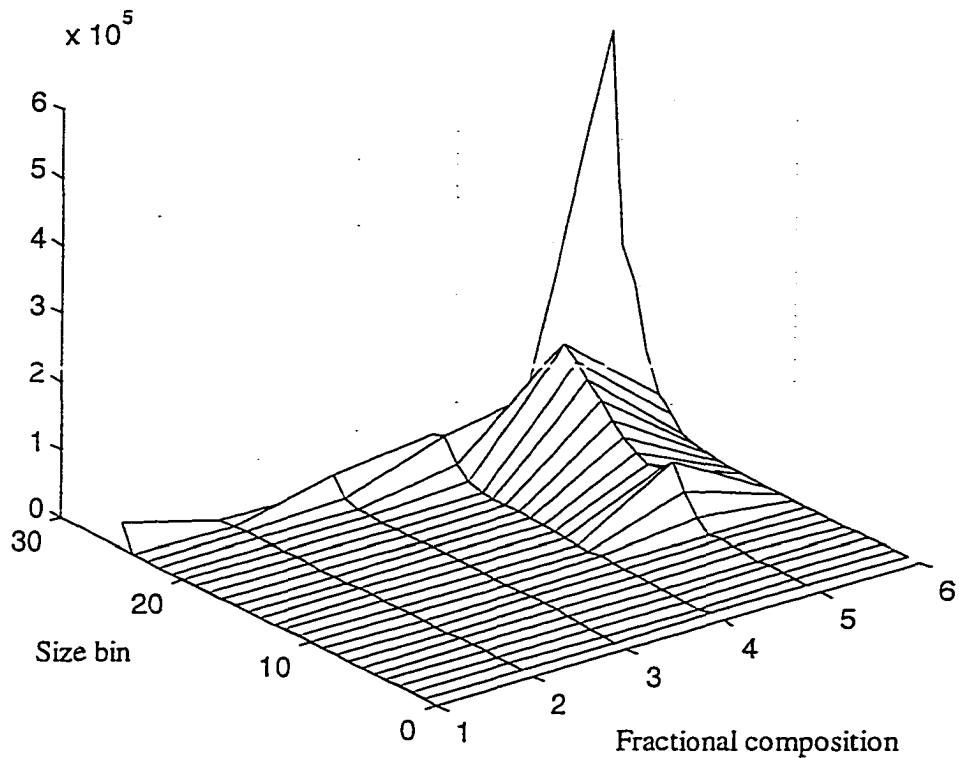


Figure 4-29 Profile - Two Reference Concentrations

Distribution of primary particles at steady state when reference concentrations are given for primary particle size bins. The reference concentration specified the particles as 90% by volume "a" material with a specific gravity of 2.65 and the remainder "b" material having a specific gravity of 1.1. The fractal dimension of all particles is 1.8 and the size is 5 microns. The reference concentration is given explicitly for 2 bins, a primary particles and b primary particles.

introduces larger aggregates which are removed more rapidly by settling.. Figures 4-28 and 4-29 show distributions of aggregates as a function of composition and aggregate size at the end of the runs. The plots are for the uppermost elevation. The distributed reference concentration reduces by a factor of 5 a spike at the primary particle concentration.

Results

Several runs were completed to determine how the model calculated the ratio of a to b particles in the water column. The turbulent energy dissipation was set to $0.01 \text{ cm}^2 \text{ s}^{-3}$. This roughly corresponds to a bed shear velocity of 1 cm s^{-1} . The reference concentration was 0.1 ppt solids by volume with 90% of the volume “a” particles and 10% “b” particles. This corresponds to a reference concentration of 250 mg l^{-1} which is high but reasonable. Particle characteristics are given in Table 4-6 and a approximates a generic inorganic matter while b approximates a generic organic matter. The reference concentration was distributed between the primary particle sizes and 2 bins smaller than the Kolmogorov scale. The distribution was set such that all bins of the same fractional composition which have explicit reference concentrations have the same number of primary particles. The number of aggregates decreases as the aggregates grow larger. Calculations were made for the 5 cases in Table 4-6. Table 4-7 presents raw output. Table 4-8 converts it to mg l^{-1} then presents ratios

Table 4-6 Depth Resolving Model Runs

run	f_a	f_b	l_a	l_b	ρ_a	ρ_b	α_1	α_2	α_3
n1	1.8	1.8	5u	5u	2.65	1.1	0.0001	0.0001	0.0001
n2	1.8	1.8	5u	5u	2.65	1.1	0.1	0.1	0.1
n3	1.8	1.8	5u	5u	2.65	1.01	0.1	0.1	0.1
n4	1.8	1.8	5u	5u	2.65	1.1	1	0.001	0.001
n5	1.8	1.8	5u	5u	2.65	1.1	0.1	0.001	0.1

Table 4-7 Depth Resolving Model Output

run	top a	top b	bottom a	bottom b
n1	1.15e5	1.51e4	1.29e5	1.52e4
n2	1.14e5	1.36e4	1.29e5	1.46e4
n3	1.14e5	1.36e4	1.29e5	1.47e4
n4	1.15e5	1.51e4	1.29e5	1.52e4
n5	1.15e5	1.51e4	1.29e5	1.52e4

Table contains number of primary particles in all size classes per ml.

Table 4-8 Concentration Ratios

run	TSS surface mg l ⁻¹	POM surface mg l ⁻¹	TSS bottom mg l ⁻¹	POM bottom mg l ⁻¹	POM/TSS surface	POM/TSS surface	ratio
n1	19.9	1.09	22.4	1.09	0.116	0.105	1.10
n2	19.8	.98	22.4	1.05	0.106	0.102	1.04
n3	19.8	.98	22.4	1.06	0.107	0.102	1.05
n4	19.9	1.09	22.4	1.09	0.116	0.105	1.10
n5	19.9	1.09	22.4	1.09	0.116	0.105	1.10

Data in Table 4-8 was converted to mg l⁻¹ assuming a particles are inorganic with densities of 2.65 mg l⁻¹ and b are organic with densities of 1.1 mg l⁻¹.

Observation of the tables reinforces the conclusion that in a two component aggregation model, stickiness between the two types of particles is the most important parameter. Comparison of the ratios in the final column of Table 4-8 with the ratio in Table 4-5 indicates that the model results for the smaller interparticle stickiness values are closer to the value in Table 4-8. This indicates that water column aggregation between organic and inorganic materials may be limited much of the time in estuarine waters.

CONCLUSION

This dissertation has two parts which essentially stand independently: the ROGTAC and the two component model. Both represent advances in endeavors which have received considerable attention in the past but which will benefit from continued study in the future.

ROGTAC

The ROGTAC is a combination of two previously successfully used aggregation devices, the rotating cylinder and the oscillating grid. Rolling cylinder devices excel at keeping particles in suspension (Shanks and Edmondson 1989) while oscillating grid devices excel at producing well behaved turbulent conditions (Brumley and Jirka 1987). Previously, the best way to introduce shear while keeping aggregates in suspension was the viscometer (van Duuren 1968). However, this device did not normally produce turbulent conditions. If it did produce turbulence, it also produced very high shear rates near the cylinder walls. Combining the rolling cylinder and turbulent grid devices results in what should prove to be a notable advance in laboratory aggregate production capability. To aid future researchers who might use this device, the hydraulic characteristics of the device were determined using a state-of-the-art laser Doppler

velocimeter system.

The energy dissipation rates in ROGTAC correspond to turbulent conditions one meter above the bed caused by shear velocities of between 5 and 10 cm sec⁻¹. These are higher than what is normally found in estuaries, one to two cm sec⁻¹ is more typical, but not unreasonable considering that the relationship between turbulent energy dissipation and shear velocity was based on a scaling relationship. Reducing the energy dissipation in ROGTAC would require wider grid spacing, which would make the turbulence less uniform, or slowing the motor speed further, which would degrade the characteristics of the turbulence.

Aggregation devices may be used to further elucidate the process of aggregation in natural water bodies. Much remains to be learned about the effect of phytoplankton species and their nutrient conditions on aggregation. Passow and Wassermann (1994), who looked at the aggregation of *Phaeocystis* colonies at senescence, is an example of this type of study. Hydrodynamic conditions may be particularly important for nutrient limitation studies because the hydrodynamic conditions may control how rapidly nutrients are delivered to living material (Logan and Hunt 1987). Although many previous studies have centered on phytoplankton characteristics, bacteria and detritus supporting bacteria are also probably important (Decho 1990). Experiments investigating species of bacteria present and resulting aggregation could add to the knowledge of aggregation in real systems. For example, one question would be how the bacteria and mucopolysaccharides

on a particle react to the transition from fresh water to saltwater?

Aggregation Model

The primary application of the two-component model in marine science appears to be in estuaries, where suspended matter can be conveniently broken into two classes, organic and inorganic. Application of aggregation models to estuaries is currently in its infancy. The current goal of applications of aggregation models in estuaries is to determine the role of aggregation in estuarine sediment dynamics. In the only application of an aggregation model to an estuarine setting to date, Lick et al. (1992) proposed that aggregation may contribute to enhanced suspended sediment concentrations near the bed. The two-component aggregation model was thus used to address basic questions about the interactions of classes of suspended materials in estuaries.

One can envision two "end member" views of aggregation. In view one, aggregates are broken up into primary particles, individual clay particles or phytoplankton cells, in the lower boundary layer. These are suspended where they again aggregate and settle out. The process repeats indefinitely. In this view, aggregation essentially dominates particle dynamics in the estuary. In the second view, aggregates of various types exist in the estuary and are cycled through the estuary. Aggregates exist, but they are created as robust pseudofeces. They do not aggregate in the water column and are strong enough that they are not broken up. In this view, aggregation is irrelevant.

As in most cases when two end members are presented, the true answer is likely somewhere in the middle. Eisma and Li (1993) working in Dollard estuary tends to support the first view while Zabawa (1978) working in northern Chesapeake Bay supports the latter. It is worth noting that Eisma and Li photographed aggregates in-situ while Zabawa captured aggregates by filtering then viewed them using a scanning electron microscope, (SEM). The SEM requires more handling of the aggregates and is therefore more likely to break them up but also allows actual observation of their structures. Also, the Dollard estuary where Eisma and Li worked had a 3m tidal range. This could have led to higher shear rates than found in Chesapeake Bay which typically has a 1m or less tidal range.

Model results do not clearly resolve these conflicting views. The two component model shows that if view one were wholly correct, aggregates of a size would have very similar fall velocities. The fact that fall velocities of aggregates vary substantially indicates that the true scenario is either the second case or somewhere between the two. The model suggests that stickiness between organic and inorganic particles is low, tending to favor view two.

A second question is the nature of how aggregates stick together. One view is that mucopolysaccharides present in the water essentially stick everything to everything (Passow et al. 1994). A second view is that the stickiness depends upon the properties of each material - realizing that organic coatings on materials may determine their adhesive

properties (Gibbs 1983). The modeling results suggest that the organic and inorganic fractions do not stick together all that well. This tends to support the second view of stickiness. The model brings into focus the fact that it is imperative to know under what conditions which materials stick or do not stick to which other materials if we are to understand the dynamics of particulates in an estuary.

To summarize, there are four main conclusions from this work.

1.) Particles aggregation has been studied in a wide variety of fields including atmospheric science, oceanography, estuarine science, colloid chemistry, process engineering, and water treatment. When faced with a challenge in this field, it is important to be aware of contributions to aggregation science from fields outside one's own.

2.) The rotating oscillating grid turbulent aggregation chamber is the most successful method yet devised to subject a particle - fluid mixture to grid turbulence while keeping particles of a different density from the fluid in suspension and minimizing interaction between the particles and the grid.

3.) The two component aggregation model simulates the behavior of two types of particles in a fluid. It does this in a manner which represents the physics of the system.

4.) As aggregation proceeds, large particles of uniform composition. Therefore,

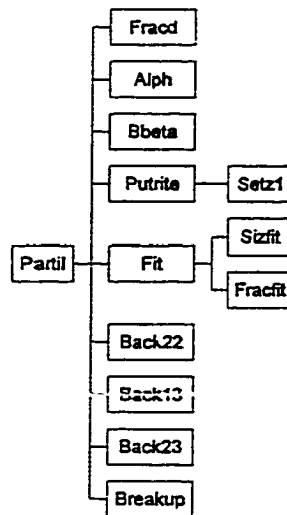
for variation in aggregate characteristics to exist in larger size aggregates, differing particle types must have low attachment probabilities between each other.

APPENDIX A

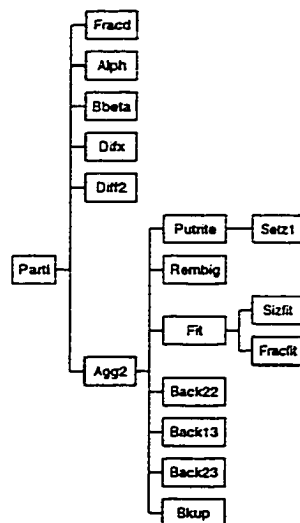
MODEL COMPUTER CODE

This appendix contain the code which composes the aggregation model. The model is given in two forms. However, the two forms use many of the same subroutines. The structure of the models is shown in the block diagrams. Comments in the code describe their functions. For detailed descriptions of algorithms refer to the main body of this dissertation.

Basic Aggregation Model



Water Column Model



```

% mfile partil
% written 1998 by Tom Chisholm
% Virginia Institute of Marine Science

% This program models aggregation of two types of particles
% particles are introduced as primary particles and removed
% by settling of from large bins.
% The two types of particles are called a and b
% there are 25 size bin and 6 fraction bins for a total of 150 bins
% For details on algorithms see Tom Chisholm's dissertation

clear all
% primary particle sizes cm
la=5e-4;      % diameter of a particles
lb=5e-4;      % diameter b particles
% fractal dimensions
ma=2.0;
mb=2.0;
% particle excess density g/ml
pa=1.65;
pb=0.1;
% stickiness
% a1 a to a; a2 a to b; a3 b to b
a1=1;
a2=0;
a3=0;

% dats includes record of adjustable parameters
dats1=['la lb ma mb pa pb a1 a2 a3']
dats2=[la, lb, ma, mb, pa, pb, a1, a2, a3];

% input for breakup
nu=0.01;      % kinematic viscosity defines units
eps=1.63;     % turbulent dissipation
dt=30;        % initial time step

% determine number of particles in each bin
% fraction bins are linearly spaced and size bins are log spaced
fa=linspace(0,1,6);
fb=1-fa;
ns=linspace(0,24,25);
ns2=2.^ns;    % bin sizes
as=ns2*fa;    % number of a particles in aggregates in each bin
bs=ns2*fb;    % number of b particles in aggregates in each bin

lam=(nu^3/eps)^0.25; % kolmogorov scale
bn=(lam./(fa.*la+fb.*lb)).^(fa.*ma+fb.*mb);
bi=log(bn)/log(2)+1;
bi=floor(bi) % bin numbers with size equal kolmogorov scale

% make sure size bin at kolmogorov scale is not out of range

```

```

for k=1:6,
    if bi(k)>24
        bi(k)=24;
    end
    if bi(k)<2
        bi(k)=2;
    end
end

% determine size density and fall velocity for each cell
[ot, w, p]=fracd(la, lb, ma, mb, pa, pb);

% calculate alpha values between bins
[alpha] =alph(la, lb, a1, a2, a3);

%Calculate beta values between bins
[bet]=bbeta(ot,w,eps);

% initial conditions
% for each bin the number of a particles, b particles,
% and aggregates it contains is specified.
n=zeros(25,6);
a=zeros(25,6);
b=zeros(25,6);
for k=1:6,
    b(1,k)= 2e5*(6-k)/5;
    n(1,k)=2e5;
    a(1,k)=2e5*(k-1)/5;
end

% initialization of counters etc.
ct=1; %loop counter for saving results
cc=1; %loop counter for saving results
t=0; %time counter
it=0; %iteration counter
tint=500; %interval for saving data
tsavtim=0; %time counter for data save routine

% main loop
while (t<3600) &(it<5000),

    it=it+1;

    %for k=1:6, %input for equilibrium run
    %b(1,k)=2e5*(6-k)/5;
    %n(1,k)=2e5;
    %a(1,k)=2e5*(k-1)/5;
    %b(20:25,k)=0;
    %n(20:25,k)=0;
    %a(20:25,k)=0;

```

```

%end

% remove aggregates due to settling from 100cm thick layer
lost=l-w/100*dt;
a=a.*lost;
b=b.*lost;
n=n.*lost;

% initialize change variables
dn=zeros(25,6);
da=zeros(25,6);
db=zeros(25,6);
dn1=zeros(25,6);
da1=zeros(25,6);
db1=zeros(25,6);

if t>tsavtim
    ttt(ct)=t; % times when results are saved
    tsavtim=tsavtim+tint; % update save time counter
    sav(:,ct)=b+a;
    tims(ct)=t;
    nsav(:,ct)=n;
    ct=ct+1;
end

%recenter bin sizes

    % puts bins outside their ranges in the proper bins
    [n, a, b, att, btt] = putrite(n, a, b);
    lsta(:,cc)=att(:); % stores mass lost in resizing operation
    lstb(:,cc)=btt(:);
    [n, a, b]=fit(n, a, b); % recenter bins
    cc=cc+1;
    [t sum(sum(a)) sum(sum(b)) sum(att) sum(btt) ] %monitor model operation

for i=2:25,
    if i==2
        % calculate interactions in first row which affect second row
        bb=bet(1,1,:);
        np=n(1:2,:);
        [dnp,dap,dbp]=back22(np,i,alpha, bb, dt);
        dn(1:2,:)=dn(1:2,:)+dnp;
        da(1:2,:)=da(1:2,:)+dap;
        db(1:2,:)=db(1:2,:)+dbp;
    else
        % treat rows 3 through 25.
        np=n(i-1:i,:);
        bb=bet(i-1,i-1,:);
        [dnp,dap,dbp]=back22(np,i, alpha, bb, dt);
        dn(i-1:i,:)=dn(i-1:i,:)+dnp;
    end
end

```

```

da(i-1:i,:)=da(i-1:i,:)+dap;
db(i-1:i,:)=db(i-1:i,:)+dbp;

np=n(i-2:i,:);
bb=bet(i,:,i-2,:);
[dnp,dap,dbp]=backi3(np,i,alpha,bb,dt);
dn(i-2:i,:)=dn(i-2:i,:)+dnp;
da(i-2:i,:)=da(i-2:i,:)+dap;
db(i-2:i,:)=db(i-2:i,:)+dbp;

bb=bet(i-1,:,i-2,:);
[dnp,dap,dbp]=back23(np,i,alpha,bb,dt);
dn(i-2:i,:)=dn(i-2:i,:)+dnp;
da(i-2:i,:)=da(i-2:i,:)+dap;
db(i-2:i,:)=db(i-2:i,:)+dbp;

    % treat interactions between rows separated by more than one row
for k=1:6,
    if (n(i,k)>1e-20) & (i>3) %avoid calculation for empty cells
        on=ones(i-3,1);
        al=on*alpha(k,:);
        clear bb
        bb=bet(1:i-3,:,i,k);
        ddn=bb.*al.*n(1:i-3,:).*n(i,k).*dt; %calculate interaction
            % calculate changes in cells
        dn(1:i-3,:)=dn(1:i-3,:)-ddn;
        da(1:i-3,:)=da(1:i-3,:)-ddn.*as(1:i-3,:);
        db(1:i-3,:)=db(1:i-3,:)-ddn.*bs(1:i-3,:);
        da(i,k)=da(i,k)+sum(sum(ddn.*as(1:i-3,:)));
        db(i,k)=db(i,k)+sum(sum(ddn.*bs(1:i-3,:)));
    end
end
end
end
end

%breakup by rupture model
[dnb,dab,dbb,bi]=breakup(bi,n,a,b);
for k=1:6, %update cells
    dn1(bi(k)-2:bi(k)+1,k)=dn1(bi(k)-2:bi(k)+1,k)+dnb(:,k);
    da1(bi(k)-2:bi(k)+1,k)=da1(bi(k)-2:bi(k)+1,k)+dab(:,k);
    db1(bi(k)-2:bi(k)+1,k)=db1(bi(k)-2:bi(k)+1,k)+dbb(:,k);
    n(bi(k)+2:25,k)=0;
    a(bi(k)+2:25,k)=0;
    b(bi(k)+2:25,k)=0;
end

% sum changes to cells
n1=n+dn+dn1;
a1=a+da+da1;
b1=b+db+db1;

```

```

% is time step causing zero errors
bul=0;
for i=1:25,
    for k=1:6,
        if n1(i,k)<-1e-20
            bul=1;
            [i k n1(i,k)];
        end
    end
end

% if zero errors decrease time step else make it bigger
if bul==1
    dt=dt/3;
    it=it-1;
    [4 it dt]
else
    if (dt<30) & (abs(it/5-ceil(it/5))<0.0001)
        dt=dt*2;
        [6 it dt]
    end
    n=n i; % use data if time step ok
    b=b i;
    a=a i;
    t=t+dt;
end

end

```

```

function [ot, w, p]=fracd(la, lb, ma, mb, pa, pb);
%calculates size of floc from number of particles in floc
%primary particle size and fractal dimension

function [ot, w, p]=fracd(la, lb, ma, mb, pa, pb);

% written 1998 by Tom Chisholm
% Virginia Institute of Marine Science
% calculates size, density, and fall velocity of floc
% from number of particles in floc
% primary particle size, fractal dimension, and density

% inputs la lb ma mb pa pb
% primary particle size, fractal dimension, and density
% output ot, p, w aggregate size, density, and fall velocity
% output is a 25x6 matrix

fa=linspace(0,1,6);
fb=1-fa;
n=i;

% determines aggregate size
for i=1:25,
    nn(i)=n;
    x1=1./(fa*ma+fb*mb);
    x2=n.^x1;
    l=(fa*la+fb*lb).*x2;
    ot(i,:)=l;
    n=n*2;
end

% calculate density
on=ones(1,25);
onh=ones(1,6);
ffa=on*fa;
ffb=on*fb;
nm=nn*onh;
p=nm.*(ffa*(la^3*pa)+ffb*(lb^3*pb))./(ot.^3);

% calculates fall velocity
k=0.6; %constant in drag coefficient
t=4*980/(3*k);
w=sqrt((0.12./(ot*k)).^2+t*ot.*p)-0.12./(ot*k);

```

```

function [alpha] =alph(la, lb, a1, a2, a3)
% written 1998 by Tom Chisholm
% Virginia Institute of Marine Science
% For details on algorithms see Tom Chisholm's dissertation

% determines the stickiness part of the kernel
% input primary particle size and stickiness values
% constants a1 a2 a3  stickiness of a to a to b and b to b respectively

% output  alpha, a symmetric 6x6 matrix which contains stickiness between aggregates

%  rows are decreasing fractions of a in particle 1
%          columns are increasing fractions of a in particle 2

fa=linspace(0,1,6);
ga=linspace(0,1,6);
onf=ones(6,1);
fa=fa*onf;
ga=onf*ga;
fb=ones(6)-fa;
gb=ones(6)-ga;

la=la*la;
lb=lb*lb;
ex=(la*fa+lb*fb);
fa=(la*fa)/ex;
fb=(lb*fb)/ex;
es=(ga*la+gb*lb);
ga=(ga*la)/es;
gb=(gb*lb)/es;
alpha=a1*fa.*ga+a2*(fb.*ga+fa.*gb)+a3*fb.*gb;
%surf(fm,gm,alpha)

```

```

function bet= bbeta( ot,w,eps)
% written 1998 by Tom Chisholm
% Virginia Institute of Marine Science
% For details on algorithms see Tom Chisholm's dissertation
% calculates interaction kernel and outputs as 4D matrix
% inputs primary particle size and fall velocity; and turbulent energy dissipation

nu=0.01; %kinematic viscosity

for i=1:25
  for j=1:6
    for k=1:25
      for m=1:6
        if ot(i,j)>ot(k,m)
          sm=ot(k,m);
        else
          sm=ot(i,j);
        end
        sd=ot(i,j)+ot(k,m);
        dw=abs(w(i,j)-w(k,m));
        gg=7.5*(eps/(30*pi*nu))^0.5;
        bet(i,j,k,m)=pi/2*sm.*sm.*(gg*sd+dw/2);
      end
    end
  end
end

```

```

function[n, a, b, att, btt ] = putrite(n, a, b);
% written 1998 by Tom Chisholm
% Virginia Institute of Marine Science
% For details on algorithms see Tom Chisholm's dissertation

% this program finds bins whose contents are outside the
% range of that bin. It then places them in the appropriate bin.

%inputs matrices for number of a and b particles and number of aggregates

% setz1 insures there are no cells with negative values or very small values
[a, b, n, att, btt]=setz1(a, b, n);

l2=log(2);
nn=linspace(1,25,25);
sz=3*2.^(nn-2);      % boundaries between size bins
sz2=2.^(nn-1);      %centers of size bins
jj=linspace(0.1, 0.9, 5); % boundaries of fraction bins
jj2=linspace(0,1,6);
n1=n;
t1=a+b;

% make n1 and t1 to avoid zero divide from on empty cells
for i=1:25,
    for j=1:6,
        if n(i,j)<1e-10
            n1(i,j)=1;
        end
        if t1(i,j)<1e-10
            t1(i,j)=1;
        end
    end
end

fr=a./(t1); % calculte fractions
ss=(a+b)./n1; % calculate sizes
tt=a+b;

%avoid errors avoiding zero divide errors
for i=1:25,
    for j=1:6,
        if tt(i,j)<1e-10
            fr(i,j)=jj2(j);
        end
        if n(i,j)<1e-10 | tt(i,j)<1e-10
            ss(i,j)=sz2(i);
        end
    end
end
end

%initialization

```

```

for i=1:25,
  for j=1:6,
    dn(i,j)=n(i,j);
    da(i,j)=a(i,j);
    db(i,j)=b(i,j);
  end
end

% do smallest row
i=1;
for j=1:6, % loop across fractions
  bool=0;
  if ss(i,j)>sz(i) % is aggregates in bin too big
    bool=1;
    s=floor(log(ss(i,j)/3)/12+3); % find correct bin
    f=j;
    if j==1 % is fraction correct, ends are special cases
      if fr(i,j)>jj(1)
        f=floor(2+5*(fr(i,j)-0.1)); % find correct fraction
      end
    elseif j==6
      if fr(i,j)<jj(5)
        f=floor(2+5*(fr(i,j)-0.1));
      end
    elseif fr(i,j)<jj(j-1) | fr(i,j)>jj(j)
      f=floor(2+5*(fr(i,j)-0.1));
    end
  else %if size is correct is fraction wrong?
    if j==1
      if fr(i,j)>jj(1)
        f=floor(2+5*(fr(i,j)-0.1));
        bool=1;
        s=i;
      end
    elseif j==6
      if fr(i,j)<jj(5)
        f=floor(2+5*(fr(i,j)-0.1));
        bool=1;
        s=i;
      end
    elseif fr(i,j)<jj(j-1) | fr(i,j)>jj(j)
      f=floor(2+5*(fr(i,j)-0.1));
      bool=1;
      s=i;
    end
  end
end

if bool==1 % make needed changes
  if s>25
    s=25;
  end
end

```

```

if s<l
    s=l;
end

dn(i,j)=dn(i,j)-n(i,j);
da(i,j)=da(i,j)-a(i,j);
db(i,j)=db(i,j)-b(i,j);
dn(s,f)=dn(s,f)+n(i,j);
da(s,f)=da(s,f)+a(i,j);
db(s,f)=db(s,f)+b(i,j);
end
end

for i=2:25, % do rest of rows
for j=1:6,
    bool=0;

% this code is about identical to that above
if ss(i,j)<sz(i-1) | ss(i,j)>sz(i) % is size correct?
    bool=1;
    s=floor(log(ss(i,j)/3)/l2+3); % determine correct size
    f=j;
    if j==1
        if fr(i,j)>jj(1)
            f=floor(2+5*(fr(i,j)-0.1));
            bool=1;
        end
    elseif j==6
        if fr(i,j)<jj(5)
            f=floor(2+5*(fr(i,j)-0.1));
            bool=1;
        end
    elseif fr(i,j)<jj(j-1) | fr(i,j)>jj(j)
        f=floor(2+5*(fr(i,j)-0.1));
    end
else
    if j==1
        if fr(i,j)>jj(1)
            f=floor(2+5*(fr(i,j)-0.1));
            bool=1;
            s=i;
        end
    elseif j==6
        if fr(i,j)<jj(5)
            f=floor(2+5*(fr(i,j)-0.1));
            bool=1;
            s=i;
        end
    elseif fr(i,j)<jj(j-1) | fr(i,j)>jj(j)

```

```

        f=floor(2+5*(fr(i,j)-0.1));
        bool=1;
        s=i;
    end

end

if bool==1
    if s>25
        s=25;
    end

    if s<1
        s=1;
    end

    dn(i,j)=dn(i,j)-n(i,j);
    da(i,j)=da(i,j)-a(i,j);
    db(i,j)=db(i,j)-b(i,j);
    dn(s,f)=dn(s,f)+n(i,j);
    da(s,f)=da(s,f)+a(i,j);
    db(s,f)=db(s,f)+b(i,j);
end
end
end

n=dn;
a=da;
b=db;

```

```

% written 1998 by Tom Chisholm
% Virginia Institute of Marine Science
% For details on algorithms see Tom Chisholm's dissertation

%this routine sets cells which have negative values to zero
%it then store the number of a and b particles amount of mass lost due to this
% process in att and btt

att=zeros(25,1);
btt=zeros(25,1);

for i=1:25,
    for j=1:6,
        if n(i,j)<0
            n(i,j)=0;
            att(i)=att(i)+a(i,j);
            a(i,j)=0;
            btt(i)=btt(i)+b(i,j);
            b(i,j)=0;
        end
        if a(i,j)<0
            att(i)=att(i)+a(i,j);
            a(i,j)=0;
        end
        if b(i,j)<0
            btt(i)=btt(i)+b(i,j);
            b(i,j)=0;
        end
    end
end
end

%If a cell has less than 1e-10 particles it is set to zero

aa=a+b;
for i=1:25,
    for j=1:6,
        if aa(i,j)<1e-10
            n(i,j)=0;
            att(i)=att(i)+a(i,j);
            a(i,j)=0;
            btt(i)=btt(i)+b(i,j);
            b(i,j)=0;
        end
    end
end
end

%[sum(att) sum(btt)]

```

```

function [n, a, b]=fit(n, a, b)
% written 1998 by Tom Chisholm
% Virginia Institute of Marine Science
% For details on algorithms see Tom Chisholm's dissertation

% puts matrix at even plaes
% input a b n  number of a particles, b particles, and aggregates
% in each size class
% output a b n  number of a particles, b particles, and aggregates
% in each size class

% fractions of a and b at nodes
f=linspace(0,1,6);
% sizes
s=linspace(0,24,25);
l=2.^s;
fl=1-f;
o1=ones(1,6);
% initialize d ab&c
da=a;
db=b;
dn=n;

% big loop
% ll is size resulting from putting to size groups
% sz is size at each node
nl=n;
t=a+b;

% avoid zero divide calculating fraction
for i=1:25
    for j=1:6
        if n(i,j)==0
            nl(i,j)=1;
        end
    end
end
end

sz=t./nl;

% zero divide stuff
for i=1:25
    for j=1:6
        if t(i,j)<1e-10
            sz(i,j)=l(i);
        end
    end
end
end
end

```

```

% i is size direction j is fraction direction
for i=1:24,
    for j=1:6,
        if (abs(sz(i,j)-l(i))/l(i))> 0.1
            % input to sizfit is a0 b0 n0 x1 x2
            a0=a(i,j);
            b0=b(i,j);
            n0=n(i,j);
            % is a node larger or smaller than it should be?

            if (sz(i,j)>l(i)) | (i==1)
                x1=l(i);
                x2=l(i+1);
                at=i;
            else
                x1=l(i-1);
                x2=l(i);
                at=i-1;
            end
            %sizfit solves simultaneous equations to recenter bins in terms of siz
            [a1, b1, n1, a2, b2, n2]=sizfit(a0, b0, n0, x1, x2);
            % update matrix
            da(at,j)=da(at,j)+a1;
            da(at+1,j)=da(at+1,j)+a2;
            db(at,j)=db(at,j)+b1;
            db(at+1,j)=db(at+1,j)+b2;
            dn(at,j)=dn(at,j)+n1;
            dn(at+1,j)=dn(at+1,j)+n2;
            dn(i,j)=dn(i,j)-n0;
            da(i,j)=da(i,j)-a0;
            db(i,j)=db(i,j)-b0;
        end
    end
end
ea=da;
eb=db;
en=dn;

% process in fraction a&b direction
dd=da+db;
ddl=dd;
% avoid zero divide
for i=1:25
    for j=1:6
        if dd(i,j)==0
            dd(i,j)=1;
        end
    end
end
end

```

```

fc=da./dd;

% avoid zero divides
for i=1:25
    for j=1:6
        if dd1(i,j)<1e-10
            fc(i,j)=f(j);
        end
    end
end

for i=1:25,
    for j=1:6,
% prepare input to fracfit
        if abs(fc(i,j)-f(j))>0.01
            % 'frac'
            a0=da(i,j);
            b0=db(i,j);
            n0=dn(i,j);
            if ((fc(i,j)>f(j))|(j==1))& (j~=6)
                f1=f(j);
                f2=f(j+1);
                k=j;
            else
                f1=f(j-1);
                f2=f(j);
                k=j-1;
            end
% fracfit solves simultaneous equations to recenter fractions
            [a1, b1, n1, a2, b2, n2]=fracfit(a0, b0, n0, f1, f2);
% update
            ea(i,k)=ea(i,k)+a1;
            ea(i,k+1)=ea(i,k+1)+a2;
            eb(i,k)=eb(i,k)+b1;
            eb(i,k+1)=eb(i,k+1)+b2;
            en(i,k)=en(i,k)+n1;
            en(i,k+1)=en(i,k+1)+n2;
            en(i,j)=en(i,j)-n0;
            ea(i,j)=ea(i,j)-a0;
            eb(i,j)=eb(i,j)-b0;
        end
    end
end
% prepare output
a=ea;
b=eb;
n=en;

```

```

function [a1, b1, n1, a2, b2, n2]=sizfit(a0, b0, n0, x1, x2);
% written 1998 by Tom Chisholm
% Virginia Institute of Marine Science
% For details on algorithms see Tom Chisholm's dissertation

% solves simultaneous equations to recenter bins
% input a0 b0 n0- values of cell  x1 x2 - center sizes of bins to reapportion to
% output a1 b1 n1 a2 b2 n2  values for cells to reapportion to

% avoid zero divide if a0=0
if a0==0
    a1=0;
    a2=0;
    b1=(x1*x2*n0-b0*x1)/(x2-x1);
    b2=b0-b1;
    n1=n0-b2/x2;
    n2=n0-n1;
else
    a1=(x1*x2*n0-x1*(b0+a0))/((x2-x1)*(1+b0/a0));
    b1=a1*b0/a0;
    a2=a0-a1;
    b2=b0-b1;
    n1=(a1+b1)/x1;
    n2=n0-n1;
end

```

```
function [a1, b1, n1, a2, b2, n2]=fracfit(a0, b0, n0, f1, f2);
% written 1998 by Tom Chisholm
% Virginia Institute of Marine Science
% For details on algorithms see Tom Chisholm's dissertation

% solve simultaneous equations to put values at even fractions
% input f1 f2 a0 b0 n0 center fractions of bins to reapportion to and value of cell
% output a1 b1 n1 a2 b2 n2 values of cells to reapportion to

%b2=(f1*(a0+b0)-a0)*(1-f2)/(f1-f2);
a2=f2*(a0*(f1-1)+f1*b0)/(f1-f2);
b2=a2*(1/f2-1);
a1=a0-a2;
b1=b0-b2;
if (a0+b0)==0
    n1=0;
else
    n1=n0*(a1+b1)/(a0+b0);
end
n2=n0-n1;
```



```
if m-mm==0.5
  dnp(2,mm)=dnp(2,mm)+nut/2;
  dap(2,mm)=dap(2,mm)+nut*(na(1,k)+na(1,l))/2;
  dbp(2,mm)=dbp(2,mm)+nut*(nb(1,k)+nb(1,l))/2;
  dnp(2,mm+1)=dnp(2,mm+1)+nut/2;
  dap(2,mm+1)=dap(2,mm+1)+nut*(na(1,k)+na(1,l))/2;
  dbp(2,mm+1)=dbp(2,mm+1)+nut*(nb(1,k)+nb(1,l))/2;
else
  dnp(2,mr)=dnp(2,mr)+nut;
  dap(2,mr)=dap(2,mr)+nut*(na(1,k)+na(1,l));
  dbp(2,mr)=dbp(2,mr)+nut*(nb(1,k)+nb(1,l));
end
end
end
end
```

```

function [dnp, dap, dbp]= back13( np,i, alpha,bb, dt)
% written 1998 by Tom Chisholm
% Virginia Institute of Marine Science
% For details on algorithms see Tom Chisholm's dissertation

%calculates interaction between aggregates in row immediately smaller
%than one being added to
% inputs
% np number of aggregates in cells
% i size class
% alpha stickiness matrix
%bb encounter kernel
% dt time step

% outputs
% changes in bins

nu=0.01;
dnp=zeros(3,6);
dap=zeros(3,6);
dbp=zeros(3,6);

%size of rows
fa=linspace(0,1,6);
fb=1-fa;
n=2^(i-3);
n1=n*4;
na(1,:)=fa.*n;
na(3,:)=fa.*n1;
nb(1,:)=fb.*n;
nb(3,:)=fb.*n1;

for k=1:6,
    for l=1:6,
        if (np(1,k)~=0) & (np(3,l)~=0)
            %nut is number of aggregates moving to new bin
            nut=np(1,k)*np(3,l)*alpha(k,l)*bb(1,l,1,k)*dt;
            dnp(1,k)=dnp(1,k)-nut;
            dnp(3,l)=dnp(3,l)-nut;
            dap(1,k)=dap(1,k)-nut*na(1,k);
            dap(3,l)=dap(3,l)-nut*na(3,l);
            dbp(1,k)=dbp(1,k)-nut*nb(1,k);
            dbp(3,l)=dbp(3,l)-nut*nb(3,l);
            m=round((1/5*k+4/5*l)); %m is fraction bin of aggregation products
            dnp(3,m)=dnp(3,m)+nut;
            dap(3,m)=dap(3,m)+nut*(na(3,l)+na(1,k));
            dbp(3,m)=dbp(3,m)+nut*(nb(3,l)+nb(1,k));
        end
    end
end
end

```

```

function [dnp, dap, dbp]= back23( np,i,alpha,bb, dt)
% written 1998 by Tom Chisholm
% Virginia Institute of Marine Science
% For details on algorithms see Tom Chisholm's dissertation

%calculates interaction between aggregates in row immediately smaller
%than one being added to
% inputs
% np number of aggregates in cells
% i size class
% alpha stickiness matrix
%bb encounter kernel
% dt time step

% outputs
% changes in bins

nu=0.01;
dnp=zeros(3,6);
dap=zeros(3,6);
dbp=zeros(3,6);

%size of rows
fa=linspace(0,1,6);
fb=1-fa;
n=2^(i-3);
n1=n*2;

na(1,:)=fa.*n;
na(2,:)=fa.*n1;
nb(1,:)=fb.*n;
nb(2,:)=fb.*n1;
%cc=1;
for k=1:6,
    for l=1:6,
        if (np(1,k)~=0) & (np(2,l)~=0)
            nut=np(1,k)*np(2,l)*alpha(k,l)*bb(1,l,1,k)*dt;
            %nut is number of aggregates moving to new bin
            dnp(1,k)=dnp(1,k)-nut;
            dnp(2,l)=dnp(2,l)-nut;
            dap(1,k)=dap(1,k)-nut*na(1,k);
            dap(2,l)=dap(2,l)-nut*na(2,l);
            dbp(1,k)=dbp(1,k)-nut*nb(1,k);
            dbp(2,l)=dbp(2,l)-nut*nb(2,l);
            m=round((1/3*k+2/3*l)); M is fraction bin of products
            dnp(3,m)=dnp(3,m)+nut;
            dap(3,m)=dap(3,m)+nut*(na(2,l)+na(1,k));
            dbp(3,m)=dbp(3,m)+nut*(nb(2,l)+nb(1,k));
        end
    end
end
end

```

```

function [dnb, dab, dbb, bi] =breakup(bi,n, a, b);
% written 1998 by Tom Chisholm
% Virginia Institute of Marine Science
% For details on algorithms see Tom Chisholm's dissertation

%inputs bi kolmogorov scale
% n a b number of aggregates a , b particles
% aggregates in bins one size larger than the kolmogorov scale to
% one bin smaller than the k scale are broken into smaller
% aggregates by rupturing in half.

for k=1:6,
    dnb(4,k)=-n(bi(k)+1,k);
    dnb(3,k)=2*n(bi(k)+1,k)-0.5*n(bi(k),k);
    dnb(2,k)=n(bi(k),k)-0.25*n(bi(k)-1,k);
    dnb(1,k)=0.5*n(bi(k)-1,k);
    dab(4,k)=-a(bi(k)+1,k);
    dab(3,k)=a(bi(k)+1,k)-0.5*a(bi(k),k);
    dab(2,k)=0.5*a(bi(k),k)-0.25*a(bi(k)-1,k);
    dab(1,k)=0.25*n(bi(k)-1,k);
    dbb(4,k)=-b(bi(k)+1,k);
    dbb(3,k)=b(bi(k)+1,k)-0.5*b(bi(k),k);
    dbb(2,k)=0.5*b(bi(k),k)-0.25*b(bi(k)-1,k);
    dbb(1,k)=0.25*b(bi(k)-1,k);
end

```

```

%m file parti
% written 1998 by Tom Chisholm
% Virginia Institute of Marine Science
% For details on algorithms see Tom Chisholm's dissertation

% This program models aggregation of two types of particles
% The two types of particles are called a and b
% there are 25 size bin and 6 fraction bins for a total of 150 bins

% calculates distribution of aggregates in water column
% includes two component aggregation model and
% vertical diffusion and settling

% bottom bc is 1 to bi-2 for columns 1 and 6

clear all
% primary particle sizes cm
la=5e-4;
lb=5e-3;
% fractal dimensions
ma=1.8;
mb=1.8;
% particle excess density g/ml
pa=1.65;
pb=0.1;
% stickiness
% a1 a to a; a2 a to b; a3 b to b
a1=1;
a2=1;
a3=1;
%
fraca=0.9; % volume fraction of reference concentration a particles
con= 0.0001; % volume concentration in reference concentration
% dats includes record of adjustable parameters
dats1=['la lb ma mb pa pb a1 a2 a3']
dats2=[la, lb, ma, mb, pa, pb, a1, a2, a3];
% input for breakup
nu=0.01;%kinnematic viscosity defines units
us=1; % shear vel cm/sec
Az=40*us; %vertical eddy diffusivity
eps=us^3/100; %turbulent dissipation
dt=100; % time step
itmax=100; %iterations dt*itmax= length of model run

%bin sizes
fa=linspace(0,1,6);
fb=1-fa;
ns=linspace(0,24,25);
ns2=2.^ns;
ns2=ns2';
as=ns2*fa;

```

```

bs=ns2*fb; %number of particles in aggregate for size classes

lam=(nu^3/eps)^0.25; % kolmogorov scale
bn=(lam./(fa.*la+fb.*lb)).^(fa.*ma+fb.*mb);
bi=log(bn)./log(2)+1;
bi=floor(bi) %size bin at kolmogorov scale
for k=1:6, %make sure size bin at kolmogorov scale is not out of range
    if bi(k)>24
        bi(k)=24;
    end
    if bi(k)<2
        bi(k)=2;
    end
end

% determine size density and fall velocity for each cell
[ot, w, p]=fracd(la, lb, ma, mb, pa, pb);
% create stickiness matrix
[alpha] =alph(la, lb, a1, a2, a3);
% create hydrodynamic interaction kernel matrix
[bet]=bbeta(ot,w,eps);

% initialization
for j=1:3,
    n(:,j)=zeros(25,6);
end
maxo(1)=bi(1)-2;
maxo(2)=bi(6)-2;
for i=1:2,
    if maxo(i)<1
        maxo(i)=1;
    end
end

%calculate reference concentrations
xx=(con*(1-frac))/(pi*(la^3)/6*maxo(1));
for j=1:maxo(1)
    coo(j,1)=xx/ns2(j);
end
xx=(con*frac)/(pi*(lb^3)/6*maxo(2));
for j=1:maxo(2)
    coo(j,2)=xx/ns2(j);
end

%initialize concentrations
it=0;
C=[0 0 0];
C=C';

%major loop
while itmax>it,

```

```

it=it+1

for ii=1:2; % include reference concentration
    i=(ii-1)*5+1;
    for j=1:maxo(ii),
        for k=1:3,
            C(k)=n(j,i,k);
        end
        Co=coo(j,ii);
        wf=w(j,i); %wf fall velocity
        %difax solves vertical distribution with reference concentration
        C= difx( wf, Az, dt, C, Co);
        n(j,i,1:3)=C;
    end
end

mm=max(maxo);

for i=2:5
    for j=1:mm
        for k=1:3,
            C(k)=n(j,i,k);
        end
        wf=w(j,i);
        %diff2 solves vertical distribution with no diffusion bottom BC
        C= diff2( wf, Az, dt, C);
        n(j,i,1:3)=C;
    end
end

for i=1:6
    for j=mm+1:25
        for k=1:3,
            C(k)=n(j,i,k);
        end
        wf=w(j,i);
        %diff2 solves vertical distribution with no diffusion bottom BC
        C= diff2( wf, Az, dt, C);
        n(j,i,1:3)=C;
    end
end

if maxo(1)>maxo(2)
    i=6;
    for j=maxo(2)+1:maxo(1)
        for k=1:3,
            C(k)=n(j,i,k);
        end
        wf=w(j,i);
        %diff2 solves vertical distribution with no diffusion bottom BC
        C= diff2( wf, Az, dt, C);
    end
end

```

```

        n(j,i,1:3)=C;
    end
end

if maxo(2)>maxo(1)
    i=1;
    for j=maxo(1)+1:maxo(2)
        for k=1:3,
            C(k)=n(j,i,k);
        end
        wf=w(j,i);
        %diff2 solves vertical distribution with no diffusion bottom BC
        C= diff2( wf, Az, dt, C);
        n(j,i,1:3)=C;
    end
end

for j=1:3
    ni=n(:,j);
    j
    %agg2 calculates aggregation
    [ni ]= agg2(dt, ni, bet,eps, bi, alpha, ns2);
    n(:,j)=ni;
    sav(:,it,j)=ni;
end
end

```

```

function C= diff2( w, Az, dt, C)
% written 1998 by Tom Chisholm
% Virginia Institute of Marine Science
% For details on algorithms see Tom Chisholm's dissertation

% calculates vertical aggregate distribution
% no diffusion bottom bc

if sum(C)>1e-20

s=-1;
dz=100; %vertical grid size cm
z=[350 250 150]; %elevations cm
tb=(2*Az-w*dz)/(2*Az+w*dz);
A=(s*w*dt*dz+s*Az*dt)/(dz*dz);
B=1-(s*w*dt*dz+2*s*Az*dt)/(dz*dz);
BB=1-(s*w*dt*dz+s*Az*dt)/(dz*dz);
D=s*Az*dt/(dz*dz);
k=[A*tb+B D 0; A B D; 0 A BB];
kk=inv(k);

C=kk*C;

end

```

```

function [C]= difx( w, Az, dt, C, C0)
% solves vertical distribution using implicit method
% written 1998 by Tom Chisholm
% Virginia Institute of Marine Science
% For details on algorithms see Tom Chisholm's dissertation
% reference concentration at bottom

s=-1;
dz=100; %vertical grid size cm
z=[350 250 150]; %elevations cm
z0=0.5;
tb=(2*Az-w*dz)/(2*Az+w*dz);
A=(s*w*dt*dz+s*Az*dt)/(dz*dz);
B=1-(s*w*dt*dz+2*s*Az*dt)/(dz*dz);
D=s*Az*dt/(dz*dz);

k=[A*tb+B D 0; A B D; 0 A B];
kk=inv(k);

C(3)=C(3)-D*C0;

C=kk*C;

```

```

function [n ]= agg2(ttot, n, bet,eps, bi, alpha, ns2)
% solves aggregation equation
% breakup is calculated each iteration
% written 1998 by Tom Chisholm
% Virginia Institute of Marine Science
% For details on algorithms see Tom Chisholm's dissertation

%inputs ttot total time modeled

%initialize bin sizes
fa=linspace(0,1,6);
fb=1-fa;
ns=linspace(0,24,25);
ns2=2.^ns;
as=ns2*fa;
bs=ns2*fb;

a=n.*as;
b=n.*bs;
dt=30;
tim=0;
it=0;
% major loop
while tim<ttot & it<3000;
    it=it+1;

%initialize
    dn=zeros(25,6);
    da=zeros(25,6);
    db=zeros(25,6);

%recenter bin
% puts bins outside their ranges in the proper bins
    [n, a, b, att, btt] = putrite(n, a, b);
% removes aggregates larger than the breakup criteria
    [ a, b, n]=rembig(bi, a, b, n, ns2);
    %lsta(:,cc)=att(:);
    %lstb(:,cc)=btt(:);
    [n, a, b]=fit(n, a, b); % recenter bins
    %cc=cc+1
% end

%
for i=2:25,
    if i==2
        bb=bet(1, :, 1, :);
        np=n(1:2, :);
        % interaction of smallest row and smallest row
        [dnp,dap,dbp]=back22(np,i,alpha, bb, dt);
        dn(1:2,:)=dn(1:2,:)+dnp;
        da(1:2,:)=da(1:2,:)+dap;
    end
end

```

```

    db(1:2,:)=db(1:2,.)+dbp;
else
    np=n(i-1:i,:);
    bb=bet(i-1, :, i-1, :);
% interaction of aggregates in row one bin smaller to add to bin i
    [dnp,dap,dbp]=back22(np,i, alpha, bb, dt);
    dn(i-1:i,:)=dn(i-1:i,.)+dnp;
    da(i-1:i,:)=da(i-1:i,.)+dap;
    db(i-1:i,:)=db(i-1:i,.)+dbp;

    np=n(i-2:i,:);
    bb=bet(i, :, i-2, :);
% interaction of row i and row i-2
    [dnp,dap,dbp]=back13(np,i, alpha, bb, dt);
    dn(i-2:i,:)=dn(i-2:i,.)+dnp;
    da(i-2:i,:)=da(i-2:i,.)+dap;
    db(i-2:i,:)=db(i-2:i,.)+dbp;

    bb=bet(i-1, :, i-2, :);
%interaction of row i-1 mnd i-2
    [dnp,dap,dbp]=back23(np,i,alpha,bb, dt);
    dn(i-2:i,:)=dn(i-2:i,.)+dnp;
    da(i-2:i,:)=da(i-2:i,.)+dap;
    db(i-2:i,:)=db(i-2:i,.)+dbp;

%interactions of row i and rows smaller than i-2
    for k=1:6,
        if (n(i,k)>1e-20) & (i>3)
            on=ones(i-3,1);
            al=on*alpha(k,:);
            clear bb
            bb=bet(1:i-3, :, i, k);
            ddn=bb.*al.*n(1:i-3, :). *n(i,k). *dt;
            dn(1:i-3, :)=dn(1:i-3,.)-ddn;
            da(1:i-3, :)=da(1:i-3,.)-ddn.*as(1:i-3, :);
            db(1:i-3, :)=db(1:i-3,.)-ddn.*bs(1:i-3, :);
            da(i,k)=da(i,k)+sum(sum(ddn.*as(1:i-3, :)));
            db(i,k)=db(i,k)+sum(sum(ddn.*bs(1:i-3, :)));
        end
    end
end
end
end

%breakup
[dn1, da1, db1]= bkup(bi, a, b, n, ns2);

[ da, db, dn]=rembig(bi, da, db, dn, ns2);

n1=n+dn+dn1;

```

```

a1=a+da+da1;
b1=b+db+db1;

% is time step causing zero errors
bul=0;
for i=1:25,
    for k=1:6,
        if ((a1(i,k)<-1) | (b1(i,k)<-1))
            bul=1;
            [i k ]
        end
    end
end

% if zero errors, decrease time step else make it bigger
if bul==1
    dt=dt/3;
    it=it-1;
    [4 it dt]
else
    if (dt<30) %
        dt=dt*2;
        [6 it dt]
    end
    n=n1; % use data if time step ok
    b=b1;
    a=a1;
    told=tim;
    tim=tim+dt;
end

end

% correct for ending time not ttot due to variable time steps
fff=(tim-ttot)/(tim-told);
n=n-dn*fff;
a=a-da*fff;
b=b-db*fff;

[n, a, b, att, btt] = putrite(n, a, b);
[n, a, b]=fit(n, a, b); % recenter bins

[tim dt sum(sum(a)) sum(sum(b)) ]

```

```

function [dn, da, db]= bkup(bi, a, b, n, ns2)
% written 1998 by Tom Chisholm
% Virginia Institute of Marine Science
% For details on algorithms see Tom Chisholm's dissertation

% aggregates close to the kolmogorov scale are
% broken up and particles produces are scattered over smaller size bins

n2=ns2';
da=zeros(25,6);
db=zeros(25,6);
per=[0.25 0.5 1]; % fraction broken up
for j=-1:1,
    for k=1:6,
        ae=bi(k)+j;
        as=a(ae,k)*per(j+2);
        ad=bi(k)+j-1;
        das=as/(1.5*n2(ad));
        da(1:ad,k)=da(1:ad,k)+0.75*n2(1:ad)*das;
        da(1,k)=da(1,k)+0.75*das;
        da(ae,k)=da(ae,k)-as;
        bs=b(ae,k)*per(j+2);
        dbs=bs/(1.5*n2(ad));
        db(1:ad,k)=db(1:ad,k)+0.75*n2(1:ad)*dbs;
        db(1,k)=db(1,k)+0.75*dbs;
        db(ae,k)=db(ae,k)-bs;
    end
end

for k=1:6
    da(bi(k)+1,k)=da(bi(k)+1,k)+sum(a(bi(k)+2:25,k));
    db(bi(k)+1,k)=db(bi(k)+1,k)+sum(b(bi(k)+2:25,k));
    da(bi(k)+2:25,k)=a(bi(k)+2:25,k);
    db(bi(k)+2:25,k)=b(bi(k)+2:25,k);
end

n22=n2*ones(1,6);

dn=(da+db)./n22;

```

```
function [ a, b, n]=rembig(bi, a, b, n, ns2)
% written 1998 by Tom Chisholm
% Virginia Institute of Marine Science
% For details on algorithms see Tom Chisholm's dissertation

% this routine remove spurious aggregates much larger than the breakup criterion

for k=1:6
    da=sum(a(bi(k)+2:25,k));
    db=sum(b(bi(k)+2:25,k));
    a(bi(k)+1,k)=a(bi(k)+1,k)+da;
    b(bi(k)+1,k)=b(bi(k)+1,k)+db;
    a(bi(k)+2:25,k)=0;
    b(bi(k)+2:25,k)=0;
    n(bi(k)+2:25,k)=0;
    n(bi(k)+1,k)=n(bi(k)+1,k)+(da+db)/ns2(bi(k)+1);
end
```

LITERATURE CITED

Acuna, J. L., D. Deibel, and S. Sooley. 1994. A Simple Device to Transfer Large and Delicate Planktonic Organisms. *Limnology and Oceanography*, 39:2001-2003.

Adrian, R. J., 1991. Particle-Imaging Techniques for Experimental Fluid Mechanics. *Annual Review of Fluid Mechanics*, 23:261-304.

Al Ani, S., K. R. Dyer and D. A. Huntley. 1991. Measurement of the Influence of Salinity on Floc Density and Strength. *Geo-Marine Letters*, 11:154-158.

Allredge, A. L. and T. Cohen, 1987. Can Microscale Chemical Patches Persist in the Sea? Microelectrode Study of Marine Snow, Fecal Pellets. *Science*, 235:689-691.

Allredge, A. L. and C. C. Gotschalk. 1988. In-Situ Settling Behavior of Marine Snow. *Limnology and Oceanography*, 33:339-351.

Allredge A. L. and M. W. Silver. 1988. Characteristics, Dynamics and Significance of Marine Snow. *Progress in Oceanography*, 20:41-82.

Allredge, A. L. and C. C. Gotschalk. 1990. The Relative Contribution of Marine Snow of Different Origins to Biological Processes in Coastal Waters. *Continental Shelf Research*, 10:41-58.

Allredge, A. L., T. C. Granata, C. C. Gotschalk, and T. D. Dickey. 1990. The Physical Strength of Marine Snow and Its Implications for Particle Disaggregation in the Ocean. *Limnology and Oceanography*, 35:1415-1428.

Allredge, A. L. and P. McGillavary. 1991. The Attachment Probabilities of Marine Snow and Their Implications for Particle Coagulation in the Ocean. *Deep Sea Research*, 38:431-443.

Allredge, A. L., U. Passow, and B. E. Logan. 1993. The Abundance and Significance of a Class of Large, Transparent Organic Particles in the Ocean. *Deep Sea Research*, 40:1131-1140.

Allredge, A. L. and G. Jackson, 1995. Aggregation in Marine Systems. *Deep-Sea Research*, 42:1-7.

Argaman, Y. and W. Kaufman. 1970. Turbulence and Flocculation. *Journal of the Sanitary Engineering Division ASCE*, 96:223-241.

Asper, V. L. 1987. Measuring the Flux and Sinking Speed of Marine Snow Aggregates. *Deep-Sea Research*, 34:1-17.

Batchelor, G. K. 1953. *Homogeneous Turbulence*. Cambridge University Press, London.

Biddanda, B. 1985. Microbial Synthesis of Macroparticulate Matter. *Marine Ecology Progress Series*, 20:241-251.

Bochdansky, A. B. and G. J. Hendl. 1992. Ecology of Amorphous Aggregations (Marine Snow) in the Northern Adriatic Sea III. Zooplankton Interactions With Marine Snow. *Marine Ecology Progress Series*, 87:135-146.

Brumley, B. H. and G. H. Jirka. 1987. Near-Surface Turbulence in a Grid Stirred Tank. *Journal of Fluid Mechanics*, 183:235-263.

Buffington, J. M. 1999. The Legend of A. F. Shields. *Journal of Hydraulic Engineering*, 125:376-387.

Burban, P.-Y., Y.-J. Xu, J. McNeil and W. Lick. 1990. Settling Speeds of Floccs in Fresh Water and Seawater. *Journal of Geophysical Research*, 95 (C10) 18213-18220.

Burd, A. and G. A. Jackson. 1997. Predicting Particle Coagulation and Sedimentation Rates for a Pulsed Input. *Journal of Geophysical Research*, 102:C5:10545-10561.

Burt, N. T. 1984. Field Settling Velocities of Estuary Muds. *Workshop on Cohesive Sediment Dynamics with Special Reference to Physical Processes in Estuaries* ed. A. J. Mehta. Springer Verlag, Berlin.

Camp, T. R. and P. C. Stein 1943. Velocity Gradients and Internal Work in Fluid Motion. *Journal of the Boston Society of Civil Engineers*, 30:219-237.

Casson, L. W. and D. F. Lawler. 1990. Flocculation in Turbulent Flow: Measurement and Modeling of Particle Size Distributions. *Journal of the American Water Works Association*, 80:54-68.

Chase R. P. 1979. Settling Behavior of Natural Aquatic Particles. *Limnology and Oceanography*, 24:417-426.

Crump, B. C., J. A. Baross, and C. A. Simenstad. 1998. Dominance of Particle-Attached Bacteria in the Columbia River Estuary, USA. *Aquatic Microbial Ecology*, 14:7-18.

Dam, H. G. and D. T. Drapeau. 1995. Coagulation Efficiency, Organic-Matter Glues and the Dynamics of Particles During a Phytoplankton Bloom in a Mesocosm Study. *Deep Sea Research*, 42:111-124.

Davies, C.N. 1952. The Separation of Airborne Dust and Particles. *Proceedings of the Institute of Mechanical Engineers London B1*, 185-213.

Decho, A. W. 1990. Microbial Exopolymer Secretions in Ocean Environments: Their Role(s) in Food Webs and Marine Processes. *Oceanography Marine Biology Annual Review*, 28:73-153.

Delichatsios, M. A. and R. F. Probstein. 1975. Coagulation in Turbulent Flow: Theory and Experiment. *Journal of Colloid and Interface Science*, 51:394-405.

Drapeau, D. T., H. G. Dam, and G. Greiner. 1994. An Improved Flocculator Design for Use in Particle Aggregation Experiments. *Limnology and Oceanography*, 39:723-729.

Ducklow, H. W., S. M. Hill, and W. D. Gardner. 1985. Bacterial Growth and the Decomposition of Particulate Organic Carbon Collected in Sediment Traps. *Continental Shelf Research*, 4:445-464.

Dyer, K. R. 1986. *Coastal and Estuarine Sediment Dynamics*, John Wiley and Sons, New York.

Dyer, K. R. and A. J. Manning. 1999. Observation of the Size, Settling Velocity, and Effective Density of Floccs, and Their Fractal Dimension. *Journal of Sea Research*, 41:87-95.

Eisma, D., J. Kalf and M. Veenhuis. 1980. The Formation of Small Particles and Aggregates in the Rhine Estuary. *Netherlands Journal of Sea Research*, 14:172-191.

Eisma, D. 1986. Flocculation and De-Flocculation of Suspended Matter in Estuaries. *Netherlands Journal of Sea Research*, 20:183-199.

Eisma, D. and A. Li. 1993. Changes in Suspended-Matter Floc Size During the Tidal Cycle in the Dollard Estuary. *Netherlands Journal of Sea Research*, 31:107-117.

Fair, G. M. and R. S. Gemmel. 1963. A Mathematical Model of Coagulation. *Journal of Colloid Science*, 19:360-372.

Farley, K. J. and F. M. M. Morel. 1986. Role of Coagulation on the Mechanics of Sedimentation. *Environmental Science and Technology*, 20:187-195.

Fennessy, M. J., K. R. Dyer, and D. A. Huntley. 1994. INSSEV: An Instrument to Measure the Size and Settling Velocity of Floccs in Situ. *Marine Geology*, 117:107-117.

- Gelbard, F., Y. Tambour, and J. Seinfeld. 1980. Sectional Dynamics for Representing Aerosol Dynamics. *Journal of Colloidal and Interface Science*, 76:541-555.
- Gibbs, R. J., M. D. Mathews, and D. A. Link. 1971. The Relationship Between Sphere Size and Settling Velocity. *Journal of Sedimentary Petrology*. 41:7-18.
- Gibbs, R. J. 1981. Floc Breakage by Pumps. *Journal of Sedimentary Petrology*, 51:670-672.
- Gibbs, R. J. 1982. Floc Stability During Coulter Counter Analysis. *Journal of Sedimentary Petrology*, 52:657-660.
- Gibbs, R. J. 1983a. Effect of Natural Organic Coatings on the Coagulation of Particles. *Environmental Science and Technology*, 17:237-240.
- Gibbs, R. J. 1983b. Coagulation Rates of Clay Materials and Natural Sediments. *Journal of Sedimentary Petrology*, 53:1193-1203.
- Gibbs, R. J. and L. N. Konwar. 1983. Sampling of Mineral Flocs Using Niskin Bottles. *Environmental Science Technology*, 17:374-375.
- Gibbs, R. J. 1985. Estuarine Flocs: Their Size, Settling Velocity and Density. *Journal of Geophysical Research*, 90:3249-3251.
- Gmachowski, L. 1996. Hydrodynamics of Aggregated Media. *Journal of Colloid and Interface Science*, 178:80-86.
- Grant, W. D. and O. S. Madsen. 1986. The Continental-Shelf Bottom Boundary Layer. *Annual Review of Fluid Mechanics*, 18:265-305.
- Griffith, P., F-W Shiah, K. Gloersen, H. W. Ducklow, and M. Fletcher. 1994. Activity and Distribution of Attached Bacteria in Chesapeake Bay. *Marine Ecology Progress Series*, 108:1-10.
- Grim, R. E. 1968. *Clay Mineralogy*,. McGraw- Hill, New York.
- Grossart, H-P and M. Simon. 1997. Formation of Macroscopic Organic Aggregates (Lake Snow) in a Large lake: The Significance of Transparent Exopolymer Particles, Phytoplankton and Zooplankton, *Limnology and Oceanography*. 42:1651-1659.
- Hamrick, J. M.. 1992. A Three-Dimensional Environmental Fluid Dynamics Computer Code: Theoretical and Computational Aspects. Special Report in Applied Marine Science and Ocean Engineering, Number 317. Virginia Institute of Marine Science, Gloucester Point, VA.

Han M. and D. F. Lawler. 1992. Interaction of Two Settling Spheres: Settling Rates and Collision Efficiency. *Journal of Hydraulic Engineering*, 117:1269-1289.

Hanson, A. T. and J. L. Cleasby. 1990. The Effects of Temperature on Turbulent Flocculation: Fluid Dynamics and Chemistry. *Journal of the American Water Works Association*, 80: 56-73.

Hawley, N. 1982. Settling Velocity Distribution of Natural Aggregates. *Journal of Geophysical Research*, 87:9489-9498.

Heffler, D. E., J. P. M. Syvitski and K. W. Asprey. 1991. The Flocc Camera. in *Principles, Methods and Applications of Particle Size Analysis*. ed. J. P. M. Syvitski. Cambridge University Press, New York, p209-221.

Hill, P. S. and A. R. M. Nowell. 1990. The Potential of Large, Fast-Sinking Particles in Clearing Nepheloid Layers. *Philosophical Transactions of the Royal Society of London*, 331:103-117.

Hill, P. 1992. Reconciling Aggregation Theory With Observed Vertical Fluxes Following Phytoplankton Blooms. *Journal of Geophysical Research*, 97:2295-2307.

Hill, P. S., A. R. M. Nowell and P. A. Jumars. 1992. Encounter Rate by Turbulent Shear of Particles Similar in Diameter to the Kolmogorov Scale. *Journal of Marine Research*, 50:643-668.

Hunt, J. R. 1982. Self-similar Particle-size Distributions During Coagulation: Theory and Experimental Verification. *Journal of Fluid Mechanics*, 122:169-185.

Hunt, J. R. 1984. Particle Aggregate Breakup by Fluid Shear. *Workshop on Cohesive Sediment Dynamics with Special Reference to Physical Processes in Estuaries*, ed. A. J. Mehta. Springer Verlag, Berlin.

Israelachvili, J. N. and P. M. McGuiggan, 1988. Forces Between Surfaces in Liquids. *Science*, 241:795-800.

Jackson, G. A.. 1990. A Model of the Formation of Marine Algal Floccs by Physical Coagulation Processes. *Deep-Sea Research*, 37:1197-1211.

Jackson, G. A. and S. E. Lochmann. 1992. Effect of Coagulation on Nutrient and Light Limitation of an Algal Bloom. *Limnology and Oceanography*, 37:77-89.

Jackson, G. A. and S. Lochmann. 1993. Modeling Coagulation of Algae in Marine Ecosystems. in *Environmental Particles vol 2* ed. J. Buffle and H. P. van Leeuwen, Lewis Publishers.

Jackson, G. A., 1994. Particle Trajectories in a Rotating Cylinder: Implications for Aggregation Incubations. *Deep Sea Research*. 41:429-437.

Jackson, G. A. 1995. Comparing Observed Changes in Particle Size Spectra with Those Predicted Using Coagulation Theory. *Deep Sea Research*, 42:159-184.

Jeffrey, D. J. and Y. Onishi. 1984. Calculation of the Resistance and Mobility Functions for Two Unequal Rigid Spheres in Low-Reynolds-Number Flow. *Journal of Fluid Mechanics*, 139:261-290.

Kaltenbock, E. and G. Herndl. 1992. Ecology of Amorphous Aggregations (Marine Snow) in the Northern Adriatic Sea IV. Dissolved Nutrients and the Autotrophic Community Associated with Marine Snow. *Marine Ecology Progress Series*, 87:147-159.

Karner M. and G. J. Herndl. 1992. Extracellular Enzymatic Activity and Secondary Production of Free-Living and Marine-Snow-Associated Bacteria. *Marine Biology*, 113:341-347.

Kawana, K. and T. Tanimoto. 1984. Turbid Bottom Water Layer and Bottom Sediment in the Seto Inland Sea. *Journal of the Oceanographical Society of Japan*, 40:175-183.

Kiorboe, T., K. P. Andersen, and H. G. Dam. 1990. Coagulation Efficiency and Aggregate Formulation in Marine Phytoplankton. *Marine Biology*, 107:235-245.

Kiorboe, T. and J. L. S. Hansen. 1993. Phytoplankton Aggregate Formation: Observations of Patterns and Mechanisms of Cell Sticking and the Significance of Exopolymeric Material. *Journal of Plankton Research*, 14:993-1018.

Kiorboe, T., C. Lundsgaard, M. Oleson and J. L. S. Hansen. 1994. Aggregation and Sedimentation Processes During a Spring Phytoplankton Bloom: A Field Experiment to Test Coagulation Theory. *Journal of Marine Research*, 52:297-323.

Klimpel, R. C. and R. Hogg. 1986. Effects of Flocculation Conditions on Agglomerate Structure. *Journal of Colloid and Interface Science*, 113:121-131.

Krank, K. 1980. Variability of Particulate Matter in a Small Coastal Inlet. *Canadian Journal of Fisheries and Aquatic Sciences*, 37:1209-1219.

Lampitt, R. S., W. R. Hillier, and P. G. Challenor. 1985. Seasonal and Diel Variation in the Open Ocean Concentration of Marine Snow Aggregates. *Nature*, 362:737-739.

Landau L. D. and E. M. Lifshitz. 1959. *Fluid Mechanics*. Addison-Wesley. Reading, MA.

Landing et al. 1991. Sample Manipulation and Speciation in Marine Particles: Analysis and Characterization eds D. C. Hurd and D. C. Spencer, American Geophysical Union, Washington, D.C., p23-32.

- Lawler, D. F. 1986. Removing Particles in Water and Wastewater. *Environmental Science and Technology*, 20:856-861.
- Lee, C. H. 1997. Resuspension Behavior of Natural Estuarine Sediment. PhD dissertation College Of William and Mary, Virginia Institute of Marine Science, Gloucester Point, VA.
- Levich, V. G. 1962. *Physicochemical Hydrodynamics*. Prentice Hall. New York.
- Libes, S. M.. 1992. *Introduction to Marine Biogeochemistry*. John Wiley and Sons, New York.
- Lick W. and J. Lick. 1988. Aggregation and Disaggregation of Fine-Grained Lake Sediments. *Journal of Great Lakes Research*, 14:514-523.
- Lick, W., Lick, J., and C. K. Zeigler. 1992. Flocculation and Its Effect on the Vertical Transport of Fine-Grained Sediments. *Hydrobiologica*, 235:1-16.
- Lick, W., H. Huang and R. Jepsen. 1993. Flocculation of Fine Grained Sediments Due to Differential Settling. *Journal of Geophysical Research*, 98(C6):10279-10288.
- Lin, M. W., H. M. Lindsay, D. A. Weitz, R. C. Ball, R. Klein, and P. Meakin. 1989. Universality in Colloid Aggregation. *Nature*, 339:360-362.
- Logan B. E. and J. R. Hunt. 1987. Advantages to Microbes of Growth in Permeable Aggregates in Marine Systems. *Limnology and Oceanography*, 32:1034-1048.
- Logan, B. E. and J. R. Kilps. 1995. Fractal Dimensions of Aggregates Formed in Different Fluid Mechanical Environments. *Water Research*, 29:443-453.
- Madsen, O.S., L. D. Wright, J. D. Boon, and T. A. Chisholm. 1993. Wind Stress, Bed Roughness, and Sediment Suspension on the Inner Shelf During and Extreme Storm Event. *Continental Shelf Research*, 13:1303-1324.
- Masliyah, J. H., G. Neale, K. Malysa, and T. G. M. van de Ven. 1987. Creeping Flow Over a Composite Sphere: Solid Core With Porous Sphere. *Chemical Engineering Science*, 42:245-253.
- Matsumoto, K. and A. Sukanuma. 1977. Settling Velocity of a Permeable Model Floc. *Chemical Engineering Science*, 32:445-447.
- McCave, I. N. 1984. Size Spectra and Aggregation of Suspended Particles in the Deep Ocean. *Deep-Sea Research*, 31:329-352.
- McCave, I. N. and T. F. Gross. 1991. In-Situ Measurements of Particle Settling Velocity in the Deep Sea. *Marine Geology*, 99:403-411.

Milligan, T. G. and D. H. Loring. 1997. The Effect of Flocculation on the Size Distributions of Bottom Sediment in Coastal Inlets: Implications for Contaminant Transport. *Water, Air and Soil Pollution*, 99:33-42.

Milligan, T. G. and P. S. Hill. 1998. A Laboratory Assessment of the Relative Importance of Turbulence, Particle Composition, and Concentration in Limiting Maximal Floc Size and Settling Behavior. *Journal of Sea Research*, 39:227-241.

Neale, G., N. Epstein, and W. Nader. 1973. Creeping Flow Relative to Permeable Spheres. *Chemical Engineering Science*, 28: 1865-1874.

Nielsen, P. 1992. *Coastal Bottom Boundary Layers and Sediment Transport*, World Scientific, Singapore.

Officer, C. B. 1976. *Physical Oceanography of Estuaries*. John Wiley and Sons, New York.

Ongley, E. D., B. G. Krishnappan, I. G. Droppo, S. S. Rao, and R. J. Maguire. 1992. Cohesive Sediment Transport: Emerging Issues for Toxic Chemical Management. *Hydrobiologia*, 235/236:177-187.

Parker, D. S., W. J. Kaufman, and D. Jenkins. 1972. Floc Breakup in Turbulent Flocculation Processes. *Journal of the Sanitary Engineering Division ASCE*. 2:79-99.

Passow, U. and P. Wassmann. 1994. On the Trophic Fate of *Phaeocystis Pouchetii* (Hariot): IV. The Formulation of Marine Snow by *P. Pouchetti*. *Marine Ecological Progress Series*, 104:153-161.

Passow, U., A. L. Alldredge, and B. E. Logan. 1994. The Role of Particulate Carbohydrate Exudates in the Flocculation of Diatom Blooms. *Deep-Sea Research*, 41:335-357.

Pierce, J. W. and M. M. Nichols. 1986. Changes of Particle Composition From Fluvial Into an Estuarine Environment: Rappahannock River, Virginia. *Journal of Coastal Research*, 2:419-425.

Pruppacher, H. R. and J. D. Klett. 1980. *Microphysics of Clouds and Precipitation*, D. Riedel, Boston.

Rennie, S. and B. Nielson. 1993. *Chesapeake Bay Atlas, U.S. Environmental Protection Agency Monitoring Program, Water Quality Data 1984-1991*. Virginia Institute of Marine Science, College of William and Mary, Gloucester Point, Virginia.

Riebesell, U. 1991. Particle Aggregation During a Diatom Bloom. I. Physical Aspects. *Marine Ecology Progress Series*. 69:273-280.

- Riebesell, U. 1992. The Formation of Large Marine Snow and Its Sustained Residence in Surface Waters. *Limnology and Oceanography*, 37:63-76.
- Rouse, H. 1938. Experimentation on the Mechanics of Sediment Suspension. Fifth International Congress for Applied Mechanics.
- Saffman, P. G. and J. S. Turner. 1956. On the Collision of Drops in Turbulent Clouds. *Journal of Fluid Mechanics*, 1:16-30.
- Schlichting, H. 1979. *Boundary Layer Theory*. McGraw-Hill, New York.
- Schulz, E. F., R. H. Wilde, and M. L. Albertson. 1954. Influence of Shape on Fall Velocity of Sedimentary Particles. Report Prepared for the Missouri River Division, Corps of Engineers, U.S. Army, through Colorado A&M Research Foundation, Fort Collins, IL.
- Shanks, A. L. and E. W. Edmondson. 1989. Laboratory-Made Artificial Marine Snow: A Biological Model of the Real Thing. *Marine Biology*, 101:463-470.
- Shanks, A. L. and E. W. Edmondson. 1990. The Vertical Flux of Metazoans (Holoplankton, Meiobenthos, and Larval Invertebrates) Due to Their Association with Marine Snow. *Limnology and Oceanography*, 35:455-463.
- Shanks, A. L. and M. L. Reeder. 1993. Reducing Microzones and Sulfide Production in Marine Snow. *Marine Ecology Progress Series*, 96:43-47.
- Sheldon, R. W., A. Prakash, and W. H. Sutcliffe, Jr. 1972. The Size Distribution of Particles in the Ocean. *Limnology and Oceanography*, 17: 327-340.
- Shimeta, J., P. A. Jumars, and E. J. Lessard. 1995. Influences of Turbulence on Suspension Feeding by Planktonic Protozoa; Experiments in Laminar Shear Fields. *Limnology and Oceanography*, 40:845-859.
- Smoluchowski, M. 1917. Versuch Einer Mathematischen Theorie der Koagulationskinetic Kolloider Losungen. *Z. Phys. Chemie.*, 92:129-168.
- Stanley, S. J. and D. W. Smith. 1995. Measurement of Turbulent Flow in Standard Jar Test Apparatus. *Journal of Environmental Engineering*, 121:902-909.
- Sternberg, R. W., A. Ogston, and R. Johnson. 1996. A Video System for In-Situ Measurement of Size and Settling Velocity of Suspended Aggregates, *Journal of Sea Research*. 36:127-130.
- Stolzenbach, K. D. 1993. Scavenging of Small Particles by Fast-Sinking Porous Aggregates. *Deep-Sea Research*, 40:359-369.

Stolzenbach, K. D. and M. Elimelech. 1994. The Effect of Particle Density on Collisions Between Sinking Particles: Implications for Particle Aggregation in the Ocean. *Deep Sea Research*, 41:469-483.

Sutherland, D. N. and C. T. Tan. 1970. Sedimentation of a Porous Sphere. *Chemical Engineering Science*, 25:1950-1951.

Swamee, P. K. and C. S. P. Ojha. 1991. Drag Coefficient and Fall Velocity of Nonspherical Particles. *Journal of Hydraulic Engineering*, 117:660-667.

Syvitski, J. P. M., K. W. Asprey, and K. W. G. LeBlanc. 1995. In-Situ Characteristics of Particles Settling Within a Deep-Water Estuary. *Deep Sea Research*, 42:223-256.

Syvitski, J. P. and E. W. H. Hutton. 1996. In-Situ Characteristics of Suspended Particles as Determined by the Floc Camera Assembly. *Journal of Sea Research*, 36:131-142.

Tambo, N. and Y. Watanabe. 1979. Physical Characteristics of Floccs - I The Floc Density Function and Aluminum Floc. *Water Research*, 13:409-419.

Taylor, G. I. 1932. The Transport of Vorticity and Heat through Fluids in Turbulent Motion. *Proceedings of the Royal Society of London. Series A*, 135:685.

ten Brinke, W. B. M. 1994. In Situ Aggregate size and Settling Velocity in the Oosterschelde Tidal Basin (the Netherlands). *Netherlands Journal of Sea Research*, 32:23-35.

Tennekes, H. and J. L. Lumley. 1972. *A First Course in Turbulence*. MIT Press. Cambridge, MA.

Thomas, D. G. 1964. Turbulent Disruption of Floccs in Small Particle Size Suspensions. *American Institute of Chemical Engineers Journal*, 10:517-523.

Thompson, S. M. and J. S. Turner. 1975. Mixing Across an Interface Due to Turbulence Generated by an Oscillating Grid. *Journal of Fluid Mechanics*, 67:349-368.

Trent, J. D., A. L. Shanks, and M. W. Silver. 1978. In Situ and Laboratory Measurements on Macroscopic Aggregates in Monterey Bay, California. *Limnology and Oceanography*, 23:626-635.

Tsai, C.-H., S. Iacobellis, and W. Lick. 1987. Flocculation of Fine-Grained Lake Sediments Due to a Uniform Shear Stress. *Journal of Great Lakes Research*, 13:135-146.

Valioli, I. and E. J. List. 1984. Numerical Simulation of a Sedimentation Basin: Model Development. *Environmental Science and Technology*, 18:242-247.

van Leussen, W. and J. M. Cornelisse. 1993. The determination of the Sizes and Settling Velocities of Estuarine Floes by an Underwater Video System. *Netherland Journal of Sea Research*, 31:231-241.

van Leussen, W. 1994. *Estuarine Macrofloes and Their Role in Fine-Grained Sediment Transport*. Ministry of Transport, Public Works and Water Management. Den Haag.

van Leussen, W. 1999. The Variability of Settling Velocities of Suspended Fine-Grained Sediment in the Ems Estuary. *Journal of Sea Research*, 41:109-118.

van Duuren, F. A. 1968. Defined Velocity Gradient Model Flocculator. *Journal of the Sanitary Engineering Division ASCE*, 94 no SA4:671-682.

Veerapaneni, S. and M. R. Weisner. 1996. Hydrodynamics of Fractal Aggregates with Radially Varying Permability. *Journal of Colloid and Interface Science*, 177:45-57.

Vold, M. J. 1963. Computer Simulation of Floe Formation in a Colloidal Suspension. *Journal of Colloid Science*, 18:684-695.

Wacholder, E. and N. F. Sather. 1974. The Hydrodynamic Interaction of Two Unequal Spheres Moving Under Gravity Through Quiescent Viscous Fluid. *Journal of Fluid Mechanics*, 65:417-437.

Weilenmann, U., C. R. O'Melia, and W. Stumm. 1989. Particle Transport in Lakes: Models and Measurements. *Limnology and Oceanography*, 34:1-18.

Wells, J. T. and A. L. Shanks. 1987. Observations and Geologic Significance of Marine Snow in a Shallow-Water, Partially Enclosed Marine Embayment. *Journal of Geophysical Research*, 92: 13,185-13,190.

White, F. M. 1979. *Fluid Mechanics*. McGraw Hill. New York.

Wright, L. D. 1995. *Morphodynamics of Intercontinental Shelves*. CRC Press, Boca Raton.

Zabawa, C. F. 1978. Microstructure of Agglomerated Suspended Sediments in Northern Chesapeake Bay Estuary. *Science*, 202:49-51.

VITA

Thomas A. Chisholm

Born in Glenn Ridge, NJ on 25 October 1960. Graduated from Slippery Rock High School in 1978. Obtained BS in Materials Engineering in 1982 and MS in Civil Engineering in 1986 both from North Carolina State University. Worked for U. S. Army Corps of Engineers for 4 years and became Registered Professional Civil Engineer - Mississippi in 1990. Received Degree of Civil Engineer from Massachusetts Institute of Technology 1993. Completed PhD in Marine Science from Virginia Institute of Marine Science 1999.